universiteit hasselt
KNOWLEDGE IN ACTION

2016 | Faculty of Sciences

DOCTORAL DISSERTATION

Characterization and modification of polyhydroxyalkanoates (PHA) for application as food packaging material

Doctoral dissertation submitted to obtain the degree of
Doctor of Science: Chemistry, to be defended by

Jens Vandewijngaarden

Promoter: Prof. Dr Robert Carleer
Co-promoters: Prof. Dr Ir Mieke Buntinx
Prof. Dr Jan Yperman

D/2016/2451/20

universiteit hasselt | imec
IMO - IMOMEC
INSTITUUT VOOR MATERIAALONDERZOEK

Voorzitter van de jury

prof. dr. Karin Coninx, UHasselt

Promotor

prof. dr. Robert Carleer, UHasselt

Co-promotor

prof. dr. ir. Mieke Buntinx, UHasselt

prof. dr. Jan Yperman, UHasselt

Leden van de jury

prof. dr. Ing. Ludwig Cardon, UGent

dr. Ing. Nadia Lepot

prof. dr. Roos Peeters, UHasselt

prof. dr. ir. Peter Ragaert, UGent

prof. dr. Sonja Schreurs, UHasselt

"Sometimes you climb out of bed in the morning and you think, I'm not going to make it, but you laugh inside, remembering all the times you've felt that way."

Charles Bukowski

ACKNOWLEDGEMENTS

Deze thesis is het resultaat van een werk van lange adem, waarbij heel wat mensen op de een of andere manier een belangrijke rol gespeeld hebben. Ik wil jullie via deze weg dan ook graag bedanken.

In eerste plaats wil ik graag mijn promotor, Robert Carleer, bedanken voor alle hulp en ondersteuning tijdens mijn doctoraat. Ik kon altijd bij u terecht voor eender welk probleem, of het nu een chemische kwestie was of gewoon een probleem van gebrek aan motivatie. Ondanks dat je het zo ontzettend druk had, vond je altijd wel een vrij moment wanneer het nodig was, bedankt!

Ook mijn copromotoren verdienen flink wat dank. Jan, ik denk dat ik van u vooral een zekere vorm van diplomatie en tact geleerd hebt, wat mogelijk wat ontbrak aan het begin van mijn tijd aan de UHasselt ☺ Je bekeek mijn werk ook altijd vanuit een andere invalshoek, wat toch wel een grote meerwaarde was. Roos en Mieke, ondanks dat ik uit een compleet andere opleiding kwam, gaven jullie mij de kans te doctoreren aan het Verpakkingscentrum, waarvoor ik jullie enorm dankbaar voor ben. Bedankt voor al jullie hulp!

Nadia en Sonja, in het kader van mijn doctoraat (maar daarbuiten wel uiteraard) hebben we niet zoveel contact gehad, maar iedere keer leidde dit wel tot nieuwe inzichten en ideeën. Jullie waren altijd geïnteresseerd en bereid om te helpen.

Graag bedank ik ook iedereen van TANC voor de gezellige en leerrijke jaren! Jullie stonden altijd klaar om me te helpen wanneer het nodig was of voor gewoon wat te babbelen wanneer ik weer moe gezeten was aan mijn bureau. Ik kon me geen beter labo gewenst hebben om al deze jaren doorgebracht te hebben!

Ook de mensen van het Verpakkingscentrum wil ik bedanken voor al hun hulp. Dimitri, bedankt om altijd een gaatje te vinden in je schema zodat ik mijn metingen kon doen, dit was essentieel voor mijn onderzoek. Gudrun, Bram en Riet, jullie stonden ook altijd klaar om te helpen of voor een praatje te slaan over eender wat. Bedankt allemaal voor de goede sfeer! Ook wil ik zeker Gert, Heleen, Stan en Griet vermelden. We zaten over veel op dezelfde golflengte, dus zeer jammer dat we maar kort collega's zijn geweest.

Niet te vergeten zijn al mijn collega doctoraatstudenten, van alle generaties. De oude garde Kenny, Koen, Inge, Mark en Lize om te beginnen. Bedankt voor de fijne werksfeer, hulp in het labo en morele steun! Marco, we started around the same time, so we've been through a lot of the same troubles. I wish you all the best for your thesis and your future in general! Ook de "nieuwe" doctoraatstudenten Sara en Jens wil ik bedanken voor de gezelligheid en veel succes wensen! Caroline en Dries, jullie starten pas jullie doctoraat, maar ik ben er zeker van dat jullie dat heel goed gaan doen! Ook de mannen van Nutec Niels en Tom, merci voor de frieten en het gezever tussen lessen in!

Ik wil graag ook Han Goossens en Benny Luijsterburg van de Technische Universiteit Eindhoven bedanken voor de hulp in het 1ste jaar van mijn doctoraat.

Bedankt aan Laurens Delva en zijn collega's van de UGent voor de hulp bij de extrusie experimenten en zeker ook voor de gezellige sfeer!

I would really like to thank Prof. Philippe Dubois for welcoming me into the Materia Nova labs for preparation of my samples. A great deal of gratitude goes out to dr. Marius Murariu of Materia Nova. You were always ready to help me with the preparation of my samples. You showed a lot of interest in my work and always provided helpful insights. Our collaboration was a vital part of my research, I can't imagine my project coming to a successful ending without your help.

Tijdens mijn doctoraat heb ik ook een gedeelte lesopdracht uitgevoerd. Bedankt dus ook aan al mijn voormalige XIOS collega's voor de leuke samenwerking. Zeker dank ik ook mijn PXL collega's Vincent en Steven voor de vele "lunchmeetings" ☺.

Ook wil ik dank betuigen aan prof. Jan D'Haen en Bart Ruttens voor het uitvoeren van de TEM en XRD analyses en voor hun inzichten en kritische kijk! Ook bedankt aan Marc Jans voor het snijden van de TEM stalen!

Graag bedank ik ook alle leden van de jury voor het nalezen van mijn thesis.

Ik wil zeker ook nog mijn ouders bedanken voor mij altijd te steunen in mijn studies en keuze om te doctoreren. Samen met het hele gezin en Lieze kon ik altijd bij jullie terecht, al was het vooral om stoom af te blazen en te klagen ☺ Jullie konden me altijd terug opnieuw moed inpraten, wat er zeker toe geleid heeft dat ik zo ver geraakt ben.

TABLE OF CONTENTS

LIST OF SYMBOLS AND ABBREVIATIONS

$\bar{M}_n$	Number average molecular weight
$\bar{M}_w$	Weight average molecular weight
A	Sample surface area
Å	Ångström
AON	Aonilex X151A
ASTM	American Society for Testing and Materials
BN	Boron nitride
c	Penetrant gas concentration
CED	Cohesive energy density
CNWs	Cellulose nanowhiskers
D	Diffusion coefficient
d	Interlayer distance
d_{50}	Median diameter
$Đ_M$	Dispersity
DSC	Differential scanning calorimetry
E	Activation energy
EVOH	Poly(ethylene vinyl alcohol) copolymer
FFV	Fractional free volume
GPC	Gel permeation chromatography
ISO	Internation Standardisation Organisation
J	Diffusive flux
k_A	Avrami crystallization rate constant
k_J	Jeziorny modified crystallization rate constant
k_O	Ozawa crystallization rate constant
MAP	Modified atmosphere packaging
n_A	Avrami exponent
n_O	Ozawa exponent
OA	Orotic acid
OMMT	Organomodified montmorillonite clay
p	Pressure
P	Permeability

PA	Polyamide
PBAT	Poly(butylene adipate-co-terephthalate)
PBS	Poly(butylene succinate)
PCL	Polycaprolactone
PCO_2	Carbon dioxide permeability
PE	Polyethylene
PET	Poly(ethylene terephthalate)
PH_2O	Water vapor permeability
PHA	Polyhydroxyalkanoates
PHB	Poly(3-hydroxybutyrate)
PHBHHx	Poly(3-hydroxybutyrate-co-3-hydroxyhexanoate)
PHBV	Poly(3-hydroxybutyrate-co-3-hydroxyvalerate)
PLA	Poly(lactic acid)
PO_2	Oxygen permeability
POM	Polarization optical microscopy
PP	Polypropylene
Q	Amount of penetrant molecule passed during time t
R	Universal gas constant
RH	Relative humidity
S	Solubility
t	Time
T	Temperature
$t_{1/2}$	Crystallization half-time
$T_{c,o}$	Crystallization onset temperature
$T_{c,p}$	Crystallization peak temperature
$T_{cc,o}$	Cold crystallization onset temperature
$T_{cc,p}$	Cold crystallization peak temperature
$T_{d,50}$	Temperature of 50 % weight loss
$T_{d,o}$	Thermal degradation onset temperature
$T_{d,p}$	Temperature of highest weight loss rate
TEM	Transmission electron microscopy
T_g	Glass transition temperature
T_m	Melting temperature

$T_{m,o}$	Melting onset temperature
$T_{m,p}$	Melting peak temperature
wt%	Weight percent
$X_{r,t}$	Relative crystallinity
Y	opacity
β	DSC cooling rate
$\delta c/\delta x$	Concentration gradient in the x-direction
ΔH_c	Crystallization enthalpy
ΔH_{cond}	Molar heat of condensation
ΔH_{mix}	Partial molar heat of mixing
ΔH_s	Heat of sorption
ΔS_m	Entropy of melting
θ	Angle between incident beam and scattering planes
λ	Wavelength
Φ	Nucleation activity

NEDERLANDSE SAMENVATTING

Dit doctoraatsonderzoek omvat de karakterisering en modificatie van polyhydroxyalkanoaten (PHA) gericht op toepassing als voedingsverpakkingsmateriaal. Op basis van een uitgebreid literatuuronderzoek werden drie types PHA geselecteerd voor verder onderzoek, namelijk poly(3-hydroxybutyraat-co-3-hydroxyvaleraat) (PHBV), poly(3-hydroxybutyraat-co-3-hydroxyhexanoaat) (PHBHHx) en Aonilex (commercieel granulaat op basis van PHBHHx). Het eerste deel van het onderzoek omvatte de karakterisering en vergelijking van deze drie polymeren om hun belangrijkste positieve en negatieve eigenschappen in kaart te brengen. Verschillende modificatietechnieken, om de toepasbaarheid van deze materialen te verbeteren, werden vervolgens onderzocht.

De **vergelijking van de geselecteerde PHA** heeft tot verschillende interessante conclusies geleid. Het verwerkingsgebied van PHBV bleek beduidend smaller te zijn dan dat van PHBHHx en Aonilex, wat betekent dat PHBV meer thermische degradatie zal ondergaan tijdens verwerking in de smelt. Qua mechanische eigenschappen is PHBV veel rigider en brosser dan PHBHHx en Aonilex. De permeabiliteit van PHBHHx en Aonilex zijn vergelijkbaar. Beide materialen vertonen een middelmatige permeabiliteit voor O_2 en CO_2 en hun waterdamppermeabiliteit is vrij laag. Deze metingen konden niet uitgevoerd worden op PHBV omwille van de brosheid van het materiaal, maar literatuurgegevens geven aan dat de zuurstofpermeabiliteit van dit type PHBV 3 à 4 keer lager kan zijn in vergelijking met de waarden van PHBHHx en Aonilex. Zowel PHBV als PHBHHx vertoonden een trage kristallisatie, die plaatsgrijpt bij vrij lage temperaturen, wat een klassiek probleem is bij de meeste types PHA. Het commercieel granulaat Aonilex had een betere kristallisatie o.w.v. additieven die niet geïndentificeerd werden. De trage kristallisatie werd vooropgesteld als de belangrijkste beperking van de geselecteerde polymeren, naast de barrière eigenschappen die, ondanks beloftevol, nog steeds voor verbetering vatbaar zijn.

Het **verbeteren van de kristallisatiesnelheid van PHBV** werd gerealiseerd door het imengen van geselecteerde nucleatiemiddelen in de smelt. De performantie van het biologisch afbreekbare orootzuur als nucleatiemiddel werd vergeleken met het meer algemeen toegepaste boornitride. Boornitride verhoogde

de piektemperatuur van kristallisatie met 30 tot 36 °C. Orootzuur verbeterde de kristallisatie-eigenschappen van PHBV ook significant, hetzij minder dan boornitride. Het toevoegen van orootzuur verhoogde de piektemperatuur van kristallisatie met 18 tot 23 °C. Ondanks de duidelijk positieve resultaten met betrekking tot de kristallisatie van PHBV, werd besloten PHBV niet langer te weerhouden voor gebruik als verpakkingsmateriaal, omwille van de inherente brosheid in vergelijking met PHBHHx en Aonilex.

Ter verbetering van de kristallisatie van PHBHHx, werd **ultrafijn talk als nucleatiemiddel** onderzocht. Talk is een bewezen nucleatiemiddel voor andere polymeren en door het verlagen van de deeltjesgrootte (≤ 1 µm) is het mogelijk om betere resultaten te bekomen met lagere concentraties. Een isotherme en niet-isotherme kristallisatiestudie toonde aan dat ultrafijn talk een zeer performant nucleatiemiddel is voor PHBHHx bij concentraties van 0,5 tot 2 m%. De halfwaardetijd voor niet-isotherme kristallisatie bij 70 °C werd verminderd met 97 % ten gevolge van het toevoegen van 2 m% ultra-fijn talk, waardoor de kristallisatiepiek smaller werd, wat duidt op snellere kristallisatie. De gaspermeabiliteit nam toe bij concentraties tot 0.5 m% en vervolgens een afname bij hogere ultra-fijn talk concentraties. Dit werd verklaard door de vorming van kleinere kristallen in aanwezigheid van de talkdeeltjes, waardoor een minder omvangrijk "doolhof" voor gasdiffusie werd gecreëerd. Door de concentratie aan ondoordringbare talkdeeltjes verder te verhogen, werd het "doolhof" opnieuw complexer. Dit laatste fenomeen kwam pas tot uiting bij concentraties hoger dan 0,5 m%. Het toevoegen van 2 m% ultra-fijn talk resulteerde in een 5 % reductie van de zuurstof- en waterdamppermeabiliteit. De elasticiteitsmodulus nam in beperkte mate toe met 13 %, terwijl de breukrek en treksterkte quasi constant bleven.

Een eerste modificatie ter verbetering van de barrière-eigenschappen van PHBHHx en Aonilex was het bereiden van **organisch gemodificeerd montmorilloniet (OMMT) nanocomposieten**. Wat betreft gaspermeabiliteit, was de combinatie Aonilex met 10 m% OMMT het meest performant en werden de zuurstof-, koolstofdioxide- en waterdamppermeabiliteit verlaagd met respectievelijk 47 %, 42 % en 37 %. Dit effect werd toegewezen aan een complexer "doolhof", ten gevolge van de plaatjesvormige structuur van OMMT. Het gebruik van hoge

concentraties OMMT resulteerde jammer genoeg in broze nanocomposieten, met een 44 % lagere breukrek. Andere geobserveerde nadelen zijn extra thermische degradatie tijdens verwerking en verlaagde kristallisatiesnelheden. Dit laatste nadeel kon voor een groot deel gecompenseerd worden door het gebruik van Aonilex in plaats van PHBHHx. Rekening houdend met alle eigenschappen van de OMMT nanocomposieten, kon geconcludeerd worden dat een OMMT concentratie van 3 m% een beloftevol compromis kan bieden tussen verbeterde barrière-eigenschappen en een aanvaardbare hoeveelheid verminderde kristallisatie en thermische stabiliteit. Verder onderzoek is echter noodzakelijk.

Een andere aanpak omvatte het bereiden van **zinkoxide nanocomposieten**. Omwille van beloftevolle literatuurgegevens voor andere polymere systemen, werd geopteerd voor zinkoxide nanostaafjes. Twee types zinkoxide nanostaafjes werden geselecteerd en toegepast, namelijk niet-gemodificeerd (ZnO) en zinkoxide met gemodificeerd oppervlak (sZnO). Een preliminaire studie toonde aan dat geen van beide types een uitgesproken effect heeft op de kristallisatie van PHBHHx. Daarom werd de rest van de studie uitgevoerd op Aonilex, o.w.v. de betere kristallisatie-eigenschappen. TEM analyses toonden aan dat het niet mogelijk was fijne dispersies van ZnO in Aonilex te bekomen bij concentraties hoger dan 1 m%, dit terwijl er geen dispersieproblemen vastgesteld werden voor sZnO bij elke geteste concentratie. Het toevoegen van 5 m% sZnO bleek geen significante veranderingen in gaspermeabiliteit te vooroorzaken. De elasticiteitsmodulus nam licht toe met 7 %, terwijl de breukrek verlaagd werd met 19 %. Een belangrijk nadeel van hogere ZnO of sZnO was de hogere opaciteit, welke toenam van 11.5 % tot 37.7 % na toevoegen van 5 m% sZnO. Een belangrijke nieuwe eigenschap die geïntroduceerd werd is het blokkeren van UV stralen met een golflengte kleiner dan 370 nm, wat reeds vastgesteld werd bij sZnO concentraties van 1 m%, wat een toegevoegde waarde kan betekenen voor voedingsverpakkingsmaterialen.

Algemeen toonde dit doctoraatsonderzoek aan dat PHBHHx potentieel toont voor gebruik als voedingsverpakkingsmateriaal. Ondanks dat de geselecteerde modificaties het niet mogelijk maakten om een goed barrièremateriaal te produceren, blijft het polymeer PHBHHx nog steeds beloftevol voor gebruik als verpakkingsmateriaal. Een succesvol implementatie van PHBHHx kan gerealiseerd

worden door de negatieve eigenschappen te verbeteren, namelijk de kristallisatiesnelheid verhogen m.b.v. ultra-fijn talc als nucleatiemiddel. De reeds aanwezig positieve eigenschappen van PHBHHx moeten op correcte wijze aangewend worden. Zo bezit PHBHHx bijvoorbeeld reeds een vrij goede waterdampbarrière en kan dus gebruikt worden als bescherming voor vochtgevoelige zuurstofbarrièrelagen. Succesvolle UV bescherming kan vrij evident gerealiseerd worden door toevoegen van lage concentraties zinkoxide (1 g%) van het materiaal. Het toevoegen van zinkoxide op dit concentratieniveau kan ook een snelle kristallisatie induceren waardoor een vochtgevoelige zuurstofbarrièrelaag (zoals EVOH) beschermd kan worden door een buitenlaag van een multilaag voedingsverpakkingsmateriaal.

ENGLISH SUMMARY

This doctoral research involves the characterization and modification of polyhydroxyalkanoates (PHA) for application as food packaging material. After an extensive literature review, three PHA were selected, namely poly(3-hydroxybutyrate-co-3-hydroxyvalerate) (PHBV), poly(3-hydroxybutyrate-co-3-hydroxyhexanoate) (PHBHHx) and Aonilex (a commercial PHBHHx granulate). The first part of the research involved the effective characterization and comparison of these three PHA and pinpointing the major positive and negative properties. Several types of modification techniques were investigated in order to enhance the applicability of these materials.

The **comparison of selected PHA** led to several interesting conclusions. The processing window of PHBV is much narrower than that of PHBHHx and Aonilex, implying PHBV will suffer more thermal degradation during melt processing. PHBV is much stiffer and more brittle than the ductile materials PHBHHx and Aonilex. The permeability properties of PHBHHx and Aonilex were similar, presenting a moderate barrier for O_2 and CO_2 and fairly low water vapor permeability. These measurements could not be performed on PHBV due to its brittleness, but literature data suggests that the oxygen permeability coefficient of this type of PHBV is about 3-4 times lower than that of PHBHHx and Aonilex. Both PHBV and PHBHHx display slow crystallization at low temperatures, which is a common issue for most PHA. The commercial granulate Aonilex performs better due to undisclosed additives. The slow crystallization rate was identified as the main limitation of the selected polymers, as well as the permeability properties which, even though promising, must be enhanced further for application as food packaging material.

In order to **enhance the crystallization rate of PHBV**, selected nucleating agents were tested. The biodegradable orotic acid was compared to the more conventional boron nitride in terms of efficiency as a nucleating agent for PHBV. Boron nitride increased the crystallization peak temperature with 30 to 36 °C. Orotic acid improved the crystallization properties of PHBV as well, but it was not as performant as boron nitride, raising crystallization peak temperatures with 18 to 23 °C. Even though positive results were obtained regarding enhancement of

PHBV crystallization, it was decided to no longer continue with PHBV as base material, due to its inherent brittleness in comparison to PHBHHx and Aonilex.

In order to enhance crystallization, the effect of **ultra-fine talc as a possible nucleating agent for PHBHHx** was investigated. Talc has been proven to be an excellent nucleating agent for other polymers and by reducing its particle size to ≤ 1 µm it is possible to obtain better results at lower concentrations. An isothermal and non-isothermal crystallization study showed that ultra-fine talc was a highly performant nucleating agent for PHBHHx, in tested concentrations of 0.5, 1 and 2 wt%. The non-isothermal crystallization half-time at 70 °C was reduced by 97 % by adding 2 wt% ultra-fine talc, changing the appearance of the crystallization peak from broad to narrow. The gas permeability coefficients showed an increasing trend at concentrations up to 0.5 wt% and then a decrease at higher ultra-fine talc concentrations. This was explained by the formation of smaller crystallites in the presence of ultra-fine talc particles, leading to a less elaborate tortuous path. However, by increasing the amount of impermeable ultra-fine talc particles, the tortuous path was enhanced again, a phenomenon which became noticeable at concentrations higher than 0.5 wt%. As a result, the addition of 2 wt% ultra-fine talc reduced oxygen and water vapor permeability coefficients with 5 %. Young's modulus increased with a maximum of 13 %, whereas the other tensile properties remained fairly constant.

In an effort to enhance the barrier properties of PHBHHx and Aonilex, **organomodified montmorillonite (OMMT) nanocomposites** were prepared. In terms of gas permeability properties, the Aonilex sample containing 10 wt% OMMT was most performant, with O_2, CO_2 and water vapor permeability coefficient reduced by 47 %, 42 % and 37 %, respectively. This effect is attributed to the increased tortuous path, due to the platelet structure of OMMT. Unfortunately, using a concentration this high renders the nanocomposite increasingly brittle, with the elongation at break reduced by 44 %. Other drawbacks were observed as well, such as extra thermal degradation during processing and reduced crystallization rates. The latter could be counteracted for a large part by using Aonilex instead of PHBHHx. Upon taking into account all properties, it can be concluded that an OMMT concentration of 3 wt% could be a promising compromise between enhanced barrier properties (about 20 % reduction) and a minor

reduction of crystallization rate and thermal stability, though further research is necessary.

A different approach involved **the preparation of zinc oxide nanocomposites**. Zinc oxide with a nanorod structure was chosen, based on promising literature data for other polymeric matrices. Two types of zinc oxide nanorods were used, unmodified (ZnO) and surface modified (sZnO). A preliminary screening showed that neither type presents a significant effect on PHBHHx crystallization. Therefore, the study involving zinc oxide was continued with Aonilex, due to its better crystallization properties. A TEM study revealed that it was not possible to obtain fine dispersions of ZnO using concentrations higher than 1 wt%, whereas there were no dispersion issues for sZnO at all tested concentrations. The addition of up to 5 wt% sZnO did not appear to present any significant changes gas permeability. The Young's modulus was increased by only 7 %, whereas the elongation at break was reduced by 19 %. An important downside of higher ZnO or sZnO concentrations is the higher opacity, which increased from 11.5 to 37.7 % upon addition of 5 wt% sZnO It is however important to note that the addition of only 1 wt% provided a novel UV shielding property, of wavelengths below 370 nm, to Aonilex, which could prove to be a valuable feature for food packaging materials as well.

Overall, this doctoral study revealed that these grades of PHBHHx certainly show promise for use as food packaging material. Despite the fact that the selected modifications did not make it possible to obtain a high barrier material, PHBHHx still shows a great deal of promise for use as a food packaging material. A successful implementation of PHBHHx could be realized by enhancing the negative properties, namely increasing the crystallization rate using ultra-fine talc as nucleating agent. The intrinsic positive properties of PHBHHx should be correctly taken advantage of. PHBHHx is a fairly good water vapor barrier and could thus be used as protection layer for moisture-sensitive oxygen barrier layers, for example. A successful UV blocking can be realized through the addition of low amounts of zinc oxide (1 wt%), as an added functionality of the material. The addition of zinc oxide in this concentration range can result in a fast crystallizing material, which can also protect a moisture-sensitive barrier layer (e.g. EVOH) in a multilayer film.

Chapter 1.

INTRODUCTION, STATE OF THE ART AND SCOPE OF THE RESEARCH

In this chapter, an introduction into bioplastics and packaging, polyhydroxyalkanoates and polyhydroxyalkanoate modifications is given. A state-of-the-art is provided, followed by a clear definition of the scope of the research. A brief overview of the dissertation is finally included.

1.1 INTRODUCTION

1.1.1 The plastics industry and sustainability

The plastics industry is of great importance for the global European industry, employing over 1.45 million people and yielding a turnover of 320 billion euro and a yearly production of 57 Mton in Europe and 299 Mton worldwide in 2013. The lion's share of this production (39.6 %) is directed towards the packaging industry, followed by building and construction (20.3 %) [1].

The plastics industry is still highly dependent on the availability of fossil resources for the production of polymers. About 4 % of the world's oil production is employed for this purpose only. As the oil supplies diminish, costs and prices will escalate. Thus the exploration of alternative resources for plastics production is of high interest for the plastics industry.

Plastics produced from natural resources could prove to be a valid and sustainable alternative. It is in this context that the so-called 'bioplastics' come into play. The term bioplastics is however often confusing and misleading.

To provide clear insight into the meaning of the term 'bioplastics' one must firstly make a distinction between biobased and biodegradable [2]:

- The term 'biobased' means that a material or product is entirely or for a large part derived from biomass (e.g. corn, sugarcane, cellulose and agricultural by-products)
- The term 'biodegradable' infers that a material is capable of undergoing a biological decomposition into substances such as water, carbon dioxide, methane etc. by micro-organisms available in the environment. As a result biodegradation takes place, without the use of artificial additives. The substances produced through biodegradation are dependent on oxygen availability, types of micro-organism, temperature etc.

With this difference clarified, it is possible to clearly categorize plastics in general, based on whether they are biodegradable or not and biobased or not. This is demonstrated in Figure 1-1. **Conventional plastics**, such as polyethylene (PE) and polypropylene (PP) are non-biodegradable as well as non-biobased. However, there are some **synthetic non-biobased polymers** in existence that are also susceptible to biodegradation, such as polycaprolactone (PCL) and poly(butylene adipate-co-terephthalate) (PBAT). The latter can be considered as bioplastics as well, however only in the broadest sense of the definition. A third category are the **biobased, non-biodegradable polymers**. Typical for these materials is that the produced polymer is identical to existing synthetic ones, but the fossil resources have been replaced by natural ones, for example polyethylene produced from ethanol obtained through biomass fermentation. A final category is set for polymers that are **biobased as well as biodegradable**, such as polyhydroxyalkanoates (PHA), poly(lactic acid) (PLA), poly(butylene succinate) (PBS) and starch blends.

In 2013, a worldwide total of 1.62 Mton of bioplastics was produced. This production is predicted to rise to about 6.73 Mton by the year 2018, indicating it is a vastly growing market [3]. In comparison to conventional plastics (299 Mton), this is still only a minor fraction. However, one must consider that global production capacity of bioplastics is not yet at the same scale as conventional plastics.

The focus of the dissertation at hand lies on the category of biobased and biodegradable plastics, more specifically polyhydroxyalkanoates. PHA are promising polymers, that show an added advantage over PLA, a different biopolymer within the same category. PHA are a family of polymers that are polymerized and accumulated intracellularly by a broad range of bacteria and are subsequently extracted for further use [4-7]. PLA on the other hand, is chemically polymerized from monomers produced by fermentation of biomass by micro-organisms [8], which means it requires an extra process step. PHA are discussed in further detail in the next paragraph.

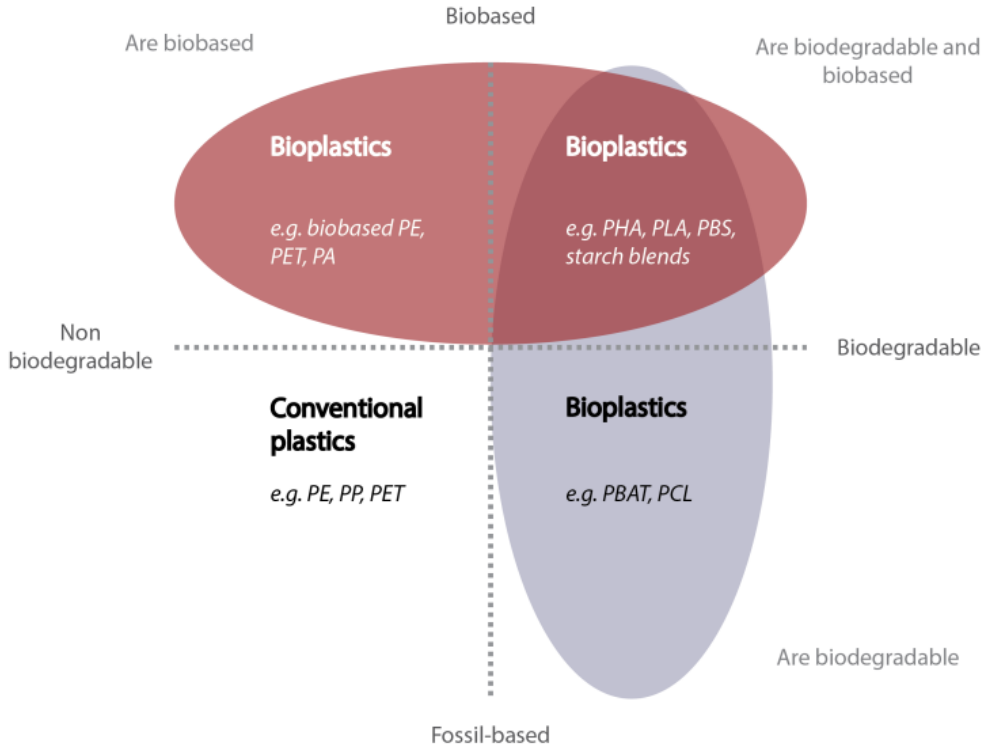

Figure 1-1: Classification of plastics (adapted from [9])

1.2 FOOD PACKAGING – A BRIEF INTRODUCTION

1.2.1 The role of food packaging

The packaging industry is the third largest industry in the world (US$ 420 billion), of which food packaging specifically is a major business sector [10]. Three basic functions of a food packaging can be defined as [11-13]:

- Containment:
  Obviously, containing the food product is the most basic function. The requirement for containment depends on size, weight, nature and shape of the enclosed food product. The containment function is closely related to the mechanical properties of the packaging.
- Protection and preservation:
  It is necessary that the packaging protects the food from mechanical damage during handling as well as deterioration caused by environmental parameters during storage and distribution. The protection and preservation function will be explained later on in this paragraph.
- Information:
  The package must communicate with the consumer and provide information regarding branding, ingredients, nutritional information etc.

Some secondary functions for a food packaging are, but not limited to:

- Traceability [11]:
  Traceability can be defined as 'the ability to follow the movement of a food through specified stage(s) of production, processing and distribution'. Food manufacturers incorporate unique codes into the packaging label, so it is possible to track the product throughout the distribution process.
- Convenience [11-13]:
  Packaging convenience has become quite an important feature in order to satisfy the consumers lifestyle. Some examples of convenience features are resealability, microwavability and ease of access and handling.
- Tamper indication [11]:
  To reduce the risk of tampering with packaged products, special features have been introduced into the packaging. Some tamper indicative features are breakaway closures, special membranes, banding etc.

However, it must be stated that in the last few years novel packaging materials have been developed that exceed these rather basic packaging demands, these are the so-called active and intelligent packaging systems. Active packaging systems contain certain components (e.g. moisture absorbers, CO_2 emitters) that release or absorb substances from or into the packed foodstuffs or the ambient environment in order to prolong shelf life and maintain the quality, safety and sensory characteristics of the food. An intelligent packaging system can provide additional information (when compared to conventional packaging systems) regarding the history of the product (e.g. storage conditions, headspace composition, microbial growth) throughout the whole food chain. The intelligent function can be obtained using indicators, sensors and/or devices able to communicate information about the packaging system. These indicators inform about a change that has occurred in the packaged product or its environment (e.g. temperature and pH) by means of visual changes [14]

Within this study, the focus lies on the protection and preservation function of the food packaging.

1.2.2 Protection and preservation

When dealing with food packaging technology, one must look for packaging systems which maintain or enhance shelf life of food. The goal is to retain the quality of a food product as much as possible during the time period between release and time of use.

When discussing food protection we can discern three types of protection. The first being physical protection, i.e. shielding food from mechanical damage during transportation, distribution and consumer use [11]. It is here that the mechanical properties of the polymer used for packaging plays a critical role.

Biological protection is also of importance, as the packaging must act as a barrier against microorganisms (pathogens and spoiling agents), insects and rodents in order to prevent disease and spoilage [11].

Finally, one can also discern chemical protection, which is necessary in order to minimalize compositional changes, triggered by environmental factors [11]. It is important to stress that the packaging objective is often to slow down specific deterioration reactions rather than reducing the reaction rates to zero [15].

A few environmental factors of great importance are:

1) Exposure of the food product to gases:

   A food product can undergo compositional changes upon exposure to certain gases, of which oxygen and water vapor are the most important for certain food products. Packaging is used to exclude, control or retain gases at a level most suited for the food product in order to maximize shelf life. Foods differ greatly in sensitivity to oxygen as well as the resulting impact on its properties. Oxidative degradation of certain compounds (e.g. unsaturated fats, vitamins etc.) can lead to color and flavor change, rancidity, loss of nutritional values etc. [16]. Atmospheric O_2 generally can have a detrimental effect, therefore it is desirable to maintain many types of foods at a low O_2 tension, or at least prevent a continuous supply of O_2 into the package. Material characteristics will therefore play an important role for this specific parameter [13]. From a different point of view, it is possible to deliberately create a specific gaseous atmosphere inside the packaging (modified atmosphere packaging (MAP)), for example a CO_2 atmosphere to retard microbial growth [13]. Water vapor interactions (loss or gain) is of course highly important as well. A change in relative humidity inside the packaging, due to permeation into or out of the packaging, can have dramatic effects on the properties of the food product, especially related with its mechanical properties (for example crispness) and water activity [13, 16].

2) Exposure to light:

   When food products are exposed to light, more specifically in the UV and lower visible part of the electromagnetic spectrum, many deteriorative reactions can be initiated or accelerated. It is known that vitamins A, B2, B6, B12 and folic acid are particularly susceptible to photo-induced degradation, which can result in flavor and color changes. The severity of the degradation is dependent on light intensity and length of exposure. Sources of light are of course natural light, as well as synthetic light from, for example, display cabinets. The incorporation of light absorbers (e.g. pigments) in packaging is well known for plenty of packaging materials [13, 16].

The focus of this study lies for the major part on reducing the exposure of the food product to gases, through enhancement of the material barrier properties against selected target gases O_2, CO_2 and water vapor. However, UV protection properties are characterized as well.

1.3 POLYMER PERMEABILITY

The reduction of gas permeability through the packaging films is one of the key parameters investigated in this study. Reduction of oxygen permeability is of high importance to reduce oxidation of packaged food stuffs, though carbon dioxide and water vapor are important to consider as well. In Table 1-1, some permeability requirements for packaging of selected food stuffs is given. A low oxygen permeability is considered to be ≤ 1 $cm^3.mm/(m^2.day.atm)$.

Table 1-1: Permeability requirements for packaging of selected food stuffs [17]

Food	Preservation time/temp.	O_2 permeability	CO_2 permeability	H_2O permeability
Red meat	6 – 14 d 0 – 5 °C	Low	Low	Low
Other meat	1 d – 6 w 0 – 5 °C	Low	Low	Low
Fish	1 – 7 d 0 – 5 °C	Low	Low	High
Fermented milk	16 – 18 d 2 – 5 °C	Low	Low	Low
Fresh pasta	4 w 2 – 5 °C	Low	Low	Low
Dried Pasta	4 w Room temp.	/	/	Low
Breakfast Cereals	1 yr Room temp.	High	High	Low
Fresh Produce	1 – 7 d 0 – 5 °C	High	High	Low

Gas permeability can be interpreted as the overall gas transport phenomenon throughout the polymer membrane. This transport can be subdivided in several steps, as illustrated in Figure 1-2 [18, 19]:

1) Sorption (ab- or ad-) of the gas by the polymer at the higher partial pressure side (by chemical affinity or by solubility)
2) Diffusion of the absorbed gas molecules (penetrant) inside the polymer membrane
3) Desorption of the diffused gas molecules at the lower partial pressure side

Events occurring within the polymer are described first, with **diffusion** being the dominant factor. The quantity of penetrant molecule, passing the polymer membrane during one unit of time and by unit of area, is the diffusive flux J [20]:

$$J = Q/A.t \qquad (1\text{-}1)$$

With t the time, A the sample surface area and Q the amount of penetrant molecule passed through the polymer membrane during time t.

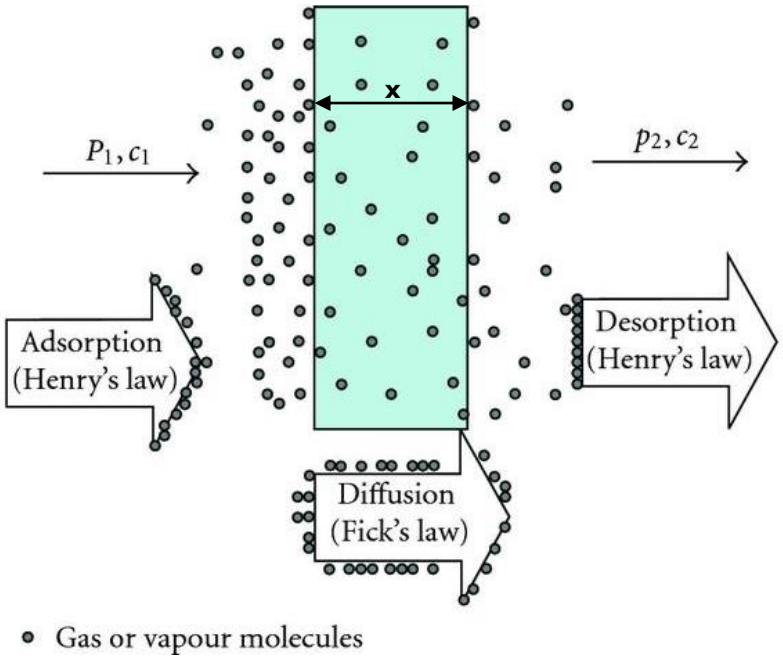

Figure 1-2: Permeation of penetrant molecules through polymers [21]

Fick's first law is applicable in steady state conditions (when diffusion equilibrium is reached). For unidirectional diffusion in the x-direction, the diffusive flux can be defined as [20]:

$$J_x = -D\frac{\delta c}{\delta x} \approx D\frac{(c_1-c_2)}{x} \quad (1\text{-}2)$$

With D the diffusion coefficient and $\delta c/\delta x$ the concentration gradient in the x-direction. This equation can be considered as correct when the value of the thickness (x-direction) is much smaller than other dimensional parameters (i.e. diameter of the tested sample area) [18].

In non-steady state, diffusion can be expressed by following Fick's second law, simplified for diffusion solely in the x-direction [18]:

$$\frac{\delta c}{\delta t} = D\left(\frac{\delta^2 c}{\delta x^2}\right) \quad (1\text{-}3)$$

Before the penetrant molecules can diffuse through the packaging, due to the partial pressure difference at both sides of the polymer membrane, they must first dissolve into the polymer. This phenomenon is characterized by the **solubility** of the penetrant gas. The local concentration c of the penetrant gas dissolved into the polymer surface can be related to the pressure using Henry's law: [22]

$$c = S.p \quad (1\text{-}4)$$

Where S is the solubility coefficient (which can be function of c or p) and p the partial pressure of the penetrant gas at the high concentration side.

Substitution of equation 1-4 into equation 1-2 yields:

$$J_x = \frac{Q}{At} = DS\,\frac{(p_1-p_2)}{x} \quad (1\text{-}5)$$

Upon understanding the previous two phenomena, it is possible to define a comprising parameter, namely the **permeability**. The permeability coefficient P can be defined as the product of the solubility coefficient S and diffusion coefficient D by reworking equation 5 into:

$$P = DS = \frac{Qx}{At(p_1-p_2)} \quad (1\text{-}6)$$

A number of factors influencing these mass transport properties can be identified and have been subdivided in three categories.

1.3.1 Extrinsic parameters

Extrinsic parameters are related to the nature of the ambient environment. Firstly, the effect of the **ambient temperature** T is elaborated [18, 23]. At temperatures sufficiently different from glass transition and melting point, permeability and diffusion can be described using an Arrhenius type equation:

$$P = P_0 \, e^{-E_P/RT} \tag{1-7}$$

$$D = D_0 e^{-E_D/RT} \tag{1-8}$$

With E_P and E_D activation energies for permeation and diffusion, P_0 and D_0 pre-exponential factors and R the universal gas constant.

The effect of temperature on solubility is often expressed by a Van't Hoff equation:

$$S = S_0 e^{-\Delta H_S/RT} \tag{1-9}$$

With S_0 a pre-exponential factor and ΔH_s the heat of sorption of penetrant in the polymer.

The activation energy of permeation can be described as the sum of activation energy for diffusion and heat of sorption of penetrant in polymer:

$$E_P = E_D + \Delta H_S \tag{1-10}$$

E_D is always a positive value as polymer chain mobility increases at higher temperature, thus facilitating penetrant diffusion.

The heat of sorption can be elaborated further:

$$\Delta H_S = \Delta H_{cond} + \Delta H_{mix} \tag{1-11}$$

With:

- ΔH_{cond} the molar heat of condensation, which is always negative and relatively small for permanent gases
- ΔH_{mix} the partial molar heat of mixing, a small and positive value

For permanent gases well above their critical point (e.g. O_2, N_2 at room temperature) the value of ΔH_{cond} will be very small, resulting in a ΔH_S mainly influenced by ΔH_{mix}. Thus, as the interactions are negligible, ΔH_S will be positive, resulting in an increase in S upon increasing the temperature T in equation (1-9) [18, 20].

When regarding more readily condensable gases and vapors (e.g. CO_2, H_2O, SO_2, NH_3, hydrocarbons), ΔH_S is often negative, due to the stronger contribution of ΔH_{cond} [18, 20]. If a negative value for ΔH_S is obtained, increasing the temperature T in equation (1-9) will result in lower S, indicative of the vapors experiencing more difficulty to condensate into the polymer at elevated temperatures.

The second extrinsic parameter of importance is the **relative humidity** (RH). Depending on the polarity of the polymer at hand, RH can have a severe deteriorative effect on polymer permeability properties. Highly apolar polymers will only experience very minor or even no changes in permeability [23], whereas more polar polymers (e.g. polyesters, ethylene vinyl alcohol, cellulose) will display much larger increases. The water vapor molecules that enter the polymer membrane can act as a plasticizing agent, resulting in an increase in polymer free volume and thus facilitating a higher oxygen permeability [24]. However, some specific cases have shown anomalous behavior. At low to moderate RH, amorphous polyamides and PET show a slight improvement in barrier properties with increasing RH. The proposed underlying mechanism is that the water molecules are not swelling the polymer, but are actually occupying some of the polymer free-volume sites instead, resulting in the reduction in permeability [23].

1.3.2 Intrinsic parameters

The first of the intrinsic properties, which are related to the nature of the polymer, is the **polymer free volume**. Polymer free volume can be interpreted as the microcavities of lower density present in a polymeric material. The permeant makes use of these cavities (transient or permanent) to diffuse through the polymer matrix, resulting in a high dependence of transport properties on the number and size of these microcavities [25, 26].

It is useful to define the term fractional free volume (FFV) as the fraction of volume in a polymer that is available to assist in permeant transport and does not include

volume occupied by polymer molecules and the volume in the polymer matrix that is otherwise unavailable for permeant transport [23].

FFV as well as the size of these microcavities are highly dependent on the cohesive energy between the macromolecules that are comprised within the polymeric membrane. One can define the cohesive energy of a substance in a condensed state as the increase in internal energy per mole of substance if all the intermolecular forces were to be eliminated [25]. The cohesive energy density (CED) is the amount of cohesive energy per unit of volume and can be used to explain the effect on permeability. High barrier polymers, such as poly(ethylene vinyl alcohol) copolymer (EVOH), are rather permeable structures but with a very high cohesive energy density (e.g. due to intermolecular bonding) and very low fractional free volume. Polymers like polyethylene on the other hand, which display much lower intermolecular cohesion and thus larger fractional free volume, possess much lower gas barrier properties [25].

A second intrinsic property is the **crystallinity** of the polymeric system. A large amount of polymers can be considered as a biphasic system, consisting of a structurally ordered crystalline phase, on one hand, and an amorphous glassy phase on the other hand. In general, one can state that increasing the crystalline fraction will decrease gas permeability [18, 23]. The crystallites, which are more dense and ordered than the amorphous zones, act as excluded volumes for the sorption process, thus reducing solubility, and can be considered as impermeable barriers for the diffusion process [18, 20, 23]. The effect of crystallites on diffusion is twofold. On one hand, they increase the effective path length of diffusion, and, on the other hand, they can reduce polymer chain mobility in the amorphous phase, due to the chain ends being trapped in neighboring crystallites, leading to an increase in E_D, and thus a decrease in permeability [18].

Closely linked to the crystallinity, is the effect of **chain orientation** on permeability. Polymer chain orientation can be induced via drawing/stretching or processing. In general, orientation will enhance the barrier properties of the polymer in a threefold manner: 1) additional orientation-induced crystallization, 2) fractionation and orientation of the existing crystallites perpendicular to permeant transport and 3) densification of the amorphous zone resulting in a reduced FFV [18, 25].

Finally, upon comparison of different types of polymers, it is the **chemical nature** of these macromolecules that also plays a highly important role. However, it is very difficult to find a distinct correlation between the nature of the polymer and its permeability, due to the fact that it is impossible to change one chemical feature of a polymer, without causing a cascade of other changes (e.g. glass transition, density, crystallinity). Nevertheless, some tendencies can be observed. For example, by varying the pendant group alongside a polymer chain, great differences in permeability can be obtained, as demonstrated in Table 1-2.

A final intrinsic parameter to be considered is the **polymer molecular architecture**. For example the introduction of branches or side groups via co-polymerization can significantly change permeability. High density polyethylene (HDPE), which is linear, has better barrier properties than its branched counterparts linear low density polyethylene (LLDPE) and low density polyethylene (LDPE). The homogeneity of the incorporated branches on the polymer backbone can also have an impact on permeability.The stereoisomerism or tacticity of the polymer can be of influence as well [25]. For example, poly(methyl methacrylate) is less permeable in its isotactic form than in its syndiotactic form, due to a denser structure and tighter stacking in the former configuration [27].

Table 1-2: Relative oxygen permeability of polymer materials based on the repetition of CH_2-CHX [25]

Polymer	Pending X unit	Relative O_2 permeability
Polyvinylalcohol	-OH	1
Polyacrylonitrile	-CN	4
Polyvinylchloride	-Cl	800
Polypropylene	$-CH_3$	15000
Polystyrene	$-C_6H_5$	42000
Polyethylene	-H	48000

1.3.3 Factors relating to the nature of the permeant

Several permeant characteristics can influence its transport properties throughout a polymer membrane, with a first one being the **shape** of the permeating molecule. For example, flattened or elongated molecules display higher diffusion coefficients than spherical molecules of similar molecular volume [25, 28].

Molecular size of the permeant also plays a crucial role. For example, it has been found that increasing the molecular size in homologous series of permeants (e.g. alkanes, esters, aldehydes or alcohols) generally causes a reduction in diffusion coefficient, due to steric reasons. The diffusion coefficient on the other hand is usually adversely influenced upon increasing molecular size of the permeant. For the light gases (e.g. He, H_2, N_2, CO_2, O_2), the kinetic diameter, which is the smallest effective dimension of a given molecule, can be used as a good measure for ease of diffusion [26]. Molecules with larger kinetic diameters will have more difficulty diffusing throughout the free volume of the polymer. When regarding solubility, one can state that the ease of sorption is almost directly proportional to properties such as boiling point and critical temperature of the gases and vapors, but only if there are no strong polymer-permeant interactions at play [18, 25]. If a molecule can condensate easier, than its solubility will increase.

Finally, the **chemical nature** of the permeant plays an important role as well. In some cases (most obvious water vapor in polymers with polar functionalities) a high affinity between permeant and polymer can lead to the replacement of initial hydrogen bonding and van der Waals forces (between adjacent polymer chains) with polymer-permeant interactions. This in turn can lead to increasing free volume and thus an increase in diffusion and solubility coefficients [25].

1.3.4 The effect of inorganic fillers

The addition of inorganic impermeable fillers, such as layered silicates, can drastically alter the permeability properties of a polymer through the formation of a so-called "tortuous path", which hinders diffusion of permeant molecules [29-31]. The layered silicates can essentially be considered as impermeable inorganic platelets. Gas molecules must diffuse around them, rather than taking a (mean) straight path perpendicular to the film surface. The diffusing molecules must follow a longer mean path length throughout the film, which is illustrated in Figure 1-3.

The simplest model to describe the effect of clay nanoparticles on gas permeability was proposed by Nielsen and assumes that the filler is evenly dispersed throughout the matrix and takes the shape of rectangular platelets of uniform size.

The Nielsen model also assumes that the increased tortuosity is the only factor influencing the gas diffusion rate, resulting in following relation: [32]

$$\frac{P_{composite}}{P_{polymer}} = \frac{1-\Phi}{1+\frac{a}{2}\Phi} \tag{1-12}$$

With $P_{composite}$ the permeability coefficient of the composite material, $P_{polymer}$ the permeability coefficient of the pristine polymer, Φ the filler volume fraction and a the aspect ratio, which is the ratio of length of the clay platelet to its width. In practice, this model is valid only for small filler loading (less than 10 %). Higher loading will result in particle agglomeration and thus reduction of the mean particle aspect ratio [30].

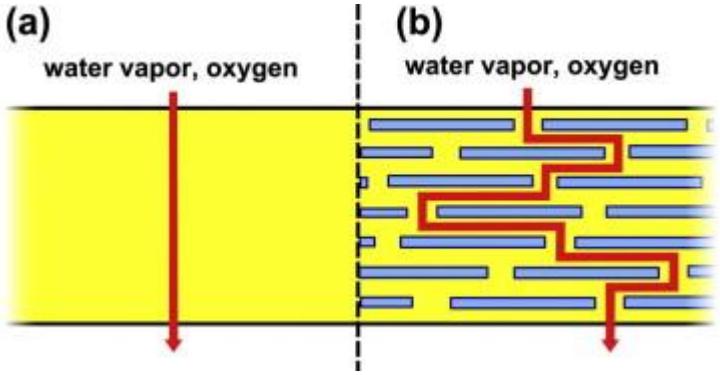

Figure 1-3: Illustration of mean path length in a) pristine polymer and b) layered silicate nanocomposite with tortuous path effect [30]

1.4 POLYHYDROXYALKANOATES

PHA are a family of (co-)polyesters of various hydroxyalkanoates, synthesized by numerous Gram negative (*Pseudomonas*, *Azotobacter* etc.) and positive bacteria (*Bacillus*, *Streptomyces* etc.) [4-7]. A general structure for PHA is given in Figure 1-4. The main monomer is usually 3-hydroxybutyrate with minor amounts of 3-hydroxyvalerate, 3-hydroxyhexanoate or 4-hydroxybutyrate.

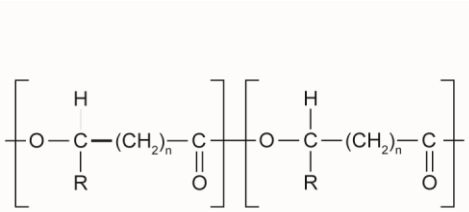

	R group	Monomer type
n = 1	hydrogen	3-hydroxypropionate
	methyl	3-hydroxybutyrate
	ethyl	3-hydroxyvalerate
	propyl	3-hydroxyhexanoate
	pentyl	3-hydroxyoctanoate
	nonyl	3-hydroxydodecanoate
n = 2	hydrogen	4-hydroxybutyrate
n = 3	hydrogen	5-hydroxyvalerate

Figure 1-4: General structure of PHA (adapted and modified from [5])

The homopolymer poly(3-hydroxybutyrate) (PHB) was first discovered in 1926 as discrete inclusions (diameter of 0.2 to 0.5 µm) inside the cell cytoplasm of *Bacillus megaterium*, in concentrations reaching up to 90 % of the dry cell weight [4, 6, 7, 33]. A transmission electron microscopy image of this type of cell is given in Figure 1-5. The PHA stored inside the cell function as a carbon- and energy-reserve when a limited amount of nutrients is available [4].

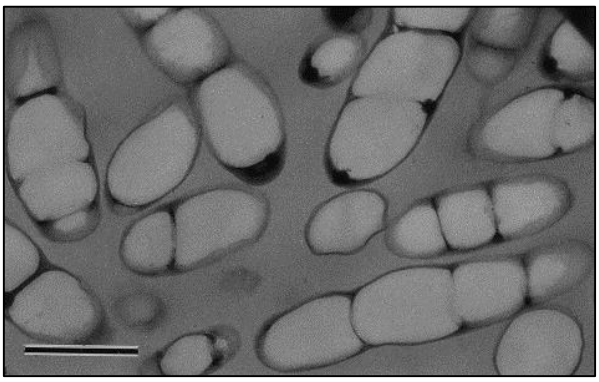

Figure 1-5: Transmission electron micrograph of recombinant *Ralstonia eutropha* PHB$^-$4 cells containing large amounts of PHBHHx. Bar represents 0.5 µm (adapted from [7])

Historically, PHB has been studied most extensively, as it was the first PHA to be discovered, and triggered a commercial interest in PHA. PHA are usually produced from, relatively, high-cost carbon substrates such as starch or purified sugars. However, a large amount of current research is applied to using organic waste streams or agricultural byproducts, such as molasses and waste water, as substrate for PHA production [34].

The homopolymer PHB is a semi-crystalline polyester with a degree of crystallinity varying between 70 and 85 %. The crystalline structure of PHB adopts a compact helical conformation with a 2-fold screw axis in an orthorhombic unit cell [7, 35, 36]. This helix conformation is stabilized by carbonyl-methyl group interaction, making it one of the few examples of helices found in nature that do not depend on hydrogen bonding for its formation and stability [36]. PHB is a thermoplastic polymer with a melting point and glass transition temperature of about 180 °C and 4°C, respectively. PHB is compostable, but also biodegradable in other environments such as marine water [37]. It also possesses fairly good barrier properties, which makes it an interesting material for food packaging [38-40]. Sanchez-Garcia et al. (2008) reported an oxygen permeability as low as 2 $cm^3.mm/(m^2.day.atm)$ for PHB [41].

Unfortunately, this polymer displays some major drawbacks, which prevents it from being widely applied. First of all, PHB is very susceptible to thermal degradation at temperatures near its melting point, which may cause problems during processing. The second drawback of PHB is its inherent brittleness, caused by formation of large cracked spherulites during crystallization from the melt (due to low nucleation density) and slow secondary crystallization [7, 42-44].

The first action to improve the properties of PHB was the introduction of 3-hydroxyvalerate monomers in varying amounts, in order to produce the copolymer poly(3-hydroxybutyrate-co-3-hydroxyvalerate) (PHBV), of which the structure is given in Figure 1-6. The incorporation of the 3-HV-monomer in the PHB polymer chain was initially expected to lower crystallinity, due to distortion of the crystal lattice, in order to reduce brittleness. However, crystallinity was reduced only slightly, due to the fact that the 3-hydroxybutyrate and 3-hydroxyvalerate units were able to co-crystallize, a phenomenon called isodimorphism. At a 3-hydroxyvalerate concentration less than 40 mol%, these units can crystallize in

the PHB lattice and at concentrations greater than 40 mol%, 3-hydroxybutyrate units can crystallize in the poly(3-hydroxyvalerate) lattice. Because the two monomer units have approximately the same shape and occupy similar volumes, it is possible to achieve relatively high levels of crystallinity in these copolyesters (see Table 1-3) [7, 35, 36].

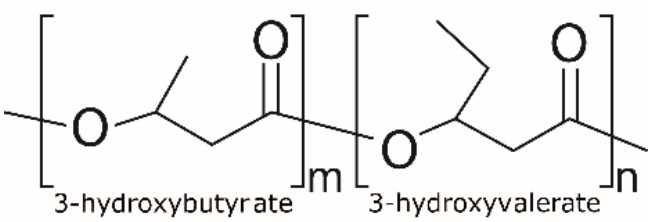

Figure 1-6: Structure of PHBV

It was shown that a substantial amount of the 3-HV units are excluded from the PHB crystal lattice upon crystallization, resulting in a molar fraction of 3-hydroxyvalerate in the crystalline phase, which is about two-thirds of the total molar ratio present in the copolymer. The helical conformation of polymer chains in an orthorhombic unit cell was retained with similar unit cell parameters. The crystallinity of PHBV is lower than that of PHB, ranging from 39 to 69 % depending on the monomer ratio. The incorporation of 3-hydroxyvalerate units also results in a melting point depression [36]. The primary nucleation rate and spherulite growth rate of PHB copolymers are reduced by the introduction of second monomer units, thus resulting in slower crystallization properties [35].

An overview of PHBV properties in function of increasing 3-hydroxyvalerate (3-HV) content is given in Table 1-3. The introduction of 3-HV monomer displayed only a minor success in altering the brittle nature of PHB. At high 3-HV contents it is possible to observe severe reductions in Young's modulus (elastic modulus), measured as the slope of the initial linear part of the stress-strain curve, and increases in notched Izod impact strength (impact strength of a material as measured by ASTM D256 or ISO 180). The tensile strength (calculated from the peak load of stress-strain curve) decreases upon with 3-HV content. High 3-HV contents also decrease crystallization properties unfortunately.

Table 1-3: Properties of PHBV with increasing 3-HV content [5]

3-HV content (mol%)	Melting temperature (°C)	Crystallinity (%)	Young's modulus (GPa)	Tensile strength (MPa)	Notched Izod impact strength (J/m)
0	179	70	3.5	40	50
3	170	69	2.9	38	60
9	162	62	1.9	37	95
14	150	56	1.5	35	120
20	145	50	1.2	32	200
25	137	-	0.7	30	400

Due to the limited success of PHBV, alternative co-monomers were investigated. A promising type of copolymer is based on 3-hydroxybutyrate with minor contents of 3-hydroxyhexanoate (3-HHx) co-monomer (PHBHHx) (See Figure 1-7).

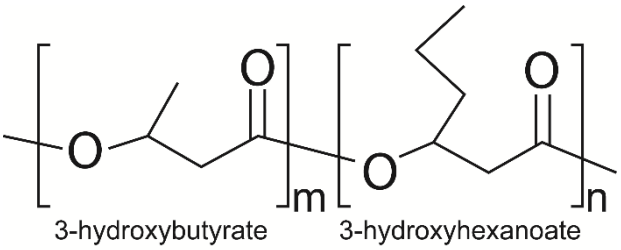

Figure 1-7: Structure of PHBHHx

The functional architecture of PHBHHx is significantly different from that of PHB and PHBV. The latter two contain side chains of maximum 2 carbon atoms long, essentially leading to PHB and PHBV being linear polymers. PHBHHx on the other hand has side chains of 3 carbon atoms long, which results in its classification as a moderately branched polymer [45].

The branches act as a molecular defect, disrupting the excessive regularity of the polymer chain and thus lowering melting temperature and crystallinity. The 3-hydroxyhexanoate units, unlike the 3-hydroxyvalerate ones, cannot co-crystallize with the 3-hydroxybutyrate units, thus excluding them from the crystalline phase, due to their sterically bulky branches. As a result, the crystallinity of the material decreases drastically at increasing 3-hydroxyhexanoate contents [35, 45]. The material is rendered less brittle and more ductile. Unfortunately, the major drawback of the incorporation of 3-hydroxyhexanoate units is the fact that the

crystallization rate is severely reduced [46, 47], which can be problematic for efficient processing of PHBHHx. The crystalline structure, on the other hand, remains identical to that of PHB, namely a helical conformation in an orthorhombic lattice [48].

The effect of increasing amounts of 3-hydroxyhexanoate units on the properties of PHBHHx is shown in Table 1-4. It is clear that a higher 3-HHx content renders the material more ductile and lowers melting point as well as degree of crystallinity, and this in a much more outspoken manner than for PHBV. One must however consider that increasing the 3-HHx content too much will result in a very low melting point, again limiting the application range of the material.

PHA co-polymers always display slower crystallization rates than the homopolymer PHB. This is due to the fact that the co-monomer units are excluded from the PHB lattice during crystallization from the melt, which significantly hinders the crystallization of the remaining 3-hydroxybutyrate units [49]. Taking all properties into account, PHBHHx (with a maximum 3-hydroxyhexanoate content of about 10 mol%) seems like a promising candidate for replacement of conventional packaging plastics.

Table 1-4: Properties of PHBHHx (n.a. = data not available)

3-HHx content (mol%)	Melting temperature (°C) [50]	Crystallinity (%) [51]	Tensile strength (MPa) [51]	Elongation at break (%) [51]
4	174.5	n.a.	n.a.	n.a.
5	n.a.	48	23.6	6.5
7	n.a.	46	20.2	73
8	132.8	n.a.	n.a.	n.a.
10	n.a.	36	15.1	388
12	114.0	37	22.9	549
18	n.a.	29	13.9	538
20	53.6	n.a.	n.a.	n.a.

1.5 MODIFICATION OF POLYHYDROXYALKANOATES

In order to further increase the applicability of PHA, several types of modifications are discussed in literature. Modifications are done in order to ameliorate processing, permeability, mechanical properties, biodegradability etc. In the following sections, a selection of modifications is made, with a focus on PHBV and PHBHHx, as these are the PHA utilized in this study. The discussed modifications are blends of PHA with other polymers, PHA based composites (nanocomposites and microcomposites), nucleating agents and various modifications, including multilayer structures, stretching etc. This overview of modifications is not complete, but provides an insight into the most important and performant modifications, relevant to this study. If a certain property of a specific type of modification is not described, then this is due to the fact that there were no data available in literature.

1.5.1 Blends

The production of polymer blends has received a great deal of attention in academia as well as the industry. In this paragraph, a few of the most studied PHA related blends are discussed. Blending is an effective way to balance and combine properties of separate polymers into one hybrid material, however it is not the most optimal way to improve barrier properties, as a blend often, but not always, results in properties in between those of the single components.

1. PHA/poly(lactic acid) blend

The combination of PHB and PLA is by far the most investigated PHA related blend, displaying mechanical properties in between both separate components, thus improving the properties of PHB [52]. The commercial viability of the separate polymers is difficult due to inherent brittleness and slow crystallization [53]. A combination of both could however prove to be interesting. A study on the effect of PLA molecular weight on its miscibility showed that PLA is miscible with PHB in all combinations for molecular weights M_w lower than 18 000 g/mol. At PLA molecular weights M_w higher than 20 000 g/mol the blend becomes immiscible [54]. The presence of PLA in the PHB matrix hinders crystallization and can possibly induce cold crystallization in subsequent heating [55, 56]. The

mechanical properties of the blends appear to be a compromise between the properties of the single components [57].

Blends of PHBV and PLA have been widely studied as well, revealing that an immiscible blend in any composition is obtained [53, 58, 59]. Mechanical properties of these blends found themselves to be in between pure polymers, which was to be expected from this type of blend [53]. Oxygen and water vapor permeability followed a similar trend, with both decreasing with increasing PHBV content, with the lowest permeability found for the pure PHBV [59]. The studies showed that the presence of PLA in a PHBV matrix induced a retarded crystallization, due to the PHBV chains being hindered by immiscible PLA chains [53, 59].

PHBHHx and PLA blends have been investigated as well and resulted in the formation of thermodynamically immiscible blends, but showing compatibility at a concentration of 20 wt% PHBHHx in PLA and vice versa. These specific compositions displayed an increase in elongation at break, toughness (area under stress-strain curve) and tensile strength. However, important to note is that the crystallization properties of the PLA matrix was retarded, most likely due to restrictions in molecular mobility [60, 61].

2. PHA/polycaprolactone blend

Blends of PHB, PHBV and PHBHHx, though the latter to a lesser extent, with polycaprolactone (PCL) have been reported to be completely immiscible [62-65]. Lovera et al. (2007) investigated the effect of PCL molecular weight and were able to prove a slight increase in miscibility upon addition of low molecular weight polycaprolactone [64].

PHB [64] and PHBV [62, 65, 66] both displayed a decrease in crystallization temperature upon addition of PCL, indicative of hindered crystallization. The mechanical properties of PHB, PHBV and PHBHHx were influenced in a similar manner, showing a decrease in Young's modulus and an increase in elongation at break [63, 64, 66]. Katsumatu et al. (2011) have also proven that the addition of low amounts (about 2.5 wt%) of PCL induced a toughening effect and significant increase in ductility, due to a change in stress deformation mechanism [67].

Some efforts have been made to improve interfacial properties of PHA/ PCL blends. One possible route is reactive blending in the presence of a reactive initiator (e.g. dicumylperoxide), resulting in the *in situ* formation of graft copolymers. For the PHB/PCL system, significant improvements in mechanical properties, upon comparison with non-reactive blends with same composition, can be observed [68]. A different route is preparing the PHA/PCL copolymer, which makes the blend more compatible, *ex situ*, thus resulting in the preparation of a ternary blend. Kim et al. (1998) prepared a compatibilizer via transesterification of PCL and PHB in the presence of dibutyl tin oxide [69]. This novel copolymer was then blended with pure PHB and pure PCL. The DSC analysis showed a clear increase in miscibility, but unfortunately no other properties were investigated.

3. PHA/starch blend

A third and often cited combination, is that of PHA and starch (modified or unmodified). Blending PHA could be an interesting route to lower the cost, due to low cost price of starch, and tailor the properties of PHA towards specific applications. Thiré et al. (2006) prepared blends of PHB and maize starch in concentrations ranging between 0 and 100 wt% [70]. At starch concentrations of 30 wt% and higher, a significant decrease in Young's modulus, elongation at break and tensile strength can be observed, most likely due to poor compatibility and adhesion between PHB and the starch granules. Innocentini-Mei et al. (2003) blended triacetin-plasticized PHB with native starch, as well as starch-adipate and starch-urethane derivatives [71]. The combination of PHB and urethane-modified starch appeared to be most promising, with a severe decrease in glass transition temperature (T_g) and melting temperature (T_m) (thus improving processability). The mechanical properties of the samples containing modified starch were better than those containing virgin starch, due to a much better chemical compatibility with PHB. In all cases, Young's modulus and tensile strength were severely reduced, whereas elongation at break was hardly affected. Ismail et al. (2010) prepared PHB/starch blends, plasticized with glycerol and compatibilized with stearic acid [72]. It was observed that a starch concentration of 10 wt% showed optimal properties, with a significant increase in Young's modulus, tensile strength and elongation at break, due to a finer morphology and better adhesion in the presence of stearic acid. They also found that biodegradation (using

actinomycetes) improved greatly by adding starch to PHB, with pure PHB and PHB containing 30 % starch showing a weight loss of about 20 % and 80 %, respectively, after 35 days of exposure.

Ramsay et al. (1993) prepared PHBV/starch blends with 25 and 50 wt% starch, using a combination of an internal mixer and compression molding [73]. Upon addition of starch, Young's modulus increased, whereas tensile strength and elongation at break showed a steady decrease, again due to poor adhesion between PHBV and starch. Reis et al. (2008) also prepared PHBV/starch blends with 0 to 50 wt% starch content [74]. Young's modulus, tensile strength and elongation at break decreased with increasing starch content. FT-IR measurements confirmed that there were no intermolecular interactions between PHBV and starch, resulting in a lack of interfacial adhesion and a heterogeneous dispersion of starch granules in the PHBV matrix. In order to overcome difficulties related to poor interfacial adhesion, Avella et al. (2000) prepared PHBV/starch blends via reactive blending in the presence of bis(tert-butylperoxyisopropyl)benzene [75]. SEM analysis clearly showed a well improved adhesion between PHBV and starch, resulting in a significant increase in impact properties. Imam et al. (1998) prepared PHBV/starch blends with 30 and 50 wt% starch and demonstrated that the weight loss upon composting after 125 days increased drastically from 7 % (pure PHBV) to 25 % (30 % starch) and 49 % (50% starch). They also proved that the presence of starch accelerated the biodegradation of the PHBV matrix [76].

1.5.2 Nanocomposites

A different route for tailoring the properties of polymers is the production of composites via the addition of micron- or nanosized particles in various concentrations. In this paragraph, a selection of nanocomposites that could show potential for food packaging is presented. One must also keep in mind that the number of publications regarding improvement of PHA barrier properties through addition of nanoparticles is very limited.

1. Organomodified montmorillonite

Montmorillonite is a layered phyllosilicate of which the surface can be organically modified, from here denoted as OMMT, in order to improve dispersion in a polymeric matrix [29]. An example of a PHBV/OMMT nanocomposite is given in Figure 1-8, showing excellent dispersion in the polymeric matrix. The effect of OMMT on PHB and PHBV mechanical properties is very similar, with the most prominent properties being a significant increase in Young's modulus and a decrease in elongation at break upon increasing concentrations of OMMT [77-80]. Due to clay aggregation, indicative of inadequate dispersion and compatibility between polymer and OMMT, it is also possible that the Young's modulus is reduced [81].

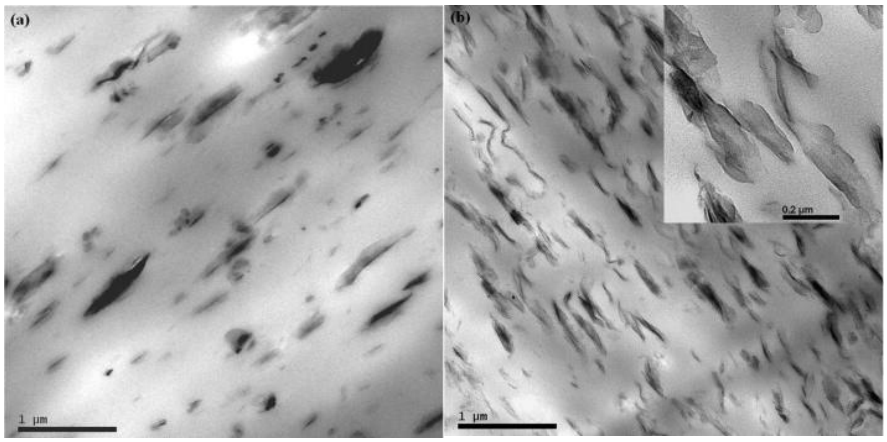

Figure 1-8: TEM image of a PHBV sample containing a) 1 wt% and b) 5 wt% of Cloisite 30B OMMT [82]

The influence of OMMT on the thermal stability of PHB and PHBV and the reported data in literature are often conflicting. Most often an increase in thermal stability (usually measured using thermogravimetric analysis) is reported, due to the

OMMT particles acting as efficient barriers for volatilized degradation products and thus causing a delay in weight loss [79, 80, 83-86]. On the other hand, a reduction in thermal stability has also been reported [41, 87-89]. Some proposed mechanisms behind reduced thermal stability are the release of tightly bound water from OMMT at elevated temperatures causing hydrolysis of PHA chains [88], Hofmann elimination of clay modifier resulting in the production of reactive species which can degrade PHA [88-90] and the formation of OMMT agglomerates which can accumulate heat and thus accelerate degradation [91].

The effect of OMMT on the crystallization of PHB and PHBV also varies from publication to publication. Some studies show that OMMT acts as a nucleating agent, increasing temperature and rate of crystallization upon cooling from the melt [77, 78, 80, 81, 86]. In other studies no significant effect [92] or even a negative effect on crystallization properties can be observed, which is usually explained by restricted mobility related to physical interactions between polymer chains and OMMT modifier [93, 94].

The amount of literature data regarding the effect of OMMT on permeability properties of PHA is very low, so it is not possible to observe one specific trend. Corrêa et al. (2012) obtained a reduction in oxygen permeability of 12.8 % and 33.8 % by adding 3 wt% of OMMT to respectively PHB and plasticized PHB [95]. The study of Crétois et al. (2014) on a PHBV/OMMT system showed an increase in carbon dioxide and water vapor permeability and a fairly constant oxygen permeability, attributed to an increase in gas solubility [90]. Sanchez-Garcia et al. (2007-2010) compared PHBV and PHB nanocomposites containing 5 wt% OMMT, resulting in a respective reduction of oxygen permeability of 26.8 % and 20.5 %. Water vapor permeability was reduced by 53.6 % and 5.9 % respectively [41, 96, 97]. The cause of only a minor reduction in water vapor permeability for the PHB nanocomposite was not elaborated.

The role of OMMT in biodegradation behavior of PHB has also been discussed on a few occasions, with varying results. The results of Maiti et al. (2007) [98] (compost as biodegradation medium) and Panayotidou et al. (2015) [99] (enzymatic degradation in aqueous solution) demonstrate that OMMT enhances the biodegradation rate of PHB. In the study of Wang et al. (2005) (soil suspension as biodegradation medium) a significant decrease in biodegradability was

demonstrated for PHB upon addition of OMMT. After 350 hours of biodegradation, the weight loss of PHBV was 46.6 %, whereas the weight losses of nanocomposites containing 3, 5 and 10 wt% were only 30.5, 4.1 and 4.2 %, respectively [100].

Literature data on PHBHHx/organomodified clay nanocomposites is very limited. Zhang et al. (2007, 2008) prepared well dispersed intercalated organomodified montmorillonite nanocomposites through solvent casting [47] as well as melt blending [101]. Their samples displayed an increase in Young's modulus, decrease in elongation at break and constant tensile strength at concentrations up to 5 wt%. Thermal stability, as evaluated by thermogravimetric analysis, was reduced at increasing nanoparticle concentrations.

After careful revision of literature data, it must be concluded that it is very difficult to identify clear patterns in the properties of PHA/OMMT nanocomposites. This is due to the fact that a great deal of parameters can influence the outcome and performance of the samples. Some important parameters are type of organic modifier, sample preparation method (melt blending or solvent casting) and degree of dispersion of OMMT in matrix.

2. Metal oxides

The addition of metal oxide nanoparticles to a polymeric matrix can result in advantageous changes in barrier properties, as well as antimicrobial properties, UV blocking etc. [102]. This paragraph will focus on zinc oxide (ZnO) and titanium dioxide (TiO_2).

The last few years, the introduction of ZnO nanoparticles in bioplastics has received more and more attention. Díez-Pascual et al. (2014) prepared PHB/ZnO nanocomposites with ZnO concentrations of 1, 2, 5 and 10 wt% via solvent casting [103]. The prepared nanocomposites displayed a higher thermal stability and the ZnO nanoparticles acted as a nucleating agent, increasing crystallization temperature. Young's modulus, tensile and impact strength of the biopolymer were enhanced by up to 43%, 32% and 26%, respectively. A maximum reduction in oxygen permeability of about 53 % was observed for PHB containing 5 wt% ZnO. The nanocomposites also displayed antimicrobial activity for Gram negative as well as Gram positive bacteria, increasing at higher ZnO contents.

PHBV based ZnO nanocomposites were prepared also in a separate study, again via solvent casting but in concentrations of 1, 2, 4 and 8 wt% [104]. The ZnO nanoparticles acted as a nucleating agent and here a gradual increase in thermal stability was also observed. Mechanical properties were influenced in a similar manner as with PHB/ZnO. In terms of barrier properties, the optimum ZnO concentration appeared to be 4 wt%, with a reduction in water vapor permeability and oxygen permeability of 46 % and 35 %, respectively. TEM images of these samples containing 4 and 8 wt% of ZnO are shown in Figure 1-9. The ZnO nanoparticles show a very good dispersion, but this is to be expected as a solvent casting technique was used for preparation of the nanocomposites.

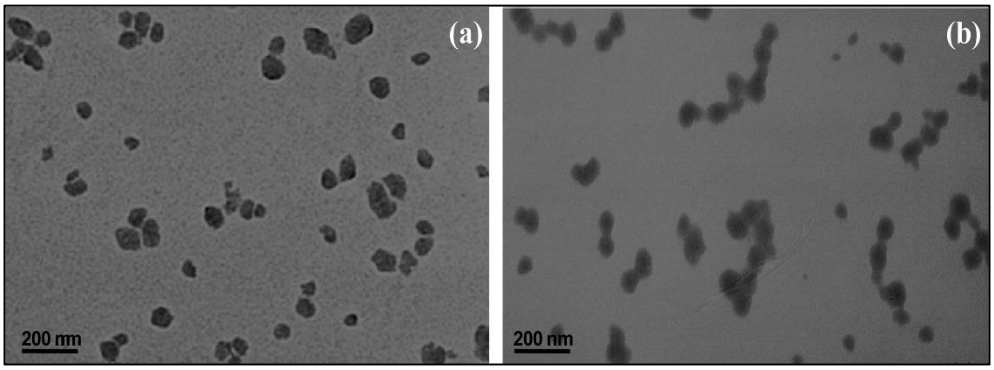

Figure 1-9: TEM images of PHBV samples containing a) 4 wt% and b) 8 wt% ZnO nanoparticles [104]

A limited amount of results on TiO_2 nanocomposites are also reported. Buzarovska et al. (2009) prepared PHBV/TiO_2 (80 % anatase, 20 % rutile) nanocomposites through solvent casting with TiO_2 contents of 0.5, 1, 2, 5 and 10 wt% [105]. At relatively high concentrations (≥ 5 wt%) a slight increase in PHBV crystallization temperature could be observed. A slight gradual increase in thermal stability could be obtained as well at increasing TiO_2 concentrations. No results on the effect of TiO_2 nanoparticles on gas permeability properties of PHA could be retrieved. However, Alberton et al. (2014) observed an increase in water vapor permeability for PLA at TiO2 concentrations up to 5 wt%, followed by a severe reduction at concentrations higher than 5 wt%, which they attributed to the hydrophilic nature of TiO_2 [106]. On the contrary, Ali et al. (2014) observed a gradual decrease in oxygen permeability (20 % reduction at 5 wt%) for PLA/TiO_2 nanocomposites

[107]. The lack of available data renders it impossible to draw any significant conclusions.

3. Cellulose nanowhiskers

Cellulose nanowhiskers (CNWs) are needle-like elementary crystals that occur naturally in cell walls of plants and can be isolated using acid hydrolysis [108]. CNWs are also one of the few organic nanofillers used for preparation of polymer nanocomposites. A TEM example of a PHBV/CNW nanocomposite is shown in Figure 1-10, which displays a very homogenous dispersion of the CNWs in PHBV. The results on the effect of CNWs on the thermal stability of PHA are not very uniform. Some studies suggest an increase in thermal stability [109], whereas other researchers demonstrate a slight decrease [110, 111]. Martínez-Sanz et al. (2014) found an increase in thermal stability at low CNWs concentration (≤ 1 wt%) and a decrease at higher concentrations [112].

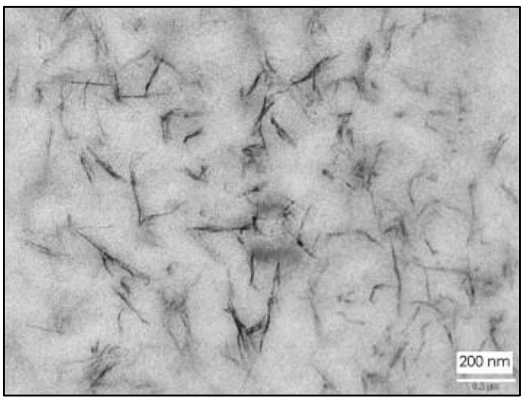

Figure 1-10: TEM image of a PHBV sample containing 5 wt% cellulose nanowhiskers [111]

For PHBV, the presence of CNWs in the polymeric matrix significantly improves crystallization properties, indicating that CNWs act as a nucleating agent [109, 111, 113, 114].

Young's modulus and tensile strength of PHBV/CNWs nanocomposites increased at higher concentrations, thus implying a reinforcing effect of the polymeric matrix [109, 111, 115].

The limited data available on permeability properties of PHBV/CNWs nanocomposites are rather contradictive. Martínez-Sanz et al. (2014) observed an increase in water vapor permeability upon addition of CNWs. In this study, oxygen permeability at 0 % relative humidity decreased, whereas the oxygen permeability at 80 % RH increased [112]. Yu et al. (2014) demonstrated a significant and gradual decrease in water vapor permeability at increasing CNWs concentration [116].

1.5.3 Nucleating agents

A major drawback of PHB [117, 118], PHBV [43, 44, 119] and PHBHHx [46, 119-121] are the slow crystallization rates from the melt, resulting in difficult processing and long processing times. An effective way to enhance the crystallization rate is the addition of a so-called nucleating agent, usually in concentrations up to 1 wt%. Nucleating agents should fulfill two functions, namely 1) speeding up the crystallization process during cooling of the molten polymer and 2) inducing the formation of a greater number of smaller and homogeneously sized crystalline spherulites [122]. The addition of these nucleating agents can thus lead to an increase in crystallization temperature and rate, narrower crystallization peak during non-isothermal cooling from the molten state and possibly also higher crystallization enthalpy. The spherulites formed in the presence of nucleating agents are often smaller than those formed by slow crystallization [44, 122].

A significant amount of literature data exists on the efficiency of certain chemical compounds as nucleating agents for PHA. These data are very difficult to compare due to the great variety of experimental parameters, sample preparation methods, but also due to the lack of a clear definition of what a 'good nucleating agent' entails from a technical point of view (i.e. how much must the crystallization temperature increase in order to correlate to a realistic processing performance).

Also, the efficiency of a specific nucleating agent tends to vary from PHA to PHA, meaning that there is no specific nucleating agent suitable for all types of PHA. One must select a nucleating agent based on the polymer (and applications) at hand. For example, boron nitride is a well-known and highly efficient nucleating agent for PHB, but cyclohexyl phosphonic acid and zinc stearate were found to be better for PHBV, especially when the 3-hydroxyvalerate content increases [122].

Another example is the case of uracil. Uracil performs slightly less than boron nitride in PHB, but is a very efficient nucleating agent for PHBHHx, whereas boron nitride performs poorly for PHBHHx [49]. The underlying mechanism behind this trend has not yet been clarified to our knowledge, however it is presumed that the length of the chains in the polymer backbone and the presence of side chains plays an important role, as they will influence the degree of interaction between the polymer and the nucleating agent.

For PHB and PHBV, boron nitride is usually considered as the best nucleating agent [43, 123, 124], resulting in its commercial use for these materials. However, a large amount of other nucleating agents have been tested for these materials with varying efficiency, including but not limited to cyclodextrin [125], terbium and lanthanum oxide [43], melamine, thymine [44], saccharin [126], lignin [127], ammonium chloride [128] and talc [124].

In terms of efficiency of nucleating agents, PHBHHx displays a lot more deviation from the behavior of PHB than is the case for PHBV. However, the last 5 years a novel generation of heterocyclic compounds have shown a great deal of promise as nucleating agents for PHBHHx. More specifically uracil [49], orotic acid [42, 129] and cyanuric acid [119] have been demonstrated to be highly efficient, displaying better performance than boron nitride and talc.

Talc is a mineral additive that has been tested as a nucleating agent for several types of PHA. For PHB, it has been shown to be highly effective when enhancing the crystallization temperature. Ye et al. (2004) found that the addition of 2 wt% talc increased the crystallization peak temperature with about 33 °C [130]. Jacquel et al. (2010) observed a 20 °C increase in PHB crystallization temperature upon addition of 1 wt% talc [129]. Talc has shown a nucleating effect for PHBV as well [124, 131], but the beneficial effect appears to vary with the 3-HV content, as was shown by Zhu et al. (2012) upon addition of 5 wt% talc to a number of PHBV samples with 3-HV contents ranging from 0 to 32.6 mol% [131]. For PHBHHx, Jacquel et al. (2010) observed no effect on crystallization of PHBHHx by adding 1 wt% talc [129]. Wang et al. (2010) reported an increase of 9 °C of crystallization peak temperature for poly(3-hydroxybutyrate-co-4-hydroxybutyrate) containing 1 wt% talc [132].

The last few years, the reduction of talc particle size for enhanced performance has been investigated, as this could lead to significant changes in properties, but at lower concentrations. For example, Petchwattana et al. (2014) studied the efficiency of talc, in concentrations of up to 10 wt%, for PLA. Three different particle sizes, namely 1, 5 and 10 µm, were investigated and it was found that the finer talc particles lead to slightly higher degrees of crystallinity [133].

1.5.4 PHA-based multilayers

Although multilayer co-extrusion is a widely used, studied and well understood domain within the synthetic polymer industry, the extrapolation towards bioplastics, however, has not been that extensive yet. This is most likely due to the fact that an optimization of several parameters is required, such as polymer viscosity, interfacial instabilities and polymer compatibility [122]. As a result, only a few publications regarding PHA-based multilayer structures can be retrieved.

A first effort regarding a multilayer structure was presented by Martin et al. (2001), through co-extrusion or compression molding, with PHBV as outerlayer and a plasticized weat starch as interlayer. The purpose of this study was to enhance the properties of the starch layer in terms of mechanical performance and moisture resistance [134]. This study did not focus on functional properties (e.g. permeability), but mostly on layer adhesion.

Fabra et al. (2014) produced 3-layered samples with a nano-scaled zein protein (extracted from corn) layer, deposited via electrospinning, protected by either plasticized PHB or plasticized PHBV on both sides [135]. The PHA layers served as a barrier against moisture, which is detrimental for the functioning of the protein layer. Water vapour permeability of the resulting multilayers were reduced by 44 % and 55 % for PHB and PHBV respectively. Oxygen permeability was lowered by 59 % and 53 %, respectively. The tensile strength and Young's modulus were reduced slightly, whereas the elongation at break was almost not affected.

Cunha et al. (2015) prepared a bilayered film, consisting of PHBV and PBAT, through co-extrusion film blowing [136]. The preparation of these bilayers did not reveal any advantageous results in terms of barrier properties, unfortunately.

The study of Thellen et al. (2013), where a poly(vinyl alcohol) barrier layer was sandwiched between two poly(3-hydroxybutyrate-co-4-hydroxybutyrate) layers,

shows the most effort towards actual application of PHA-based multilayers for food packaging, as it simulates more conventional food packaging multilayer films [137]. Oxygen permeability (at 23 °C and 60-90 % relative humidity) of the PHA was successfully reduced by about 85-90 % by introducing a poly(vinyl alcohol) interlayer. A thin-gauge adhesion layer of maleated PHA was used to promote compatibility between both layers.

1.6 AIMS AND SCOPE OF THE RESEARCH

Biobased and biodegradable plastics enjoy more and more attention, but the application of these polymers is still rather limited due to their performance, that is not yet up to par with conventional polymers. The use of these materials as food packaging is a rather demanding application, as a great deal of properties (e.g. gas permeability, mechanical properties, processability) must be considered.

In this study, two polyhydroxyalkanoates have been selected for investigation and further modification, namely poly(3-hydroxybutyrate-co-3-hydroxyvalerate) (PHBV) and poly(3-hydroxybutyrate-co-3-hydroxyhexanoate) (PHBHHx). These polymers were chosen based on available literature data, showing a certain potential for food packaging applications. Both display fairly good gas permeability properties, are commercially available and show rapid biodegradation (in comparison with PLA for example).

The main goal of this study can be defined as:

To provide an in-depth characterization of selected polyhydroxyalkanoates, with an identification of properties that could render the application of the material for food packaging on one hand promising or on the other hand difficult. Dedicated modifications, using a variety of analysis techniques, are performed and investigated in order to enhance these properties

This goal can by subdivided in the following aims:

Aim 1

Provide an in-depth characterization of selected polyhydroxyalkanoates in order to gain understanding of their intrinsic properties as well as to pinpoint specific properties that could prove to promote or hinder the application of the materials for food packaging purposes.

This is done by analyzing the most relevant intrinsic properties of the selected virgin polymers using a large array of techniques. The properties that are investigated are molecular weight distribution, thermal stability, thermal behavior (melting point, crystallization etc.), tensile properties and gas permeability (O_2, CO_2 and water vapor).

Aim 2

Validation of selected nucleating agents on the crystallization properties of the polyhydroxyalkanoates, which is a known drawback of this type of polymers.

Slow and inadequate crystallization is a problem common to most types of PHA. Therefore, the effect of certain nucleating agents (orotic acid, boron nitride and talc) on polymer crystallization is investigated, with differential scanning calorimetry as the primary analysis technique. These specific nucleating agents were chosen based on their performance, as reported in available literature data. Though not directly related to the applicability for food packaging, the crystallization properties of a polymer are of great importance for the conversion of polymer powder or granulates into actual films, trays etc., using conventional processing techniques (e.g. extrusion, injection molding). Thus, the crystallization is still of high importance for the eventual application.

Aim 3

Evaluate the efficiency and applicability of the introduction of (nanosized) additives towards the production of a high-end food packaging material.

Even though the barrier properties of PHA are fairly good, they should be enhanced even further in order to find application as a high-end food packaging material. Based on extensive literature research, a few modification techniques have been selected and performed, both based on the formation of PHA based nanocomposites. The nanoparticles used in this study are organically modified montmorillonite clay and zinc oxide nanorods. The effect of these nanoparticles on several properties (mechanical properties, gas permeability, thermal stability and thermal behavior) is subsequently investigated. The underlying mechanisms involved in the alteration of properties are thoroughly investigated as well. During characterization of the samples, the focus will lie on gas permeability properties.

Finally, it will be possible to combine all results in order to assess which modification techniques show most potential for production of a performant food packaging material.

1.7 MANUSCRIPT OVERVIEW

Chapter 2 provides an in-depth characterization of the three polymers that were selected for further use in this thesis, namely PHBV and two types of PHBHHx. Thermal, mechanical and barrier properties of these polymers were compared in order to highlight the properties that can promote or hinder the applicability of the materials.

Chapter 3 presents a comparison of the conventional nucleating agent boron nitride with an alternative and biodegradable nucleating agent orotic acid, for use in PHBV, which displays slow crystallization rates. The effect of different concentrations of both nucleating agents on non-isothermal crystallization of PHBV is discussed and described by three known models (Jeziorny modified Avrami, Ozawa and Mo model).

In chapter 4, an in-depth characterization of ultra-fine talc as a nucleating agent for PHBHHx is performed. Talc is nucleating agent for a large number of polymers, thus the crystallization properties are firstly characterized. The effect of this filler on mechanical properties, permeability, color/opacity and thermal stability is investigated as well

In chapter 5, a thorough investigation of the applicability of PHBHHx/OMMT nanocomposites as a food packaging material is presented. Besides material properties such as nanoparticle dispersion/morphology, thermal stability and crystallization, specific end-use properties concerning color/opacity and gas permeability are discussed in depth as well.

Chapter 6 explores the influence of zinc oxide nanorods on the thermal stability, crystallization, mechanical properties, gas permeability, color/opacity and UV absorption properties of PHBHHx. The nanofiller dispersion is investigated as well.

Finally, chapter 7 summarizes the main findings of this doctoral research. Possible routes for further research are suggested as well, based on these findings.

1.8 REFERENCES

1. PlasticsEurope, *Plastics – the Facts 2014/2015: An analysis of European plastics production, demand and waste data.* 2015.

2. Chen, Y., *Advantages of bioplastics and global sustainability.* Applied Mechanics and Materials, 2013. **420**: p. 209-214.

3. EuropeanBioplastics, *Bioplastics - Facts and Figures*. 2014.

4. Braunegg, G., G. Lefebvre, and K.F. Genser, *Polyhydroxyalkanoates, biopolyesters from renewable resources: Physiological and engineering aspects.* Journal of Biotechnology, 1998. **65**(2–3): p. 127-161.

5. Lee, S.Y., *Bacterial polyhydroxyalkanoates.* Biotechnology and Bioengineering, 1996. **49**(1): p. 1-14.

6. Reddy, C.S.K., et al., *Polyhydroxyalkanoates: an overview.* Bioresource Technology, 2003. **87**(2): p. 137-146.

7. Sudesh, K., H. Abe, and Y. Doi, *Synthesis, structure and properties of polyhydroxyalkanoates: biological polyesters.* Progress in Polymer Science, 2000. **25**(10): p. 1503-1555.

8. Garlotta, D., *A Literature Review of Poly(Lactic Acid).* Journal of Polymers and the Environment, 2001. **9**(2): p. 63-84.

9. EuropeanBioplastics. *http://en.european-bioplastics.org/*. 2015 [cited 2015.

10. Han, J.H., *Chapter 1 - A Review of Food Packaging Technologies and Innovations*, in *Innovations in Food Packaging (Second Edition)*, J.H. Han, Editor. 2014, Academic Press: San Diego. p. 3-12.

11. Marsh, K. and B. Bugusu, *Food Packaging—Roles, Materials, and Environmental Issues.* Journal of Food Science, 2007. **72**(3): p. R39-R55.

12. Yam, K.L. and D.S. Lee, *1 - Emerging food packaging technologies: an overview*, in *Emerging Food Packaging Technologies*, K.L. Yam and D.S. Lee, Editors. 2012, Woodhead Publishing. p. 1-9.

13. Robertson, G.L., *Food Packaging and Shelf Life*, in *Food Packaging and Shelf Life*. 2009, CRC Press. p. 1-16.

14. Realini, C.E. and B. Marcos, *Active and intelligent packaging systems for a modern society.* Meat Science, 2014. **98**(3): p. 404-419.

15. Figura, L. and A. Teixeira, *Permeability*, in *Food Physics*. 2007, Springer Berlin Heidelberg. p. 233-255.

16. Brown, H., J. Williams, and M. Kirwan, *Packaged Product Quality and Shelf Life*, in *Food and Beverage Packaging Technology*. 2011, Wiley-Blackwell. p. 59-83.

17. Petersen, K., et al., *Potential of biobased materials for food packaging.* Trends in Food Science and Technology, 1999. **10**(2): p. 52-68.

18. Klopffer, M., H. and B. Flaconneche, *Transport de molécules gazeuses dans les polymères : revue bibliographique.* Oil & Gas Science and Technology - Rev. IFP, 2001. **56**(3): p. 223-244.

19. Han, J.H. and M.G. Scanlon, *Chapter 3 - Mass Transfer of Gas and Solute Through Packaging Materials*, in *Innovations in Food Packaging (Second Edition)*, J.H. Han, Editor. 2014, Academic Press: San Diego. p. 37-49.

20. Rogers, C.E., *Permeation of Gases and Vapours in Polymers*, in *Polymer Permeability*, J. Comyn, Editor. 1985, Springer Netherlands. p. 11-73.

21. Siracusa, V., *Food Packaging Permeability Behaviour: A Report.* Int J Polym Sci, 2012. **2012**: p. 11.

22. Van Krevelen, D.W.T.N., K., *Properties of Polymers*. 2009, Amsterdam: Elsevier. 1004.

23. Mark, H.F., *Encyclopedia of Polymer Science and Technology*. 2003, Hoboken, New Jersey: John Wiley & Sons.

24. Hong, S.-I. and J.M. Krochta, *Oxygen barrier performance of whey-protein-coated plastic films as affected by temperature, relative humidity, base film and protein type.* J Food Eng, 2006. **77**(3): p. 739-745.

25. Lagarón, J.M., *1 - Multifunctional and nanoreinforced polymers for food packaging*, in *Multifunctional and Nanoreinforced Polymers for Food Packaging*, J.-M. Lagarón, Editor. 2011, Woodhead Publishing. p. 1-28.

26. Matteucci, S., et al., *Transport of Gases and Vapors in Glassy and Rubbery Polymers*, in *Materials Science of Membranes for Gas and Vapor Separation*. 2006, John Wiley & Sons, Ltd. p. 1-47.

27. Min, K.E. and D.R. Paul, *Effect of tacticity on permeation properties of poly(methyl methacrylate).* Journal of Polymer Science Part B: Polymer Physics, 1988. **26**(5): p. 1021-1033.

28. George, S.C. and S. Thomas, *Transport phenomena through polymeric systems.* Progress in Polymer Science, 2001. **26**(6): p. 985-1017.

29. Alexandre, M. and P. Dubois, *Polymer-layered silicate nanocomposites: preparation, properties and uses of a new class of materials.* Materials Science and Engineering: R: Reports, 2000. **28**(1–2): p. 1-63.

30. Duncan, T.V., *Applications of nanotechnology in food packaging and food safety: Barrier materials, antimicrobials and sensors.* Journal of Colloid and Interface Science, 2011. **363**(1): p. 1-24.

31. Sinha Ray, S. and M. Okamoto, *Polymer/layered silicate nanocomposites: a review from preparation to processing.* Prog Polym Sci, 2003. **28**(11): p. 1539-1641.

32. Nielsen, L.E., *Models for the Permeability of Filled Polymer Systems.* Journal of Macromolecular Science: Part A - Chemistry, 1967. **1**(5): p. 929-942.

33. Madison, L.L. and G.W. Huisman, *Metabolic Engineering of Poly(3-Hydroxyalkanoates): From DNA to Plastic.* Microbiology and Molecular Biology Reviews, 1999. **63**(1): p. 21-53.

34. Du, C., et al., *Polyhydroxyalkanoates Production From Low-cost Sustainable Raw Materials.* Current Chemical Biology, 2012. **6**(1): p. 14-25.

35. Sudesh, K. and H. Abe, *Practical Guide to Microbial Polyhydroxyalkanoates*. 2010, Shawbury: iSmithers.

36. Volova, T., *Microbial Polyhydroxyalkanoates — Plastic Materials of the 21st Century (Biosynthesis, Properties, Applications)*. 2004, New York: Nova Science Publishers, Inc. 282.

37. Bugnicours, E., et al., *Polyhydroxyalkanoate (PHA): Review of synthesis, characteristics, processing and potential applications in packaging.* Express Polymer Letters, 2014. **8**(11): p. 791-808.

38. Corre, Y.-M., et al., *Morphology and functional properties of commercial polyhydroxyalkanoates: A comprehensive and comparative study.* Polymer Testing, 2012. **31**(2): p. 226-235.

39. Dhar, P., et al., *Poly (3-hydroxybutyrate)/cellulose nanocrystal films for food packaging applications: Barrier and migration studies.* Polymer Engineering & Science, 2015: p. n/a-n/a.

40. Follain, N., et al., *Structure and Barrier Properties of Biodegradable Polyhydroxyalkanoate Films.* The Journal of Physical Chemistry C, 2014. **118**(12): p. 6165-6177.

41. Sanchez-Garcia, M.D., E. Gimenez, and J.M. Lagaron, *Morphology and barrier properties of nanobiocomposites of poly(3-hydroxybutyrate) and layered silicates.* Journal of Applied Polymer Science, 2008. **108**(5): p. 2787-2801.

42. Jacquel, N., et al., *Effect of Orotic Acid as a Nucleating Agent on the Crystallization of Bacterial Poly(3-hydroxybutyrate-co-3-hydroxyhexanoate) Copolymers.* Journal of Applied Polymer Science, 2009. **114**(2): p. 1287-1294.

43. Liu, W.J., et al., *Effect of nucleating agents on the crystallization of poly(3-hydroxybutyrate-co-3-hydroxyvalerate).* Journal of Applied Polymer Science, 2002. **86**(9): p. 2145-2152.

44. Qian, J., et al., *Comparison of different nucleating agents on crystallization of poly(3-hydroxybutyrate-co-3-hydroxyvalerates).* Journal of Polymer Science Part B: Polymer Physics, 2007. **45**(13): p. 1564-1577.

45. Noda, I., S.B. Lindsey, and D. Caraway, *Nodax™ Class PHA Copolymers: Their Properties and Applications*, in *Plastics from Bacteria*, G.G.-Q. Chen, Editor. 2010, Springer Berlin Heidelberg. p. 237-255.

46. Yu, F., et al., *Nucleation Effect of Layered Metal Phosphonate on Crystallization of Bacterial Poly[(3-hydroxybutyrate)-co-(3-hydroxyhexanoate)].* Macromolecular Materials and Engineering, 2011. **296**(2): p. 103-112.

47. Zhang, X., et al., *Some novel layered-silicate nanocomposites based on a biodegradable hydroxybutyrate copolymer.* European Polymer Journal, 2007. **43**(8): p. 3128-3135.

48. Sato, H., et al., *Thermal Behavior and Molecular Interaction of Poly(3-hydroxybutyrate-co-3-hydroxyhexanoate) Studied by Wide-Angle X-ray Diffraction.* Macromolecules, 2004. **37**(10): p. 3763-3769.

49. Pan, P., et al., *Uracil as Nucleating Agent for Bacterial Poly[(3-Hydroxybutyrate)-co-(3-hydroxyhexanoate)] Copolymers.* Macromolecular Bioscience, 2009. **9**(6): p. 585-595.

50. Qu, X.-H., et al., *Effect of 3-hydroxyhexanoate content in poly(3-hydroxybutyrate-co-3-hydroxyhexanoate) on in vitro growth and differentiation of smooth muscle cells.* Biomaterials, 2006. **27**(15): p. 2944-2950.

51. Alata, H., T. Aoyama, and Y. Inoue, *Effect of Aging on the Mechanical Properties of Poly(3-hydroxybutyrate-co-3-hydroxyhexanoate).* Macromolecules, 2007. **40**(13): p. 4546-4551.

52. Ramachandran, H., et al., *CHAPTER 4 Blends of Polyhydroxyalkanoates (PHAs)*, in *Polyhydroxyalkanoate (PHA) based Blends, Composites and Nanocomposites*. 2015, The Royal Society of Chemistry. p. 66-97.

53. Nanda, M.R., M. Misra, and A.K. Mohanty, *The Effects of Process Engineering on the Performance of PLA and PHBV Blends.* Macromolecular Materials and Engineering, 2011. **296**(8): p. 719-728.

54. Koyama, N. and Y. Doi, *Miscibility of binary blends of poly[(R)-3-hydroxybutyric acid] and poly[(S)-lactic acid].* Polymer, 1997. **38**(7): p. 1589-1593.

55. Blümm, E. and A.J. Owen, *Miscibility, crystallization and melting of poly(3-hydroxybutyrate)/ poly(l-lactide) blends.* Polymer, 1995. **36**(21): p. 4077-4081.

56. Furukawa, T., et al., *Structure, Dispersibility, and Crystallinity of Poly(hydroxybutyrate)/Poly(l-lactic acid) Blends Studied by FT-IR Microspectroscopy and Differential Scanning Calorimetry.* Macromolecules, 2005. **38**(15): p. 6445-6454.

57. Zhang, M. and N.L. Thomas, *Blending polylactic acid with polyhydroxybutyrate: The effect on thermal, mechanical, and biodegradation properties.* Advances in Polymer Technology, 2011. **30**(2): p. 67-79.

58. Modi, S., K. Koelling, and Y. Vodovotz, *Miscibility of poly(3-hydroxybutyrate-co-3-hydroxyvalerate) with high molecular weight poly(lactic acid) blends determined by thermal analysis.* Journal of Applied Polymer Science, 2012. **124**(4): p. 3074-3081.

59. Zembouai, I., et al., *A study of morphological, thermal, rheological and barrier properties of Poly(3-hydroxybutyrate-Co-3-Hydroxyvalerate)/polylactide blends prepared by melt mixing.* Polymer Testing, 2013. **32**(5): p. 842-851.

60. Lim, J.S., et al., *Effect of composition ratio on the thermal and physical properties of semicrystalline PLA/PHB-HHx composites.* Materials Science and Engineering: C, 2013. **33**(4): p. 2131-2137.

61. Zhao, Q., et al., *Phase morphology, physical properties, and biodegradation behavior of novel PLA/PHBHHx blends.* Journal of Biomedical Materials Research Part B: Applied Biomaterials, 2012. **100B**(1): p. 23-31.

62. Chun, Y.S. and W.N. Kim, *Thermal properties of poly(hydroxybutyrate-co-hydroxyvalerate) and poly(ϵ-caprolactone) blends.* Polymer, 2000. **41**(6): p. 2305-2308.

63. Lim, J., et al., *Biocompatibility studies and characterization of poly(3-hydroxybutyrate-co-3-hydroxyhexanoate)/polycaprolactone blends.* Journal of Biomedical Materials Research Part B: Applied Biomaterials, 2013. **101B**(5): p. 752-761.

64. Lovera, D., et al., *Crystallization, Morphology, and Enzymatic Degradation of Polyhydroxybutyrate/Polycaprolactone (PHB/PCL) Blends.* Macromolecular Chemistry and Physics, 2007. **208**(9): p. 924-937.

65. Qiu, Z., et al., *Miscibility and crystallization behavior of biodegradable blends of two aliphatic polyesters. Poly(3-hydroxybutyrate-co-hydroxyvalerate) and poly(ε-caprolactone).* Polymer, 2005. **46**(25): p. 11814-11819.

66. Del Gaudio, C., et al., *Assessment of poly(ε-caprolactone)/poly(3-hydroxybutyrate-co-3-hydroxyvalerate) blends processed by solvent casting and electrospinning.* Materials Science and Engineering: A, 2011. **528**(3): p. 1764-1772.

67. Katsumata, K., et al., *The toughening effect of a small amount of poly([epsiv]-caprolactone) on the mechanical properties of the poly(3-hydroxybutyrate-co-3-hydroxyhexanoate)/PCL blend.* Polym J, 2011. **43**(5): p. 484-492.

68. Immirzi, B., et al., *Blends of biodegradable polyesters by reactive blending: preparation, characterisation and properties.* Journal of Materials Science, 1999. **34**(7): p. 1625-1639.

69. Kim, B.O. and S.I. Woo, *Compatibilizing capability of poly(β-hydroxybutyrate-,co-ε-caprolactone) in the blend of poly(β-hydroxybutyrate) and poly(ε-caprolactone).* Polymer Bulletin, 1998. **41**(6): p. 707-712.

70. Thiré, R.M.S.M., T.A.A. Ribeiro, and C.T. Andrade, *Effect of starch addition on compression-molded poly(3-hydroxybutyrate)/starch blends.* Journal of Applied Polymer Science, 2006. **100**(6): p. 4338-4347.

71. Innocentini-Mei, L.H., J.R. Bartoli, and R.C. Baltieri, *Mechanical and thermal properties of poly(3-hydroxybutyrate) blends with starch and starch derivatives.* Macromolecular Symposia, 2003. **197**(1): p. 77-88.

72. Ismail, A.M. and M.A.B. Gamal, *Water resistance, mechanical properties, and biodegradability of poly(3-hydroxybutyrate)/starch composites.* Journal of Applied Polymer Science, 2010. **115**(5): p. 2813-2819.

73. Ramsay, B.A., et al., *Biodegradability and mechanical properties of poly-(beta-hydroxybutyrate-co-beta-hydroxyvalerate)-starch blends.* Applied and Environmental Microbiology, 1993. **59**(4): p. 1242-1246.

74. Reis, K.C., et al., *Characterization of polyhydroxybutyrate-hydroxyvalerate (PHB-HV)/maize starch blend films.* Journal of Food Engineering, 2008. **89**(4): p. 361-369.

75. Avella, M. and M.E. Errico, *Preparation of PHBV/starch blends by reactive blending and their characterization.* Journal of Applied Polymer Science, 2000. **77**(1): p. 232-236.

76. Imam, S.H., et al., *Biodegradation of Injection Molded Starch-Poly (3-hydroxybutyrate-co-3-hydroxyvalerate) Blends in a Natural Compost Environment.* Journal of environmental polymer degradation, 1998. **6**(2): p. 91-98.

77. Botana, A., et al., *Effect of modified montmorillonite on biodegradable PHB nanocomposites.* Applied Clay Science, 2010. **47**(3–4): p. 263-270.

78. Branciforti, M.C., et al., *Crystallinity study of nano-biocomposites based on plasticized poly(hydroxybutyrate-co-hydroxyvalerate) with organo-modified montmorillonite.* Polymer Testing, 2013. **32**(7): p. 1253-1260.

79. Bruzaud, S. and A. Bourmaud, *Thermal degradation and (nano)mechanical behavior of layered silicate reinforced poly(3-hydroxybutyrate-co-3-hydroxyvalerate) nanocomposites.* Polymer Testing, 2007. **26**(5): p. 652-659.

80. Mook Choi, W., et al., *Preparation and characterization of poly(hydroxybutyrate-co-hydroxyvalerate)–organoclay nanocomposites.* Journal of Applied Polymer Science, 2003. **90**(2): p. 525-529.

81. Chen, G.X., et al., *Crystallization kinetics of poly(3-hydroxybutyrate-co-3-hydroxyvalerate)/clay nanocomposites.* Journal of Applied Polymer Science, 2004. **93**(2): p. 655-661.

82. Carli, L.N., J.S. Crespo, and R.S. Mauler, *PHBV nanocomposites based on organomodified montmorillonite and halloysite: The effect of clay type on the morphology and thermal and mechanical properties.* Composites Part A, 2011. **42**(11): p. 1601-1608.

83. Achilias, D.S., E. Panayotidou, and I. Zuburtikudis, *Thermal degradation kinetics and isoconversional analysis of biodegradable poly(3-hydroxybutyrate)/organomodified montmorillonite nanocomposites.* Thermochimica Acta, 2011. **514**(1–2): p. 58-66.

84. Erceg, M., T. Kovačić, and I. Klarić, *Poly(3-hydroxybutyrate) nanocomposites: Isothermal degradation and kinetic analysis.* Thermochimica Acta, 2009. **485**(1–2): p. 26-32.

85. Erceg, M., T. Kovačić, and S. Perinović, *Isothermal degradation of poly(3-hydroxybutyrate)/organically modified montmorillonite nanocomposites.* Polymer Composites, 2010. **31**(2): p. 272-278.

86. Mohamed El-Hadi, A., *Investigation of the effect of nano-clay type on the non-isothermal crystallization kinetics and morphology of poly(3(R)-hydroxybutyrate) PHB/clay nanocomposites.* Polymer Bulletin, 2014. **71**(6): p. 1449-1470.

87. Bordes, P., et al., *Effect of clay organomodifiers on degradation of polyhydroxyalkanoates.* Polymer Degradation and Stability, 2009. **94**(5): p. 789-796.

88. Cabedo, L., et al., *Studying the degradation of polyhydroxybutyrate-co-valerate during processing with clay-based nanofillers.* Journal of Applied Polymer Science, 2009. **112**(6): p. 3669-3676.

89. Hablot, E., et al., *Thermal and thermo-mechanical degradation of poly(3-hydroxybutyrate)-based multiphase systems.* Polymer Degradation and Stability, 2008. **93**(2): p. 413-421.

90. Crétois, R., et al., *Microstructure and barrier properties of PHBV/organoclays bionanocomposites.* Journal of Membrane Science, 2014. **467**(0): p. 56-66.

91. Lim, S., et al., *Preparation and characterization of microbial biodegradable poly(3-hydroxybutyrate)/organoclay nanocomposite.* Journal of Materials Science Letters, 2003. **22**(4): p. 299-302.

92. D'Amico, D.A., L.B. Manfredi, and V.P. Cyras, *Crystallization behavior of poly(3-hydroxybutyrate) nanocomposites based on modified clays: Effect of organic modifiers.* Thermochimica Acta, 2012. **544**(0): p. 47-53.

93. D'Amico, D.A., V.P. Cyras, and L.B. Manfredi, *Non-isothermal crystallization kinetics from the melt of nanocomposites based on poly(3-hydroxybutyrate) and modified clays.* Thermochimica Acta, 2014. **594**(0): p. 80-88.

94. Naguib, H.F., M.S.A. Aziz, and G.R. Saad, *Effect of Organo-Modified Montmorillonite on Thermal Properties of Bacterial Poly(3-hydroxybutyrate).* Polymer-Plastics Technology and Engineering, 2013. **53**(1): p. 90-96.

95. Corrêa, M.C.S., et al., *Elaboration and Characterization of Nano-Biocomposites Based on Plasticized Poly(Hydroxybutyrate-Co-Hydroxyvalerate) with Organo-Modified Montmorillonite.* Journal of Polymers and the Environment, 2012. **20**(2): p. 283-290.

96. Sanchez-Garcia, M.D., E. Gimenez, and J.M. Lagaron, *Novel PET Nanocomposites of Interest in Food Packaging Applications and Comparative Barrier Performance With Biopolyester Nanocomposites.* Journal of Plastic Film and Sheeting, 2007. **23**(2): p. 133-148.

97. Sanchez-Garcia, M.D. and J.M. Lagaron, *Novel clay-based nanobiocomposites of biopolyesters with synergistic barrier to UV light, gas, and vapour.* Journal of Applied Polymer Science, 2010. **118**(1): p. 188-199.

98. Maiti, P., C.A. Batt, and E.P. Giannelis, *New Biodegradable Polyhydroxybutyrate/Layered Silicate Nanocomposites.* Biomacromolecules, 2007. **8**(11): p. 3393-3400.

99. Panayotidou, E., et al., *Nanocomposites of poly(3-hydroxybutyrate)/organomodified montmorillonite: Effect of the nanofiller on the polymer's biodegradation.* Journal of Applied Polymer Science, 2015. **132**(11): p. n/a-n/a.

100. Wang, S., et al., *Characteristics and biodegradation properties of poly(3-hydroxybutyrate-co-3-hydroxyvalerate)/organophilic montmorillonite (PHBV/OMMT) nanocomposite.* Polymer Degradation and Stability, 2005. **87**(1): p. 69-76.

101. Zhang, X., et al., *Biodegradable Nanocomposites Based on the Polyester Poly(3-hydroxybutyrate-co-3-hydroxyhexanoate) and Layered Silicate or Expanded Graphite.* Journal of Macromolecular Science, Part A, 2008. **45**(6): p. 431-439.

102. Llorens, A., et al., *Metallic-based micro and nanocomposites in food contact materials and active food packaging.* Trends in Food Science & Technology, 2012. **24**(1): p. 19-29.

103. Díez-Pascual, A.M. and A.L. Díez-Vicente, *Poly(3-hydroxybutyrate)/ZnO Bionanocomposites with Improved Mechanical, Barrier and Antibacterial Properties.* International Journal of Molecular Sciences, 2014. **15**(6): p. 10950-10973.

104. Díez-Pascual, A.M. and A.L. Díez-Vicente, *ZnO-Reinforced Poly(3-hydroxybutyrate-co-3-hydroxyvalerate) Bionanocomposites with Antimicrobial Function for Food Packaging.* ACS Applied Materials & Interfaces, 2014. **6**(12): p. 9822-9834.

105. Buzarovska, A., et al., *Poly(hydroxybutyrate-co-hydroxyvalerate)/titanium dioxide nanocomposites: A degradation study.* Journal of Applied Polymer Science, 2009. **114**(5): p. 3118-3124.

106. Alberton, J., et al., *Mechanical and moisture barrier properties of titanium dioxide nanoparticles and halloysite nanotubes reinforced polylactic acid (PLA).* IOP Conference Series: Materials Science and Engineering, 2014. **64**(1): p. 012010.

107. Ali, N.A. and F.T.M. Noori, *Gas Barrier Properties of Biodegradable Polymer Nanocomposites Films.* Chemistry and Materials Research, 2014. **6**(1).

108. Ten, E., L. Jiang, and M.P. Wolcott, *Crystallization kinetics of poly(3-hydroxybutyrate-co-3-hydroxyvalerate)/cellulose nanowhiskers composites.* Carbohydrate Polymers, 2012. **90**(1): p. 541-550.

109. Yu, H.-Y., et al., *Simultaneous improvement of mechanical properties and thermal stability of bacterial polyester by cellulose nanocrystals.* Carbohydrate Polymers, 2012. **89**(3): p. 971-978.

110. Long Jiang, et al., *Study of the Poly(3-hydroxybutyrate-co-3-hydroxyvalerate)/Cellulose Nanowhisker Composites Prepared by Solution Casting and Melt Processing.* Journal of Composite Materials, 2008. **42**(24): p. 2629-2645.

111. Ten, E., et al., *Thermal and mechanical properties of poly(3-hydroxybutyrate-co-3-hydroxyvalerate)/cellulose nanowhiskers composites.* Polymer, 2010. **51**(12): p. 2652-2660.

112. Martínez-Sanz, M., et al., *Characterization of polyhydroxyalkanoates synthesized from microbial mixed cultures and of their nanobiocomposites with bacterial cellulose nanowhiskers.* New Biotechnology, 2014. **31**(4): p. 364-376.

113. Ten, E., et al., *Effects of Cellulose Nanowhiskers on Mechanical, Dielectric, and Rheological Properties of Poly(3-hydroxybutyrate-co-3-hydroxyvalerate)/Cellulose Nanowhisker Composites.* Industrial & Engineering Chemistry Research, 2012. **51**(7): p. 2941-2951.

114. Yu, H.-y., Z.-y. Qin, and Z. Zhou, *Cellulose nanocrystals as green fillers to improve crystallization and hydrophilic property of poly(3-hydroxybutyrate-co-3-hydroxyvalerate).* Progress in Natural Science: Materials International, 2011. **21**(6): p. 478-484.

115. S. de O. Patrício, P., et al., *Increasing the elongation at break of polyhydroxybutyrate biopolymer: Effect of cellulose nanowhiskers on mechanical and thermal properties.* Journal of Applied Polymer Science, 2013. **127**(5): p. 3613-3621.

116. Yu, H., C. Yan, and J. Yao, *Fully biodegradable food packaging materials based on functionalized cellulose nanocrystals/poly(3-hydroxybutyrate-co-3-hydroxyvalerate) nanocomposites.* RSC Advances, 2014. **4**(104): p. 59792-59802.

117. Zhu, C., et al., *The effect of nucleating agents on physical properties of poly-3-hydroxybutyrate (PHB) and poly-3-hydroxybutyrate-co-3-hydroxyvalerate (PHB-co-HV) produced by Burkholderia cepacia ATCC 17759.* Polymer Testing, 2012. **31**(5): p. 579-585.

118. Babu, R., K. O'Connor, and R. Seeram, *Current progress on bio-based polymers and their future trends.* Prog. Biomat., 2013. **2**(1): p. 1-16.

119. Pan, P., et al., *Crystallization kinetics of bacterial poly(3-hydroxylbutyrate) copolyesters with cyanuric acid as a nucleating agent.* Journal of Applied Polymer Science, 2013. **129**(3): p. 1374-1382.

120. Luo, R., K. Xu, and G. Chen, *Effects of L-phenylalanine as a nucleation agent on the nonisothermal crystallization, melting behavior, and mechanical properties of poly(3-hydroxybutyrate-co-3-hydroxyhexanoate).* Journal of Applied Polymer Science, 2008. **110**(5): p. 2950-2956.

121. Lim, J.S., I. Noda, and S.S. Im, *Miscibility and crystallization behavior of poly(3-hydroxybutyrate-co-3-hydroxyhexanoate) and methoxy poly(ethylene glycol) blends.* Journal of Polymer Science Part B: Polymer Physics, 2006. **44**(19): p. 2852-2863.

122. Khandal, D., E. Pollet, and L. Averous, *CHAPTER 6 Polyhydroxyalkanoate-based Multiphase Materials*, in *Polyhydroxyalkanoate (PHA) based Blends, Composites and Nanocomposites*. 2015, The Royal Society of Chemistry. p. 119-140.

123. Puente, J.A.S., et al., *Effect of boron nitride as a nucleating agent on the crystallization of bacterial poly(3-hydroxybutyrate).* Journal of Applied Polymer Science, 2013. **128**(5): p. 2586-2594.

124. Kai, W., Y. He, and Y. Inoue, *Fast crystallization of poly(3-hydroxybutyrate) and poly(3-hydroxybutyrate-co-3-hydroxyvalerate) with talc and boron nitride as nucleating agents.* Polym Int, 2005. **54**(5): p. 780-789.

125. Dong, T., et al., *Rapid crystallization of poly(3-hydroxybutyrate-co-3-hydroxyhexanoate) copolymer accelerated by cyclodextrin-complex as nucleating agent.* Carbohydrate Polymers, 2010. **80**(2): p. 387-393.

126. Black, S.N., et al., *Crystal chemistry and nucleating agents; saccharin and poly-3-hydroxybutyrate.* Journal of Materials Science Letters, 1990. **9**(1): p. 51-52.

127. Weihua, K., et al., *Effect of lignin particles as a nucleating agent on crystallization of poly(3-hydroxybutyrate).* Journal of Applied Polymer Science, 2004. **94**(6): p. 2466-2474.

128. Organ, S.J. and P.J. Barham, *Nucleation of poly(hydroxy butyrate) by epitaxy on nitrogen-containing compounds.* Journal of Materials Science, 1992. **27**(12): p. 3239-3242.

129. Jacquel, N., et al., *Nucleation mechanism of polyhydroxybutyrate and poly(hydroxybutyrate-co-hydroxyhexanoate) crystallized by orotic acid as a nucleating agent.* Journal of Applied Polymer Science, 2010. **115**(2): p. 709-715.

130. He, Y. and Y. Inoue, *Effect of α-cyclodextrin on the crystallization of poly (3-hydroxybutyrate).* Journal of Polymer Science Part B: Polymer Physics, 2004. **42**(18): p. 3461-3469.

131. Zhu, C., et al., *The effect of nucleating agents on physical properties of poly-3-hydroxybutyrate (PHB) and poly-3-hydroxybutyrate-co-3-hydroxyvalerate (PHB-co-HV) produced by Burkholderia cepacia ATCC 17759.* Polym. Test., 2012. **31**(5): p. 579-585.

132. Wang, L., et al., *Effect of nucleation agents on the crystallization of poly(3-hydroxybutyrate-co-4-hydroxybutyrate) (P3/4HB).* J. Appl. Polym. Sci., 2010. **116**(2): p. 1116-1123.

133. Petchwattana, N., S. Covavisaruch, and S. Petthai, *Influence of talc particle size and content on crystallization behavior, mechanical properties and morphology of poly(lactic acid).* Polym. Bull., 2014. **71**(8): p. 1947-1959.

134. Martin, O., et al., *Properties of Biodegradable Multilayer Films Based on Plasticized Wheat Starch.* Starch - Stärke, 2001. **53**(8): p. 372-380.

135. Fabra, M.J., A. Lopez-Rubio, and J.M. Lagaron, *Nanostructured interlayers of zein to improve the barrier properties of high barrier polyhydroxyalkanoates and other polyesters.* Journal of Food Engineering, 2014. **127**(0): p. 1-9.

136. Cunha, M., et al., *Film blowing of PHBV blends and PHBV-based multilayers for the production of biodegradable packages.* Journal of Applied Polymer Science, 2015: p. n/a-n/a.

137. Thellen, C., S. Cheney, and J.A. Ratto, *Melt processing and characterization of polyvinyl alcohol and polyhydroxyalkanoate multilayer films.* Journal of Applied Polymer Science, 2013. **127**(3): p. 2314-2324.

Chapter 2.

CHARACTERIZATION OF VIRGIN POLYMERS

In this chapter, a general characterization of the selected virgin polymers is presented. The primary properties that are investigated are molecular weight distribution, thermal stability, crystallization properties, tensile behavior and gas permeability. The material properties of each polymer are compared and critical drawbacks are identified. A (large) part of this chapter was published as Vandewijngaarden, J., Murariu, M., Dubois, P., Carleer, R., Yperman, J., Adriaensens, P., Schreurs, S., Lepot, N., Peeters, R., Buntinx, M.: Gas Permeability Properties of Poly(3-hydroxybutyrate-co-3-hydroxyhexanoate), Journal of Polymers and the Environment 22:4, p. 501-507

2.1 MATERIALS AND METHODS

2.1.1 Materials

PHBV in pure powdered form was purchased from Tianan Biologic (Ningbo City, China). The 3-hydroxyvalerate content of the material was determined to be 2.8 mol% with ^{1}H-NMR in deuteroform. PHBHHx (pure powdered form) and Aonilex pellets (based on PHBHHx) were kindly provided by Kaneka (Westerlo-Oevel, Belgium). The 3-hydroxyhexanoate content of these samples were determined to be 10.5 mol%. The polymer samples were dried *in vacuo* at 70 °C for 5 days before use and stored in a desiccator.

2.1.2 Sample preparation

Most analyses were performed on the virgin powders or pellets. For permeability testing, about 1.8 g of PHBHHx or Aonilex was compressed and molded at 170 °C to prepare films in a polyimide mold (100 mm x 100 mm x 0.150 mm) using an Agila PE20 hydraulic press. The polymer was pre-heated for 3 min without pressure before being pressed at 30 bar for 120 s, followed by two degassing cycles. Finally, the films were pressed at high pressure of 150 bar for 120 s,

followed by 20 min slow cooling at 50 bar and 60 °C to allow film crystallization and easy demolding.

For tensile testing, thicker plates of about 6.9 g were produced in a stainless steel mold (100 mm x 100 mm x 0.5 mm) at 160 °C (for PHBHHx and Aonilex) or 190 °C (for PHBV) with a pre-heating time of 3 min before being pressed at 30 bar for 200 s. Subsequently two degassing cycles were used before finally molding the sample at 150 bar for 150 s. The samples were slowly cooled at 50 bar and 60 °C for 20 min.

2.1.3 Gel permeation chromatography (GPC)

The molecular weight distribution of PHBHHx was analyzed using a GPC apparatus composed of a SpectroSeries P100 pump, equipped with a Shodex RI71 refractometer detector and two PL-gel 10 µl Mixed-B columns in series, thermostated at 35 °C. The eluent was chloroform (VWR, HPLC grade) at a flow rate of 1.0 ml/min. Dried polymer samples were dissolved in chloroform at a concentration of 1 g/l. The injection volume was 100 µl. Calibration was performed using polystyrene standards (474 to 3 150 000 g/mol) dissolved in chloroform with a concentration of 1 g/l.

2.1.4 Differential scanning calorimetry (DSC)

Differential scanning calorimetry (DSC) was performed under inert atmosphere (50 ml/min nitrogen) using a TA Instruments Q200. About 3-4 mg of the polymer in a sealed aluminium pan was used to perform the measurements. The sample pan was heated from -30 °C to 150 °C (for PHBHHx and Aonilex) and 190 °C (for PHBV). After being kept isothermal for 2 min, the sample was cooled at -30 °C and kept constant for 2 min before heating again to 150 °C and 190 °C. Separate experiments using heating/cooling rates of 10 °C/min and 20 °C/min were performed. All measurements were performed in duplicate.

2.1.5 Thermogravimetric analysis (TGA)

The thermal stability of the samples was analysed using a TA Instruments Hi-Res TGA 2950 thermogravimetric analyser. Samples of about 10 mg were heated from room temperature to 350 °C at a heating rate of 20 °C/min with a N_2 gas flow of 80 ml/min. To provide a mean value, measurements were performed at least in duplicate.

2.1.6 Tensile testing

The tensile test was performed using a MTS/10 tensile tester at a crosshead speed of 1 mm/min and a distance of 25.4 mm between the grips. PHBHHx and Aonilex samples were cut into dumbbell shapes (ASTM D638-02 type V). Due to their brittleness, PHBV samples could not be cut into dumbbell shapes and were thus cut into strips of 150 x 15 mm and tested according to ISO 527 (sample type 2) using a crosshead speed of 1 mm/min. All samples were conditioned at 23 °C and 50 % relative humidity (RH) for at least two days prior to testing. At least 10 samples of each polymer were analyzed in order to obtain a representative average

2.1.7 Thickness measurements

Sample thickness was measured prior to permeability testing using a MTS MI20 thickness gauge. The thickness was taken as the average of five measurements for different locations of each sample.

2.1.8 Gas permeability

The oxygen transmission rate (OTR), at 23 °C and 0 % RH, of the produced samples was measured using a Mocon Ox-Tran 702 (ASTM D3985). OTR measurements at varying RH (same RH on both sides of the film) and temperature were performed using a Mocon Ox-Tran 2/20 (ASTM F1927). Carbon dioxide transmission rate (CO_2TR) at 23 °C and 0 % RH was measured using a Mocon Permatran-C 4/41 (ASTM F2476). Water vapor transmission rate (WVTR) was measured using a Mocon Permatran-W 700 (ASTM F1249). Test gases (O_2 and CO_2) and carrier gas (N_2, N_2/H_2) with a purity of 99.999 % were purchased from Westfalen, Münster (Germany). Samples were placed between 2 aluminium masks with an effective testing area of 5 cm². The sample was exposed to the test gas on one side and to a continuously flushing carrier gas on the other side, both at a

total pressure of 1 atm. For OTR measurements a carrier gas N_2/H_2 (95/5) was used, for all other measurements pure N_2. The test gas diffuses through the sample and is guided by the carrier gas towards the detector. The gas transmission rate or gas flux *J*, in cm³/m².day.atm (for OTR and CO_2TR) or g/m².day (for WVTR) of the specific test gas, is reported when the concentration of test gas in the carrier gas changes less than 1 % during a test cycle of 30 min. The gas flux *J* can be defined as the quantity of test gas or permeant *Q*, which passes through the polymeric film per unit area *A* during one unit of time *t* [1-3]:

$$J = Q / (A.t) \quad (2\text{-}1)$$

In order to obtain a thickness-independent criterion for comparison, the gas flux *J* can be normalized for sample thickness *d* and permeant pressure *p* to obtain the permeability coefficient *P* :

$$P = J.d / p \quad (2\text{-}2)$$

Of each sample, at least two specimen were measured in duplicate.

2.2 RESULTS AND DISCUSSION

2.2.1 Molecular weight distribution

The molecular weight distribution of the virgin polymers is analyzed using GPC, yielding the number average molecular weight $\bar{M}_n$, the weight average molecular weight $\bar{M}_w$ and the dispersity $Đ_M$, which is defined as the ratio of $\bar{M}_w$ to $\bar{M}_n$. These results are presented in Table 2-1.

Table 2-1: Molecular weight distribution of virgin polymers

Sample	$\bar{M}_n$ (x 10^3 g/mol)	$\bar{M}_w$ (x 10^3 g/mol)	$Đ_M$
PHBV	134	442	3.3
PHBHHx	272	686	2.5
Aonilex	247	557	2.3

Virgin PHBV has a significantly lower molecular weight than PHBHHx and the dispersity is higher as well, indicative of a broader range of molecular weights. From the results, it can also be derived that the molecular weight of Aonilex is lower than that of PHBHHx. This is logical since Aonilex is a commercial granulate produced from thermally processed PHBHHx. PHBHHx is the pristine polymer, not yet undergone any processing, and thus displays a higher molecular weight.

2.2.2 Thermal properties

Firstly the thermal stability of the virgin polymers was investigated using TGA, a technique which yields weight loss curves as function of temperature. It is widely accepted that thermal degradation of PHBV and PHBHHx occurs through the same mechanism as PHB, which is random chain scission (*cis*-elimination), involving a six-membered ring transition state (as shown in), followed by an auto-accelerated degradation due to the formation of low molecular weight reaction products [4-7].

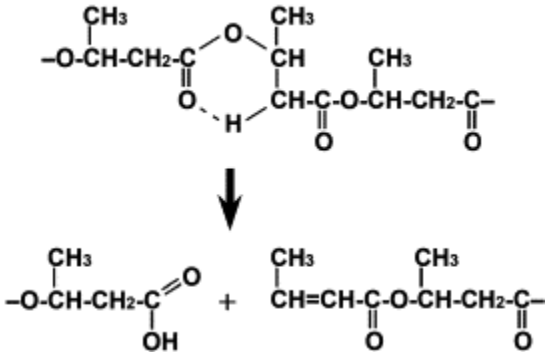

Figure 2-1: cis-elimination of poly(3-hydroxybutyrate) [7]

From the weight loss curve and its first derivative (d*m*/d*t*) the thermal degradation onset temperature $T_{d,o}$, calculated as the intersection of the extrapolated initial base line and the tangent to the inflection point, $T_{d,50}$, the temperature at 50 % weight loss, and the degradation peak temperature $T_{d,p}$, peak of the first derivative of the weight loss curve, were determined. This terminology is illustrated in Figure 2-2 and the results are presented in Table 2-2.

Upon comparison of PHBV and PHBHHx it is clear that PHBV is slightly less stable than PHBHHx the thermal degradation behavior is fairly similar for both polymers, with PHBHHx displaying a $T_{d,o}$, $T_{d,50}$ and $T_{d,p}$ of about 11 to 13 °C higher.

The thermal stability of Aonilex is practically the same as that of PHBHHx, which was to be expected as these materials are based on the same polymer.

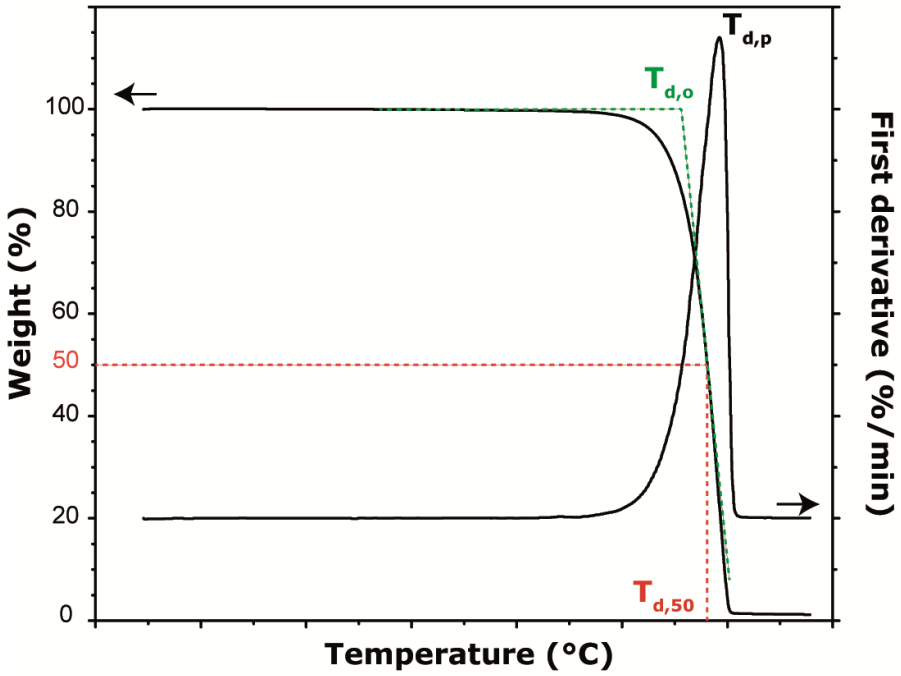

Figure 2-2: Terminology for TGA interpretation

From a processing point of view, the parameter processing window was introduced. In this study, the processing window was calculated as the difference between $T_{d,o}$ and the melting peak temperature (determined using the heat flow curve from the DSC measurement). The processing window is an indication of the suitable temperature interval for melt processing of the polymer. However, one must keep in mind that this is a bit smaller for practical applications, as the processing temperature is usually kept well below the degradation temperature.

Table 2-2: Thermal stability of virgin polymers

Sample	$T_{d,o}$ (°C)	$T_{d,50}$ (°C)	$T_{d,p}$ (°C)	Processing window (°C)
PHBV	278.5	289.6	296.9	106
PHBHHx	291.8	302.9	308.1	157
Aonilex	290.5	301.0	307.0	162

PHBV was determined to have a processing window of about 106 °C, whereas PHBHHx and Aonilex display significantly larger values of 157 °C and 162 °C, respectively. These results present a clear advantage of PHBHHx over PHBV in terms of thermal stability. The difference between PHBHHx and Aonilex can be attributed to the slightly lower melting temperature of the latter.

The thermal properties investigated by differential scanning calorimetry (DSC) are melting behavior, crystallization and glass transition. The first melting run, crystallization run and second melting run (performed with a heating rate of 20 °C/min) are presented in Figure 2-3. The values corresponding to all relevant parameters, for both heating rates (10 and 20 °C/min), can be found in Table 2-3. The first heating run was not discussed in detail, as the production history (processing, extractions etc.) of the polymers was not disclosed by the supplier of the materials. Though the first heating run of PHBV is rather simple, displaying only a single melting peak, those of PHBHHx and Aonilex are far too complex to interpret without any knowledge of history or pretreatment. Only the onset of melting $T_{m,o}$ and melting peak temperature of the melting peak $T_{m,p}$ at the highest temperature is given in order to have an idea of the melting temperature that should be kept in mind during melt processing. The onset of melting is determined as the intersect of the slope of the peak and the extrapolated baseline. It is clear that PHBV shows a significantly higher $T_{m,p}$ (around 173 °C) than PHBHHx and Aonilex (around 129-135 °C), indicating that the latter two require less energy to be brought into the molten state during processing.

After the first heating run, the samples are cooled to -30 °C in order to investigate the crystallization behavior. DSC measurements were performed at two different heating/cooling rates to observe any phenomena induced by rate of cooling. At the slow cooling rate of 10 °C/min, PHBV displays a crystallization peak with an onset temperature $T_{c,o}$ and peak temperature $T_{c,p}$ at 95.9 and 86.6 °C, respectively, corresponding to a crystallization enthalpy ΔH_c of 68.2 J/g.

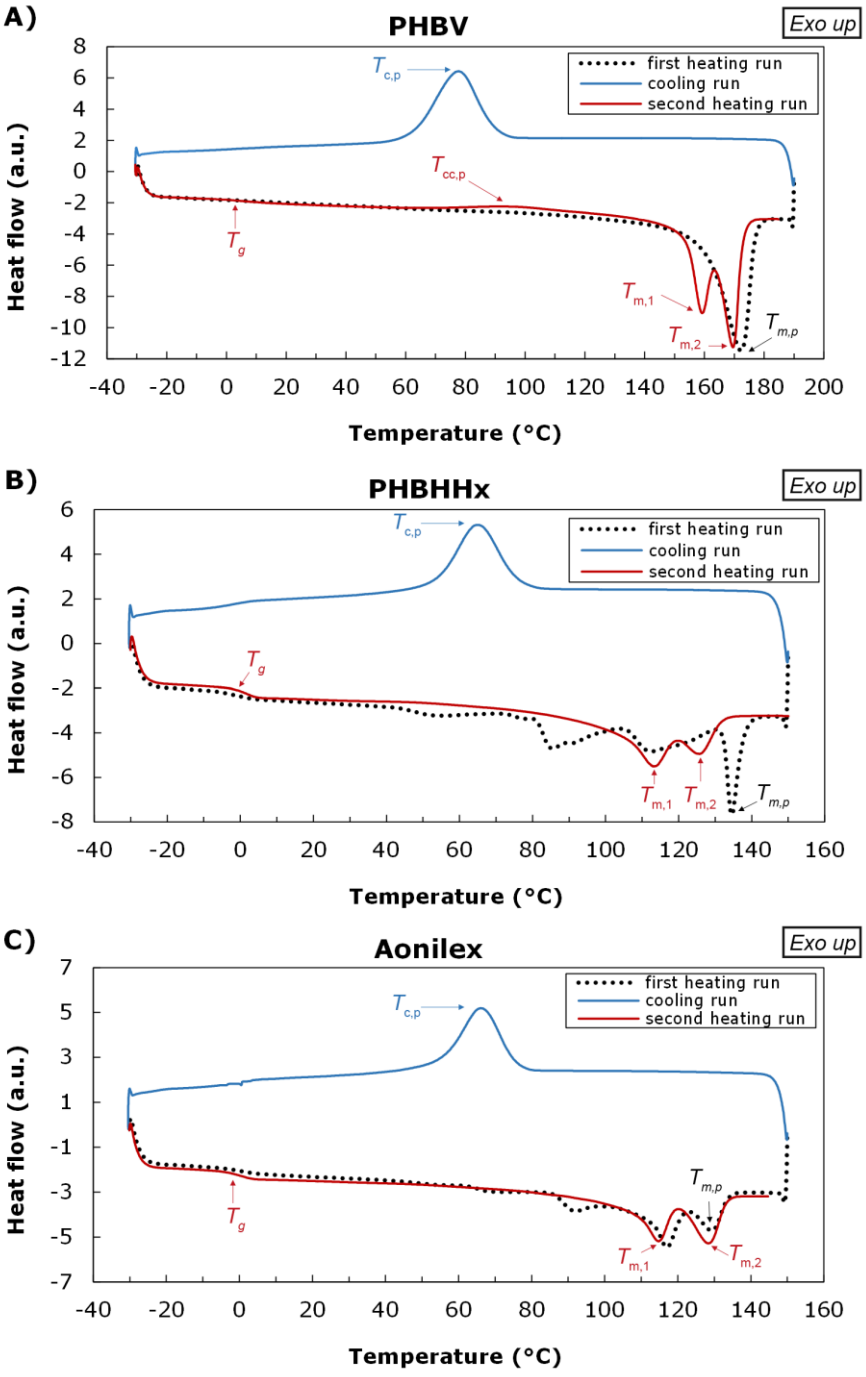

Figure 2-3: DSC thermograms at 20 °C/min of A) PHBV, B) PHBHHx and C) Aonilex powder or granulates

When using a higher cooling rate (20 °C/min), $T_{c,o}$ and $T_{c,p}$ shift to a slightly lower temperature. However, ΔH_c was reduced significantly to a value of 61.2 J/g, indicative of a crystallization not being able to be completed during the cooling run. PHBHHx and Aonilex both showed a $T_{c,o}$ and $T_{c,p}$ significantly lower than that of PHBV. Aonilex seemed to perform slightly better than PHBHHx in terms of crystallization. $T_{c,p}$ occurred a few degrees higher at around 76.4 °C (at 10 °C/min) than for PHBHHx. It can also be noted that, during crystallization, Aonilex displayed a slightly higher ΔH_c, namely 35.4 J/g, than PHBHHx (31.5 J/g). It is clear that the commercial granulate Aonilex contains certain processing aids that slightly increase the crystallization rate, but also raise the degree of crystallinity during cooling. This same trend could be observed for cooling at 20 °C/min.

In general, one can conclude that all three materials display a rather broad crystallization peak, occurring at relatively low temperatures, which could prove to be problematic for processing. PHBV crystallizes at slightly higher temperatures than PHBHHx and Aonilex, but displays a much higher crystallization enthalpy.

By observing the second heating run, extra insights into the melt crystallization that preceded it can be obtained. A first observation is the occurrence of a double melting peak for all three samples during the second heating run. This phenomenon is usually explained by the melting-recrystallization-remelting model. According to this model, the observed double melting curve is actually a superposition of three thermal contributions, namely 1) an endothermal transition associated with the melting of the original crystals formed before the heating scan, 2) an exothermal transition corresponding to recrystallization following the initial melting and 3) another endothermal transition associated with the melting of crystals formed by the recrystallization process [8, 9].

A second observation that can be made, is the occurrence of a small cold crystallization peak in the second heating run of PHBV (with cooling rate of 20 °C/min), with an onset temperature $T_{cc,o}$ and peak temperature $T_{cc,p}$ of 73.1 and 92.0 °C, respectively. This is indicative of crystallization not being able to complete during crystallization from the melt. During subsequent heating, enough energy will be provided to the polymeric system to complete crystallization. The surface area of the peak was too small to calculate the cold crystallization enthalpy.

Table 2-3: Thermal properties measured by DSC with a heating/cooling rate of 10 °C/min and 20 °C/min

Heating/cooling rate: 10 °C/min								
	melting (1st heating run)			*crystallization (cooling run)*			*melting (2nd heating run)*	
Sample	$T_{m,o}$	$T_{m,p}$	ΔH_m	$T_{c,o}$	$T_{c,p}$	ΔH_c	$T_{m,1}$	$T_{m,2}$
PHBV	162.2	172.9	86.9	95.9	86.6	68.2	162.0	171.7
PHBHHx	n.d.	133.2	n.d.	83.9	75.0	31.5	115.7	127.2
Aonilex	n.d.	129.1	n.d.	82.9	76.4	35.4	118.0	130.6

Heating/cooling rate: 20 °C/min											
	melting (1st heating run)				*crystallization (cooling run)*			*melting (2nd heating run)*			
Sample	$T_{m,o}$	$T_{m,p}$	ΔH_m	T_g	$T_{c,o}$	$T_{c,p}$	ΔH_c	$T_{m,1}$	$T_{m,2}$	$T_{cc,o}$	$T_{cc,p}$
PHBV	159.7	172.3	87.1	4.0	90.5	78.1	61.2	162.0	171.7	73.1	92.0
PHBHHx	n.d.	134.5	n.d.	1.4	76.2	64.7	31.2	113.3	125.5	n.d.	n.d.
Aonilex	n.d.	128.9	n.d.	1.1	75.8	66.2	34.8	114.8	128.5	n.d.	n.d.

n.d. = not detected

2.2.3 Tensile properties

The tensile properties of the virgin polymers, after compression molding into plates of about 0.5 mm thick, are presented in Table 2-4. From the tensile test, following parameters were obtained: Young's modulus (slope of initial linear part of stress-strain curve), maximum tensile strength, nominal strain at maximum load (strain where load/tensile strength reaches a maximum) and nominal strain at break (final strain of sample upon breaking).

At first glance, it becomes clear that the properties of PHBHHx and Aonilex are fairly similar, though Aonilex seems to present slightly lower values for nominal strain at break and strain at max. load, which is most likely due to the presence of certain additives in the commercial granulate Aonilex. Aonilex and PHBHHx display a rather low Young's modulus and a rather high degree of ductility, which can be observed from the nominal strain at break. PHBV, on the other hand, is obviously much more brittle and stiffer. The Young's modulus for PHBV is much higher (2.5 GPa) than that for PHBHHx (804 MPa). For PHBV, the nominal strain at max. load is not reported, as this coincided with the nominal strain at break, due to its brittleness.

Table 2-4: Tensile properties of virgin polymers

Sample	Young's modulus (MPa)	Max. tensile strength (MPa)	Nominal strain at max. load (%)	Nominal strain at break (%)
PHBV	2503 (± 134)	15.7 (± 2.4)	/	0.6 (± 0.1)
PHBHHx	804 (± 24)	21.5 (± 0.5)	6.8 (± 0.2)	8.4 (± 0.4)
Aonilex	734 (± 43)	19.3 (± 0.3)	5.7 (± 0.2)	7.1 (± 0.3)

2.2.4 Gas permeability

A major criterion to decide for which food packaging applications a polymer can be considered is its gas permeability (barrier properties) for gases such as O_2, CO_2 and water vapor. In order to compare the barrier properties with those of other polymers, the gas transmission rate must be converted to the permeability coefficient by multiplying with sample thickness (mm).

Due to the brittleness of the PHBV samples, it was not possible to measure the gas permeability. In this paragraph, the permeability properties of PHBHHx Aonilex are investigated.

The permeability coefficients at 23 °C and 0 % RH for PHBHHx and Aonilex are presented in Table 2-5. It is clear that PCO_2 (54 $cm^3.mm/m^2.day.atm$) is much higher than PO_2 (8.3 $cm^3.mm/m^2.day.atm$), which can be attributed to a difference in kinetic diameter of the gas molecules, which is 3.46 Å for O_2 and 3.3 Å for CO_2 [10]. A smaller kinetic diameter will facilitate a higher permeability throughout the polymer. PH_2O was determined to be 1.42 (± 0.04) $g.mm/m^2.day$. It can also be seen that the permeability values of Aonilex are slightly higher than those of PHBHHx, an observation that recurs in Chapter 5. However, both materials still reside in the same range of applicability and can thus be considered as practically equally performant in permeability properties.

Table 2-5: Permeability properties of PHBHHx

	PHBHHx	**Aonilex***
PO_2 ($cm^3.mm.m^{-2}.day^{-1}.atm^{-1}$)	8.3 (± 0.2)	9.3 (± 0.4)
PCO_2 ($cm^3.mm.m^{-2}.day^{-1}.atm^{-1}$)	54 (± 1)	55 (± 1)
PH_2O ($g.mm.m^{-2}.day^{-1}$)	1.42 (± 0.04)	1.51 (± 0.05)

* The permeability values for Aonilex were taken as the average of the values obtained in Chapters 5 and 6

Comparison with common packaging plastics:

For evaluation of PHBHHx as a packaging material, the permeability coefficients were compared to literature data of more conventional packaging polymers (see Table 2-6 [11-15]). PO_2 of PHBHHx is 6 to 25 times lower than PO_2 of conventional packaging materials such as PP, PE and polystyrene (PS). However, PO_2 value of PHBHHx is about 1.5 to 8 times higher than that of poly(ethylene terephthalate) (PET) and even 8 to 80 times higher than that of polyamide (PA). Compared to the known high-performance oxygen barrier of EVOH (used in multilayer systems), PO_2 of PHBHHx is much higher (900 to 9000 times).

The permeability coefficient for water vapor of PHBHHx is rather low, but still slightly higher than PP and PE, which is most likely due to the highly apolar nature of the latter two. PH_2O is very similar to those of PS, PA, PET, EVOH and PLA, but about 20 times lower than PH_2O of PVOH.

The permeability coefficient for CO_2 of PHBHHx is lower than for materials such as PP, PE and PS (2 to 20 times). However PCO_2 is higher than that of PET (7 to 18 times), PA (12 to 30 times) and EVOH/PVOH (about 1300 times). Unfortunately, plenty of different testing conditions are employed in the literature, so it must be noted that values of PCO_2 must be compared critically, when the testing conditions, i.e. temperature and RH, vary from the conditions used in this study.

Overall, PHBHHx showed a performance most comparable with PLA.

Effect of relative humidity and ambient temperature on PHBHHx gas permeability:

In order to further explore the application of PHBHHx as a packaging material, the effect of ambient RH and temperature on the oxygen permeability coefficient was investigated. This is valuable information, considering that a packaged product can be subjected to varying environmental conditions. It is known that RH can have a deteriorating effect on PO_2, especially for hydrophilic polymers [14, 16-20]. The results of this study are given in Figure 2-4 A. When increasing RH to 50 %, PO_2 increased slightly to 9.0 ± 0.3 $cm^3.mm/m^2.day.atm$, which corresponds to an increase of about 8.4 %. An 18.4 % increase, compared to 0 % RH, in PO_2 was observed at a RH of 70 %, reaching a PO_2 value of 9.8 ± 0.3 $cm^3.mm/m^2.day.atm$.

Table 2-6: Permeability properties of common packaging plastics

Polymer	PO_2 at 23 °C ($cm^3.mm/m^2.day.atm$) [9]	PCO_2 ($cm^3.mm/m^2.day.atm$) [10]	PH_2O 23 °C, 85 % RH ($g.mm/m^2.day$) [9]
Ethylene vinyl alcohol (EVOH)	0.001-0.01 (0% RH)	0.01-0.08 (23 °C, 0 % RH)	1-3
Poly(vinyl alcohol) (PVOH)	0.02 (0% RH)	0.04 (23 °C, 0 % RH)	30
Polyamide (PA)	0.1-1 (0% RH)	1.8-4.6 (23 °C; 0 % RH)	0.5-10
Poly(ethylene terephthalate) (PET)	1-5 (50 % RH)	3-7 (23 °C, 75 % RH)	0.5-2
Polylactic acid (PLA)	3.5-15 [8,11] (50 % RH)	35-72 [7,11] (23-30 °C, 0 % RH)	1.6-3.6 [8]
Polypropylene (PP)	50-100 (50 % RH)	200-900 (unknown conditions)	0.2-0.4
Polyethylene (PE)	50-200 (50 % RH)	100-1000 (23-25 °C, unknown RH)	0.5-2
Polystyrene (PS)	100-150 (50 % RH)	270-1000 (23 °C, 0 % RH)	1-4

Finally, the most pronounced increase of about 33.2 %, compared to 0 % RH, occurred at 90 % RH, with PO_2 reaching a value of 11.1 ± 0.4 cm³.mm/m².day.atm. Overall, it is clear that the ambient RH has a deteriorating effect on PO_2, but not as severe as compared to other hydrophilic polymers such as polyamide 6, cellophane and EVOH, of which PO_2 can increase up to 10, 100 and 1000 times respectively at a RH of 90 % [21, 22]. The increase in PO_2 of PHBHHx at higher RH can be explained by the slightly hydrophilic character of PHBHHx. The water vapor molecules that enter the polymer membrane can act as a plasticizing agent, resulting in an increase in polymer free volume and thus facilitating a higher oxygen permeability [17].

Oxygen permeability measurements at temperatures of 10, 16, 30 and 38 °C were additionally performed in order to assess the effect of ambient temperature. The results are presented in Figure 2-4 B. Upon lowering the ambient temperature from 23 °C to 10 °C a decrease in PO_2 of about 62 % was observed, with an absolute PO_2 of 3.3 ± 0.2 cm³.mm/m².day.atm. At a higher temperature of 38 °C, PO_2 shows a dramatic increase of about 200 %, reaching a PO_2 value of 26 ± 1 cm³.mm/m².day.atm. The temperature dependence of oxygen permeability can be described by an Arrhenius-type equation [23-26]:

$$PO_2 = P_0.e^{(-E/R.T)} \quad (2\text{-}3)$$

With P_0 the pre-exponential constant, T the temperature, R the molar gas constant and E the activation energy associated with permeability.

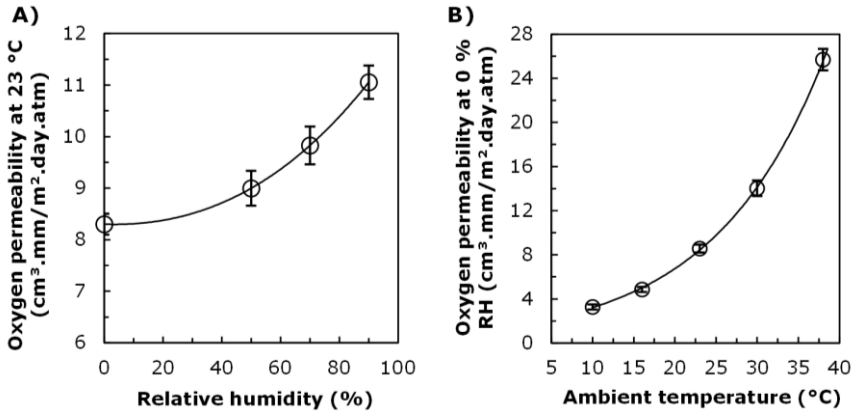

Figure 2-4: Effect of A) relative humidity at 23 °C and B) ambient temperature at 0 % RH on oxygen permeability of PHBHHx (n = 4)

Plotting of ln(PO_2) *versus* 1/T yielded a straight line with a slope of -6.519 and intercept of 24.2 (r^2 = 0.9982). The activation energy, calculated from the slope of the curve, is about 54 kJ/mol. The equation of the Arrhenius plot can be employed to estimate the oxygen permeability of PHBHHx at other temperatures.

Due to its inherent brittleness, it was not possible to produce thin PHBV films for permeability measurements. However, in order to be able to make some comparison, a concise overview of literature data on oxygen permeability of PHBV, with varying 3-hydroxyvalerate concentrations, is presented in Table 2-7. Though there is a great amount of variation between these literature data, it can be concluded that low 3-hydroxyvalerate PHBV samples display a slightly lower PO_2 than the PHBHHx used in this study. However, these types of PHBV are usually highly brittle. Upon increasing the 3-hydroxyvalerate content, in order to render the polymer less brittle, it is possible to observe an increasing trend in PO_2. As a result, less brittle types of PHBV possess values for oxygen permeability very similar to PHBHHx.

Table 2-7: Oxygen permeability data for PHBV with varying 3-hydroxyvalerate concentrations

3-HV content (mol%)	*T* (°C)	RH (%)	PO_2 ($cm^3.mm.m^{-2}.day^{-1}.atm^{-1}$)	
3	25	80	2.2	[27]
5	25	80	5.9	[28]
5	23	0	4.9	[29]
7	24	0	7.1	[30]
7	24	80	4.6	[30]
8	21	40	8.8	[31]
8	23	0	4.9	[29]
12	24	80	12.6	[32]
12	24	80	15.6	[33]
12	23	0	3.9	[29]
12	25	54	5.9	[34]
40	24	0	9.4	[30]
40	24	80	12.3	[30]

2.3 CONCLUSIONS

In this chapter, several basic properties of the three selected virgin polymers (PHBV, PHBHHx and Aonilex) were investigated. From the comparison of these results, the following conclusions can be drawn:

- The **processing window** of PHBV is rather narrow in comparison to PHBHHx and Aonilex, due to the lower melting temperatures for PHBHHx and Aonilex, whereas the thermal degradation temperature is fairly similar.
- Both PHBV and PHBHHx display flaws in **crystallization properties**, mostly in terms of rather low crystallization temperature and wide crystallization peaks, as measured by DSC. The commercial granulate Aonilex performs a bit better than the pure PHBHHx polymer.
- In terms of **tensile properties**, PHBHHx and Aonilex are quite similar and act as flexible polymers, with rather low Young's moduli. PHBV, on the other hand, appeared to be very brittle and stiff, which renders the application of this type of PHBV as flexible packaging material difficult.
- It was found that PHBHHx and Aonilex possess a relatively low oxygen **permeability** (compared to conventional polymers used in flexible film packaging) and a water vapor permeability slightly higher than highly apolar polymers (i.e. PE and PP). The carbon dioxide permeability of PHBHHx is rather high in comparison to known barrier materials such as PET, PA and EVOH, but still substantially lower than for common packaging materials PP and PE. This study also revealed that the oxygen permeability of PHBHHx shows only relatively minor increases of 8 % and 34 % upon increasing RH to 50 and 90 %, respectively. In addition, within the temperature range of 10 and 38°C (0% RH), the PO_2 increased from 3.3 ± 0.2 to 26 ± 1 $cm^3.mm/m^2.day.atm$. Investigation of the permeability properties of PHBV was not possible, due to its highly brittle nature.

From the results of Chapter 2, it must be concluded that slow crystallization is the main limitation of the selected PHA. The barrier properties, though showing a lot of potential, must be enhanced further as well for use as a food packaging material.

2.4 REFERENCES

1. Bronlund, J.E., G.P. Redding, and T.R. Robertson, *Modelling Steady-State Moisture Transport Through Corrugated Fibreboard Packaging.* Packag Technol Sci, 2013. **27**: p. 193-201.

2. Cagnon, T., et al., *Nanostructuring and Microstructuring of Materials from a Single Agropolymer for Sustainable MAP Preservation of Fresh Food.* Packag Technol Sci, 2013. **26**(3): p. 137-148.

3. Kuorwel, K.K., et al., *Physico-Mechanical Properties of Starch-Based Films Containing Naturally Derived Antimicrobial Agents.* Packag Technol Sci, 2013. **27**: p. 149-159.

4. Ariffin, H., et al., *Determination of multiple thermal degradation mechanisms of poly(3-hydroxybutyrate).* Polym Degrad Stab, 2008. **93**(8): p. 1433-1439.

5. Morikawa, H. and R.H. Marchessault, *Pyrolysis of bacterial polyalkanoates.* Can J Chem, 1981. **59**(15): p. 2306-2313.

6. Vogel, C., et al., *Thermal Degradation of Poly(3-hydroxybutyrate) and Poly(3-hydroxybutyrate-co-3-hydroxyhexanoate) in Nitrogen and Oxygen Studied by Thermogravimetric–Fourier Transform Infrared Spectroscopy.* Appl Spectrosc, 2007. **61**(7): p. 755-764.

7. Kim, K.J., Y. Doi, and H. Abe, *Effects of residual metal compounds and chain-end structure on thermal degradation of poly(3-hydroxybutyric acid).* Polymer Degradation and Stability, 2006. **91**(4): p. 769-777.

8. Ding, C., B. Cheng, and Q. Wu, *DSC analysis of isothermally melt-crystallized bacterial poly(3-hydroxybutyrate-co-3-hydroxyhexanoate) films.* Journal of Thermal Analysis and Calorimetry, 2011. **103**(3): p. 1001-1006.

9. Xu, C. and Z. Qiu, *Nonisothermal melt crystallization and subsequent melting behavior of biodegradable poly(hydroxybutyrate)/multiwalled carbon nanotubes nanocomposites.* Journal of Polymer Science Part B: Polymer Physics, 2009. **47**(22): p. 2238-2246.

10. Matteucci, S., et al., *Transport of Gases and Vapors in Glassy and Rubbery Polymers*, in *Materials Science of Membranes for Gas and Vapor Separation*. 2006, John Wiley & Sons, Ltd: Chichester. p. 1-47.

11. Bao, L., et al., *Gas permeation properties of poly(lactic acid) revisited.* Journal of Membrane Science, 2006. **285**(1–2): p. 166-172.

12. Drieskens, M., et al., *Structure versus properties relationship of poly(lactic acid). I. Effect of crystallinity on barrier properties.* Journal of Polymer Science Part B: Polymer Physics, 2009. **47**(22): p. 2247-2258.

13. Lange, J. and Y. Wyser, *Recent innovations in barrier technologies for plastic packaging—a review.* Packag Technol Sci, 2003. **16**(4): p. 149-158.

14. Massey, L.K., *Permeability Properties of Plastics and Elastomers*. 2002, New York: William Andrew Inc.

15. Siracusa, V., et al., *Poly(lactic acid)-modified films for food packaging application: Physical, mechanical, and barrier behavior.* J Appl Polym Sci, 2012. **125**(S2): p. 390-401.

16. Aulin, C., M. Gällstedt, and T. Lindström, *Oxygen and oil barrier properties of microfibrillated cellulose films and coatings.* Cellulose, 2010. **17**(3): p. 559-574.

17. Hong, S.-I. and J.M. Krochta, *Oxygen barrier performance of whey-protein-coated plastic films as affected by temperature, relative humidity, base film and protein type.* J Food Eng, 2006. **77**(3): p. 739-745.

18. Mujica-Paz, H. and N. Gontard, *Oxygen and Carbon Dioxide Permeability of Wheat Gluten Film: Effect of Relative Humidity and Temperature.* J Agric Food Chem, 1997. **45**(10): p. 4101-4105.

19. Muramatsu, M., et al., *Oxygen permeability and free volume hole size in ethylene–vinyl alcohol copolymer film: temperature and humidity dependence.* Radiat Phys Chem, 2003. **68**(3–4): p. 561-564.

20. Siracusa, V., *Food Packaging Permeability Behaviour: A Report.* Int J Polym Sci, 2012. **2012**: p. 11.

21. Dhoot, S.N., B.D. Freeman, and M.E. Stewart, *Barrier Polymers*, in *Encyclopedia of Polymer Science and Technology*. 2002, John Wiley & Sons, Inc. p. 198-263.

22. Gontard, N., et al., *Influence of Relative Humidity and Film Composition on Oxygen and Carbon Dioxide Permeabilities of Edible Films.* J Agric Food Chem, 1996. **44**(4): p. 1064-1069.

23. Gajdoš, J., et al., *Gas permeability and DSC characteristics of polymers used in food packaging.* Polym Test, 2000. **20**(1): p. 49-57.

24. Mrkić, S., K. Galić, and M. Ivanković, *Effect of Temperature and Mechanical Stress on Barrier Properties of Polymeric Films Used for Food Packaging.* J Plast Film Sheet, 2007. **23**(3): p. 239-256.

25. Mrkic, S., et al., *Gas transport and thermal characterization of mono- and di-polyethylene films used for food packaging.* J. Appl. Polym. Sci., 2006. **99**(4): p. 1590-1599.

26. Wang, Y., A.J. Easteal, and X.D. Chen, *Ethylene and oxygen permeability through polyethylene packaging films.* Packag Technol Sci, 1998. **11**(4): p. 169-178.

27. Fabra, M.J., A. López-Rubio, and J.M. Lagaron, *On the use of different hydrocolloids as electrospun adhesive interlayers to enhance the barrier properties of polyhydroxyalkanoates of interest in fully renewable food packaging concepts.* Food Hydrocolloids, 2014. **39**: p. 77-84.

28. Fabra, M.J., A. Lopez-Rubio, and J.M. Lagaron, *Nanostructured interlayers of zein to improve the barrier properties of high barrier polyhydroxyalkanoates and other polyesters.* Journal of Food Engineering, 2014. **127**(0): p. 1-9.

29. Thellen, C., et al., *A Processing, Characterization and Marine Biodegradation Study of Melt-Extruded Polyhydroxyalkanoate (PHA) Films.* Journal of Polymers and the Environment, 2008. **16**(1): p. 1-11.

30. Martínez-Sanz, M., et al., *Characterization of polyhydroxyalkanoates synthesized from microbial mixed cultures and of their nanobiocomposites with bacterial cellulose nanowhiskers.* New Biotechnology, 2014. **31**(4): p. 364-376.

31. Cava, D., et al., *Comparative performance and barrier properties of biodegradable thermoplastics and nanobiocomposites versus PET for food packaging applications.* Journal of Plastic Film and Sheeting, 2006. **22**(4): p. 265-274.

32. Sanchez-Garcia, M.D., J.M. Lagaron, and S.V. Hoa, *Effect of addition of carbon nanofibers and carbon nanotubes on properties of thermoplastic biopolymers.* Composites Science and Technology, 2010. **70**(7): p. 1095-1105.

33. Sanchez-Garcia, M.D. and J.M. Lagaron, *Novel clay-based nanobiocomposites of biopolyesters with synergistic barrier to UV light, gas, and vapour.* J Appl Polym Sci, 2010. **118**(1): p. 188-199.

34. Díez-Pascual, A.M. and A.L. Díez-Vicente, *ZnO-Reinforced Poly(3-hydroxybutyrate-co-3-hydroxyvalerate) Bionanocomposites with Antimicrobial Function for Food Packaging.* ACS Applied Materials & Interfaces, 2014. **6**(12): p. 9822-9834.

Chapter 3.

EFFECT OF NUCLEATING AGENTS ON NON-ISOTHERMAL CRYSTALLIZATION PROPERTIES OF POLY(3-HYDROXYBUTYRATE-CO-3-HYDROXYVALERATE)

In this chapter, the effect of orotic acid, a novel nucleating agent for polyhydroxyalkanoates, on the crystallization of poly(3-hydroxybutyrate-co-3-hydroxyvalerate) is investigated and compared to the more conventional ceramic nucleating agent boron nitride. Both nucleating agents were added in two concentrations (0.5 and 1.0 wt%) and the effect on non-isothermal crystallization was extensively investigated and modelled.

3.1 INTRODUCTION TO POLYMER CRYSTALLIZATION

The crystallization of a polymer from the liquid molten state can be subdivided into two phenomena: 1) the formation of small nuclei (nano-sized seed crystals) and 2) the growth of these nuclei into large crystallites (micron-sized) in one, two or three dimensions.

Upon cooling of a molten polymer to a temperature below its melting temperature, small nuclei of different sizes and shapes are initially formed as a result of density fluctuations in the liquid [1]. In order to effectively grow into larger crystals, these nuclei must reach a critical radius. Sub-critical sized nuclei dissolve back into the polymer melt, whereas the supercritical nuclei can grow and eventually complete crystallization [1, 2].

If absolutely no preformed nuclei or foreign particles are present, **homogeneous nucleation** occurs [2]. This phenomenon is however rare as it is very tasking to synthesize a material completely absent of impurities [3]. If a foreign substance is introduced into the polymer, it is possible that the critical radius of the nuclei is

reduced, resulting in a process called **heterogeneous nucleation**, occurring on the surface of these foreign particles [2].

These foreign particles can be added involuntary (e.g. catalyst residues) or purposely in order to effectively enhance the polymer crystallization properties. In the latter case, these foreign surfaces are called nucleating agents. Over the years, two types of heterogeneous nucleation have been proposed. The first type is called **epitaxial nucleation**, a physical interaction during which compatibility in crystalline structure of the polymer and the nucleating agent will facilitate the formation of nuclei on the surface of the nucleating agent [3, 4]. The second type of heterogeneous nucleation is called **chemical nucleation**. For polymers with reactive groups in the main chain (i.e. polyesters and polyamides), it is possible that a chemical reaction occurs between these groups and the nucleating agent. Poly(ethylene terephthalate), for example, is often nucleated with salts of benzoic acid. These salts can dissolve into the polymer melt and act as chemical reagents. As a result, a decrease in molecular weight, together with the formation of ionic clusters, which act as nuclei for crystal growth, is observed [4, 5].

The addition of nucleating agents leads to the continuous presence of a large amount of sites from which crystallites can grow, leading to decreasing crystallite sizes and increasing crystallization rates [6]. This in contrary to homogeneous nucleation, in which the crystallization rate is dependent on the random occurrence of nuclei.

PHBV generally displays a slow crystallization rate [6-9], which leads to major processing difficulties, for example a PHBV film will stick to itself, even after cooling, especially at higher 3-hydroxyvalerate (3-HV) content [6, 8]. Therefore, this chapter is dedicated to studying the rate of crystallization by adding nucleating agents, rather than to increase the total degree of crystallinity, as this is already high for this type of PHBV.

Several kinds of chemical compounds have been investigated as nucleating agents for PHBV, including, but not limited to, boron nitride (BN) [6, 8, 9], talc [6, 8, 10], thymine [9], terbium oxide, lanthanum oxide [8] and fumed silica [11]. However, from these results it must be concluded that BN, the most commonly used

nucleating agent for PHBV, most often shows the highest efficiency. Unfortunately, this ceramic material is not biodegradable nor biobased.

Orotic acid (OA), a heterocyclic compound (see Figure 3-1), was recently discussed in a publication by Pan et al. (2013), where it was added to a PHBV sample with a 3-HV content of 12 %, resulting in an improved crystallization peak temperature during non-isothermal crystallization from the melt [12]. However, this combination of materials was barely elaborated.

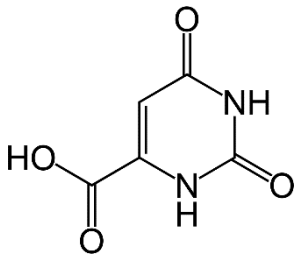

Figure 3-1: Chemical structure of orotic acid

In this chapter however, the effect of OA on the non-isothermal crystallization kinetics of PHBV is discussed in more detail and compared to that of BN. OA has also already been proven to be a good nucleating agent for other polymeric systems, such as PHBHHx, PHB [7] and PLA [13]. Non-isothermal crystallization has been chosen over isothermal crystallization, because the study of crystallization in a continuously changing environment resembles more the actual processing conditions [14, 15]. Low concentrations of 0.5 and 1 wt% were used, because enhanced crystallization is the main objective and does not require high loading.

3.2 EXPERIMENTAL

3.2.1 Materials

PHBV in pure powdered form was purchased from Tianan Biologic. The 3-HV content of the material was determined to be 2.8 % with ^{1}H-NMR, after dissolving in deuteroform. The powder was dried at 70 °C for 2 days before use and stored in a desiccator. OA and hexagonal BN were purchased from respectively Sigma-

Aldrich and Momentive and were ground in a mortar and dried at 110 °C before use.

3.2.2 Sample preparation

Samples with a total weight of about 40 g were weighed and premixed in polyethylene bottles. Melt mixing of the samples was performed using a Haake Rheomix OS kneader at a temperature of 185 °C for 6 min with a screw speed of 40 rpm. OA and BN were added in concentrations of 0.5 and 1 wt%. A sample of neat PHBV was prepared in the same manner, in order to take into account any effects due to the melt mixing. After removal from the mixer, the samples were cooled at room temperature and stored in a desiccator for two weeks prior to analysis.

3.2.3 Differential scanning calorimetry (DSC)

The non-isothermal crystallization of the pure and nucleated PHBV under inert atmosphere (nitrogen) was analyzed using a TA Instruments Q200 DSC. Sample sizes of about 3 mg in an aluminium pan were used to perform the measurements. The samples were heated from 25 °C to 190 °C and held isothermal for 4 min in order to erase any thermal history. The samples were then cooled to -10 °C at cooling rates of 7, 11, 15, 19 and 23 °C/min. The measurements were performed under a constant flow of 50 ml/min nitrogen gas. The obtained data were analyzed as described in the following paragraph. Selected measurements were performed in triplicate in order to check reproducibility.

3.2.4 Description of theoretical models

The use of DSC allows us to monitor the energy released during non-isothermal crystallization of a polymeric system upon cooling from the amorphous melt. For the modelling of these results, it is necessary to calculate the relative crystallinity:

$$X_{r,t} = \int_{T_0}^{T} (dH_c / dT) dT \; / \; \int_{T_0}^{T_e} (dH_c / dT) dT \qquad (3\text{-}1)$$

where T_0 and T_e represent the temperatures at which crystallization respectively starts and ends. T is the temperature at time t at which a relative crystallinity $X_{r,t}$ is reached. We define dH_c as the enthalpy of crystallization released during an infinitesimal temperature interval dT.

For analysis of non-isothermal kinetics, according to certain theoretical models, it is necessary to transform the temperature scale into a time scale, using following relationship between crystallization time and crystallization temperature:

$$t = |T_0 - T| / \beta \quad (3\text{-}2)$$

Where T is the temperature at time t, T_0 the temperature at which crystallization starts and β the maintained cooling rate during melt crystallization of the polymer [16, 17].

From the relationship between relative degree of crystallinity and crystallization time, it will be possible to calculate the crystallization half-time $t_{1/2}$, which will be used as a model-free parameter for comparison of nucleating agents. The crystallization half-time is defined as the time needed to obtain a relative degree of crystallinity of 50 % [18].

In this work, the applicability of three theoretical models for the non-isothermal crystallization has been investigated. Finally, the nucleation ability, as described by Dobreva and Gutzow [19, 20], was also used as a possible parameter for determination of the effectiveness of BN and OA as nucleating agents for PHBV.

A) Jeziorny modified Avrami model:

The well-known Avrami equation is often used to analyse isothermal crystallization kinetics and is not restricted to polymers. This equation relates the relative degree of crystallinity to the crystallization time in the following way [14, 15, 17, 21, 22]:

$$1 - X_{r,t} = \exp(-k_A \cdot t^{n_A}) \quad (3\text{-}3)$$

With $X_{r,t}$ the relative degree of crystallinity at time t, k_A the crystallization rate constant (including nucleation and growth rate parameters) and n_A the Avrami exponent, which contains information about nucleation mechanism and growth geometry [14, 15, 17, 21, 22].

When the non-isothermal crystallization data are transformed from temperature scale to the time scale (equation 3-2), the same Avrami equation can also be applied, despite being performed under non-isothermal conditions, resulting in the calculation of the non-isothermal parameters k_A and n_A. However, it is important to realize that k_A and n_A do not have the same physical meaning as for isothermal

crystallization, due to the fact that they are susceptible to changes when the crystallization conditions are variable, i.e. upon non-isothermal crystallization. This implies that k_A and n_A are two adjustable parameters to be fitted to the data [14, 23].

Jeziorny stated that modification of the crystallization rate constant k_A, by taking into account the cooling rate, results in a parameter than can be used for characterizing the kinetics of non-isothermal crystallization [15]. The Jeziorny modified crystallization rate constant k_J can be calculated, using the cooling rate β, as follows:

$$\log k_J = \log k_A / \beta \tag{3-4}$$

The extraction of k_A and n_A from the experimental data can be performed by linearization of equation 3-3 [14, 15, 17, 21, 22]:

$$\log [- \ln (1 - X_{r,t})] = n_A \cdot \log t + \log k_A \tag{3-5}$$

Plotting of log [-ln (1 - $X_{r,t}$)] as a function of log t for each applied cooling rate will yield a linear curve. The slope and intercept of this curve can be used to calculate n_A and k_A respectively.

Alternatively, a direct substitution of equation 3-4 into equation 3-5, yields following expression:

$$\log [- \ln (1 - X_{r,t})] = n_A \cdot \log t + \beta \cdot \log k_J \tag{3-6}$$

B) Ozawa model:

Ozawa reconsidered the general Avrami equation in order to take into account the cooling rate at which the non-isothermal crystallization is performed. The time variable was replaced by an expression containing the constant cooling rate β [24]:

$$1 - X_{r,t} = \exp \left(\frac{-k_O}{\beta^{n_O}} \right) \tag{3-7}$$

Where k_O is the Ozawa crystallization rate constant, which is a function of the cooling rate β, and n_O the Ozawa exponent, depending on the crystal growth and nucleating mechanism. The data needed for this model can be taken directly from the raw $X_{r,t}(T)$ data [17, 18, 22, 24].

Linearization of the above equation can be performed by taking the double logarithm, yielding following equation [17, 18, 22, 24]:

$$\log [- \ln (1 - X_{r,t})] = - n_O \cdot \log \beta + \log k_O \quad (3\text{-}8)$$

Plotting log [- ln (1 - $X_{r,t}$)] versus log β for each cooling rate, at a particular temperature during crystallization, yields a linear curve, from which intercept and slope can be used to calculate k_O and n_O.

C) Mo model:

Mo et al. (1997, 2000) suggested a different kinetic equation by combining the Ozawa and Avrami equations [16, 25]:

$$\log k_A + n_A \cdot \log t = \log k_O - n_O \cdot \log \beta \quad (3\text{-}9)$$

Equation 3-8 can be rewritten further into:

$$\log \beta = \log F(T) - b \cdot \log t \quad (3\text{-}10)$$

Where b is the ratio of the Avrami exponent n_A to the Ozawa exponent n_O. The parameter $F(T) = (k_O/k_A)^{1/n_O}$ refers to the value of the cooling rate at a certain relative degree of crystallinity at unit crystallization time [16, 25]. The lower the value of F(T), the higher the crystallization rate, meaning F(T) has a definite physical and practical meaning [26].

Plotting of log β as a function of log t will yield a straight line with an intercept log F(T) and a slope of –b [16, 25].

D) Determination of nucleation ability:

In order to actually quantify the effect of the nucleating agents on polymer crystallization, a relatively simple method, developed by Dobreva and Gutzow [19, 20, 27], is employed. This method allows us to calculate the nucleating activity of foreign substrates in a polymer melt. The nucleation activity ϕ is an experimentally determined factor by which the energy required for three-dimensional nucleation decreases upon addition of a foreign substrate, i.e. the nucleating agent. If the nucleating agent is very active, ϕ will approach 0. However, non-active particles will show a nucleation activity ϕ closer to 1.

For homogeneous nucleation, as is the case for the pure unmodified polymer, the cooling rates can be written as:

$$\ln\beta = A - (B/\Delta T_p^2) \quad (3\text{-}11]$$

While for heterogeneous nucleation, i.e. upon addition of a nucleating agent, it is stated that:

$$\ln\beta = A - (B^*/\Delta T_p^2) \quad (3\text{-}12)$$

Here β is the applied cooling rate, A is a constant and ΔT_p is the degree of supercooling, which can be calculated as the difference between the temperature of the polymer melt T_m and the crystallization peak temperature $T_{c,p}$ ($\Delta T_p = T_m - T_{c,p}$). B and B* are the slopes of the curves obtained for respectively neat and nucleated polymer.

The nucleation activity is then calculated as:

$$\phi = B^*/B \quad (3\text{-}13)$$

B is also a parameter than can be calculated from the following equation [19, 20, 27]:

$$B = (\omega \cdot \sigma^3 \cdot V_m^2)/(3 \cdot n_A \cdot k_B \cdot T_m^0 \cdot \Delta S_m^2) \quad (3\text{-}14)$$

Where ω is a geometrical factor, σ is the specific energy, V_m is the molar volume of the crystallizing substance, n_A is the Avrami exponent, ΔS_m is the entropy of melting, k_B the Boltzmann constant and T_m^0 is the infinite crystal melting temperature.

3.3 RESULTS AND DISCUSSION

3.3.1 Crystallization parameters

Crystallization peak temperature $T_{c,p}$, onset of crystallization $T_{c,o}$, crystallization half time $t_{1/2}$ and enthalpy ΔH_c from non-isothermal crystallization of PHBV, neat and nucleated with BN and OA, at different cooling rates are given in Table 3-1. For visual comparison, the DSC exotherm of cooling at 7 °C/min from the amorphous melt of each sample is given in Figure 3-2.

Based on these data, it is clear that for every sample, $t_{1/2}$, $T_{c,o}$ and $T_{c,p}$ decrease with an increasing cooling rate, meaning the overall crystallization proceeds at higher temperatures with increasing cooling rate. The known nucleating agent BN clearly exhibits a positive effect on the crystallization parameters of PHBV. $T_{c,p}$ has increased by about 30 to 36 °C for each heating rate, meaning the crystallization process reaches its maximum at a much higher temperature, which is a very interesting property for melt processing of the polymer.

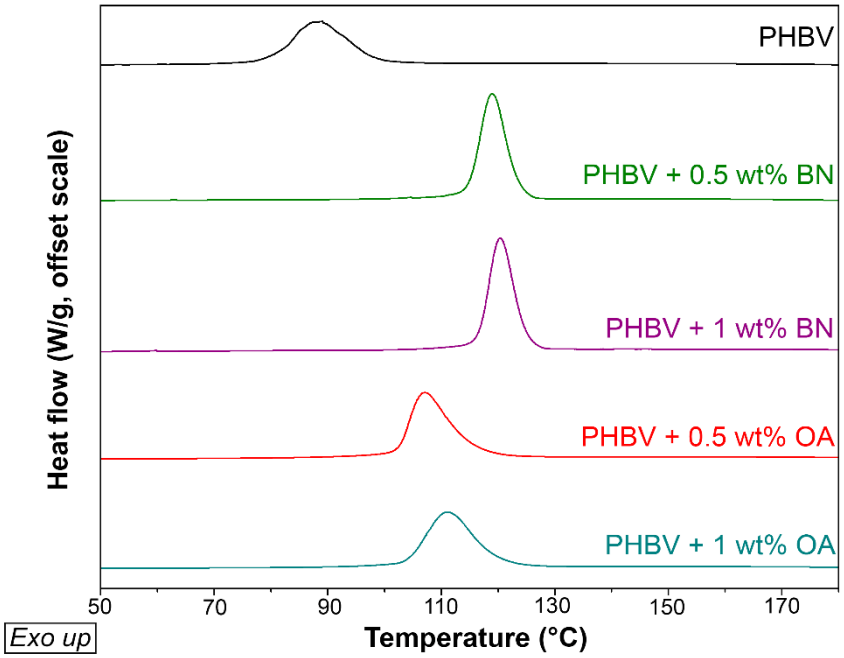

Figure 3-2: Exotherms of non-isothermal crystallization from the melt at 7 °C/min for neat and nucleated PHBV

When comparing the crystallization half time of the BN nucleated samples with the pure material, it is clear that $t_{1/2}$ has drastically decreased to about half the value of neat PHBV. This means completion of crystallization will be reached roughly twice as fast. $T_{c,o}$ is 26 to 29 °C higher for BN nucleated samples, when compared to neat PHBV. ΔH_c is slightly higher than for neat PHBV and appears to decrease at higher cooling rates. Also important to note is that doubling the amount of BN in the sample, does not seem to affect the performance of the nucleating agent. $T_{c,p}$ and $t_{1/2}$ are similar for the samples containing 0.5 and 1 % BN. Practically this means that one can obtain the same improvement in crystallization features with only half the amount of BN. The shape of the crystallization peak, as can be seen from the DSC curve in Figure 3-2, is rather sharp and steep at the beginning and end of crystallization. This is usually a feature found during crystallization in the presence of a large number of pre-formed nuclei, indicating that crystallization starts quickly and is completed in a relatively short time [28].

In this work, OA is presented as a novel nucleating agent for PHBV. The peak temperatures were influenced in a manner similar to BN, shifting them to temperatures about 18 to 23 degrees higher than for neat PHBV. The crystallization half time however was hardly influenced by the addition of OA. Thus, it can be concluded that the crystallization will proceed at higher temperatures due to the addition of OA, but the phase transformation will not be completed at a higher rate. This can also be clearly seen in Figure 3-2, where the addition of OA resulted in a shift of the crystallization peak to higher temperatures, however remaining equally broad. Similar to the BN nucleated samples, ΔH_c decreases with rising cooling rate. Doubling the concentration of OA resulted in only a slight improvement. The peak temperatures are slightly higher in the sample containing 1 % OA than in the one containing 0.5 % OA.

Table 3-1: Characteristic parameters of neat and nucleated PHBV during non-isothermal crystallization (n = 2)

Sample	β (°C/min)	$T_{c,p}$ (°C)	$T_{c,o}$ (°C)	ΔH_c (J/g)	$t_{1/2}$ (min)
PHBV	7	89	98	70	2.5
	11	84	94	58	1.7
	15	81	91	63	1.2
	19	78	89	57	1.0
	23	76	89	60	0.9
PHBV + 0.5 % BN	7	119	124	83	1.2
	11	116	121	84	0.9
	15	114	119	80	0.7
	19	112	117	79	0.6
	23	111	116	80	0.5
PHBV + 1 % BN	7	120	125	86	1.2
	11	117	122	84	0.8
	15	115	120	77	0.6
	19	114	118	76	0.5
	23	112	117	77	0.5
PHBV + 0.5 % OA	7	107	116	80	2.5
	11	103	110	73	1.7
	15	101	107	70	1.2
	19	100	105	66	1.0
	23	99	103	64	0.9
PHBV + 1 % OA	7	110	119	76	2.4
	11	107	117	76	1.7
	15	103	115	75	1.4
	19	100	112	69	1.2
	23	98	107	67	1.0

The relative error on ΔH_c and $T_{c,p}$ of nucleated samples is determined to be of an order of magnitude of respectively 1-3 % and 0.5-1 %. For neat PHBV the relative error is substantially higher at an order of magnitude of 7 and 4 % for respectively ΔH_c and $T_{c,p}$.

Regarding $T_{c,o}$, it is clear that higher values can be obtained upon doubling the concentration of OA. Compared to neat PHBV, the addition of 0.5 % OA raises $T_{c,o}$ with 14 to 18 °C, whereas an OA concentration of 1 % results in a raise of 18 to 24 °C. The crystallization half time was rather similar for both samples nucleated with OA. The shape of the crystallization peak (see Figure 3-2) resembles more that of neat PHBV in contrast to the BN nucleated samples. The rather broad DSC crystallization peak could possibly be caused by the hindered nucleation due to a broad distribution of induction times [28].

These results clearly indicate that OA is not quite as efficient at enhancing crystallization as BN for this specific type of PHBV, this in contrary to the limited amount of literature data available. Pan et al. (2013) found that OA was about equally effective as BN for a PHBV sample with 3-HV content of 12 %, reaching a non-isothermal crystallization peak temperature of about 85 °C [12]. Jacquel et al. (2009) presented a comparison of OA and BN as nucleating agents for PHB and PHBHHx. They showed that OA had an influence on the non-isothermal crystallization of PHB similar to BN, raising $T_{c,p}$ with about 27 °C. However, for PHBHHx, OA appears to be far more effective than BN. $T_{c,p}$ of OA nucleated samples was 11 to 18 °C higher than of BN nucleated samples. Samples with a high 3-HHx content of 18 % even showed no change in crystallization upon addition of BN [7]. The non-isothermal crystallization peak temperature of PLA was raised by about 30 °C upon addition of OA [13].

Jacquel et al. (2009) compared the efficiency of BN and OA as nucleating agents for PHBHHx with a 3-HHx content of 10 mol%. It was observed that OA raised the non-isothermal crystallization peak temperature to 76.1 °C, whereas for BN it was increased to only 65.5 °C [7]. This in contrary to the results reported in this chapter, where BN performs better than OA for PHBV.

3.3.2 Analysis of non-isothermal crystallization kinetics

The first kinetic model applied to the experimental data is the Avrami model, as modified by Jeziorny for non-isothermal crystallization. Plots of log [-ln (1 - $X_{r,t}$)] versus log t for each sample are given in Figure 3-3. The calculated kinetic parameters can be found in Table 3-2. Only the $X_{r,t}$ data in the range of 10 to 90 % were used in the fitting of the model.

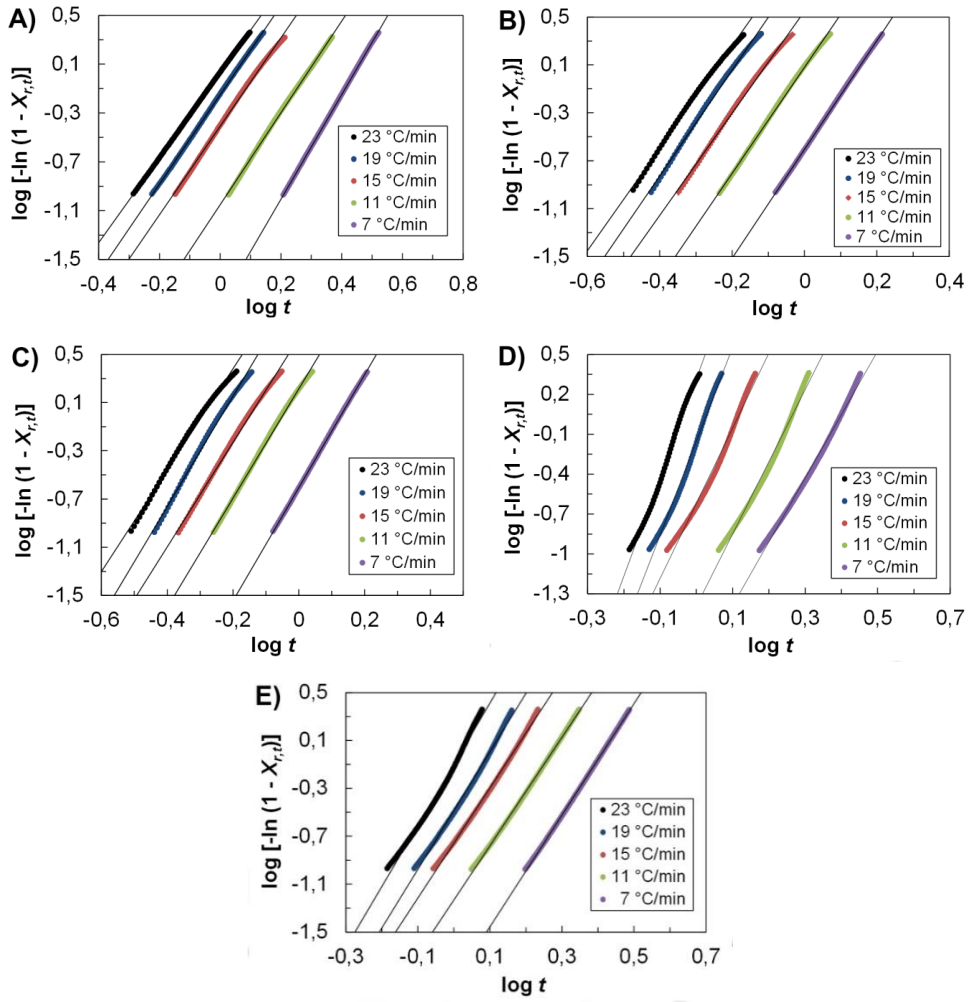

Figure 3-3: Jeziorny modified Avrami plots of A) neat PHBV and PHBV nucleated with B) 0.5 % BN, C) 1 % BN, D) 0.5 % OA and E) 1 % OA

The experimental data of neat PHBV display a very high correlation with the Jeziorny modified Avrami model ($r^2 > 0.997$) showing only minor deviations from the linear curve at the high or low end of relative crystallinity. The Avrami constant n_A varies between 3.48 and 4.28. The calculated crystallization rate constant k_A increases with increasing cooling rate, indicating that crystallization proceeds faster at higher cooling rates. This is consistent with the crystallization half time $t_{1/2}$ which appears to decrease at higher cooling rates.

However, in his original paper, Jeziorny obtained a constant cooling rate independent kinetic parameter k_J with his proposed modification [15]. From our results it is clear that k_J still increases at higher cooling rates, yet less obvious at cooling rates of 15, 19 and 23 °C/min. This seems rather contradictory when regarding the very high correlation between log t and log [-ln (1 - $X_{r,t}$).]. It is however important to note that a double logarithmic function in general is not very sensitive to relatively small changes in argument. This means high correlation coefficients are expected even if the Jeziorny modified Avrami model is not completely fulfilled. Thus, it must be concluded that this model is not very suitable to describe the non-isothermal crystallization of neat PHBV, despite the high correlation coefficient r^2.

For both BN nucleated samples a high degree of correlation with the Jeziorny modified Avrami model ($r^2 > 0.99$) can be observed. A slight deviation from linearity can however be visually noted from the graphs, despite the very high correlation coefficient. This is again due to the low sensitivity of double logarithmic functions to small changes in argument. Both samples show a slightly fluctuating n_A, with values ranging from 4.21 to 4.69 and from 4.26 to 4.54 for respectively 1 % and 0.5 % BN. The calculated crystallization rate constant k_A increases with rising cooling rate, again indicating that crystallization proceeds faster at higher cooling rates. The Jeziorny modified crystallization rate constant k_J increases only slightly with rising cooling rate. The almost identical values of the Avrami parameters for both BN concentrations again indicates that doubling the BN concentration does not have an effect on its effectiveness as a nucleating agent. Overall, the Jeziorny modified Avrami model fits moderately for BN nucleated PHBV.

Table 3-2: Non-isothermal crystallization kinetic parameters based on Jeziorny modified Avrami model (n = 3)

sample	β (°C/min)	r^2	n_A (± 0.05)	k_A (± 0.04)	k_A (± 0.05)
PHBV	7	0.9999	4.28	0.01	0.54
	11	0.9991	3.75	0.09	0.80
	15	0.9973	3.58	0.39	0.94
	19	0.9998	3.66	0.71	0.98
	23	0.9999	3.48	1.08	1.00
PHBV + 0.5 % BN	7	0.9999	4.54	0.25	0.82
	11	0.9986	4.42	1.21	1.02
	15	0.9968	4.26	3.56	1.09
	19	0.9967	4.42	8.77	1.12
	23	0.9966	4.28	13.2	1.12
PHBV + 1 % BN	7	0.9998	4.69	0.25	0.82
	11	0.9982	4.54	1.65	1.05
	15	0.9969	4.33	14.4	1.10
	19	0.9955	4.58	11.8	1.14
	23	0.9942	4.21	16.8	1.13
PHBV + 0.5 % OA	7	0.9947	4.78	0.01	0.54
	11	0.9882	5.42	0.04	0.75
	15	0.9858	5.65	0.24	0.91
	19	0.9903	7.06	0.71	0.98
	23	0.9939	7.42	2.10	1.03
PHBV + 1 % OA	7	0.9996	4.66	0.01	0.53
	11	0.9990	4.52	0.06	0.77
	15	0.9974	4.59	0.18	0.89
	19	0.9950	4.90	0.33	0.94
	23	0.9915	5.10	0.80	0.99

The novel nucleating agent OA shows a slightly lower correlation to the Jeziorny modified Avrami model, with a correlation coefficient higher than 0.98. Visually, it can be seen from the graphs that the deviations from linearity are much more severe than for BN nucleated samples. The Avrami parameter n_A appears to

increase from 4.52 to 5.10 and 4.78 to 7.42 for respectively 1 % and 0.5 % OA. The crystallization rate constant k_A increases with rising cooling rate, but has lower absolute values than the BN nucleated samples. This means that crystallization proceeds faster at higher cooling rates, but in general proceeds slower than is the case for BN. This conclusion correlates well with the crystallization half times. The Jeziorny modified crystallization rate constant seems to increase with rising temperature. Again, this does not correlate well with Jeziornys original findings [15]. From our results it must be concluded that the Jeziorny Avrami model is not very effective at describing the crystallization of PHBV nucleated with OA.

An analysis based on the Ozawa model, which is a modification of the Avrami equation, was also performed on the experimental data. Figure 3-4 shows plots of log [-ln (1 - $X_{r,t}$)] versus log β for a selected range of temperatures for each separate sample. Crystallization temperatures were chosen in order to obtain at least 4 (and for obvious reasons at most 5) data points to perform a linear regression. The calculated kinetic parameters n_O and k_O are given in Table 3-3.

For neat PHBV, the Ozawa model has been applied to crystallization temperatures between 73 and 88 °C. The correlation coefficient of these linear fits are fairly good ($0.989 \leq r^2 \leq 0.9992$). The absolute value of the crystallization rate constant k_O varies only slightly when the temperature is lowered from 88 to 76 °C, indicating that the crystallization proceeds at roughly the same rate within this temperature range. At 73 °C, k_O is slightly lower, meaning the crystallization proceeds slower. However, the uncertainties on these values are very high. The Ozawa exponent n_O decreases systematically with decreasing temperature, varying between 2.8 and 1.5. However, the high uncertainties on the values for k_O make the Ozawa model not suitable and not applicable to the non-isothermal crystallization of neat PHBV. Again, we must conclude that a high correlation is obtained due to the insensitivity of a double logarithmic function.

For the samples nucleated with BN, the degree of correlation of the linear fitted curves varies greatly from poor to good. The calculated Ozawa constants n_O also decrease with decreasing temperature. The crystallization rate constant k_O also decreases, but shows very high uncertainties. In general, it must be concluded that the Ozawa model is not suitable to describe the non-isothermal crystallization of PHBV nucleated with BN.

The correlation coefficient between the data of the samples with the proposed nucleating agent OA and the Ozawa equation also varies greatly. The parameter k_O increases with decreasing temperature and, again, displays very high uncertainty. The Ozawa constant n_O however appears to remain fairly constant, except at a temperature of 98 °C, where it decreases significantly. Again, the Ozawa model is not able to properly fit the non-isothermal crystallization kinetics of PHBV nucleated with OA.

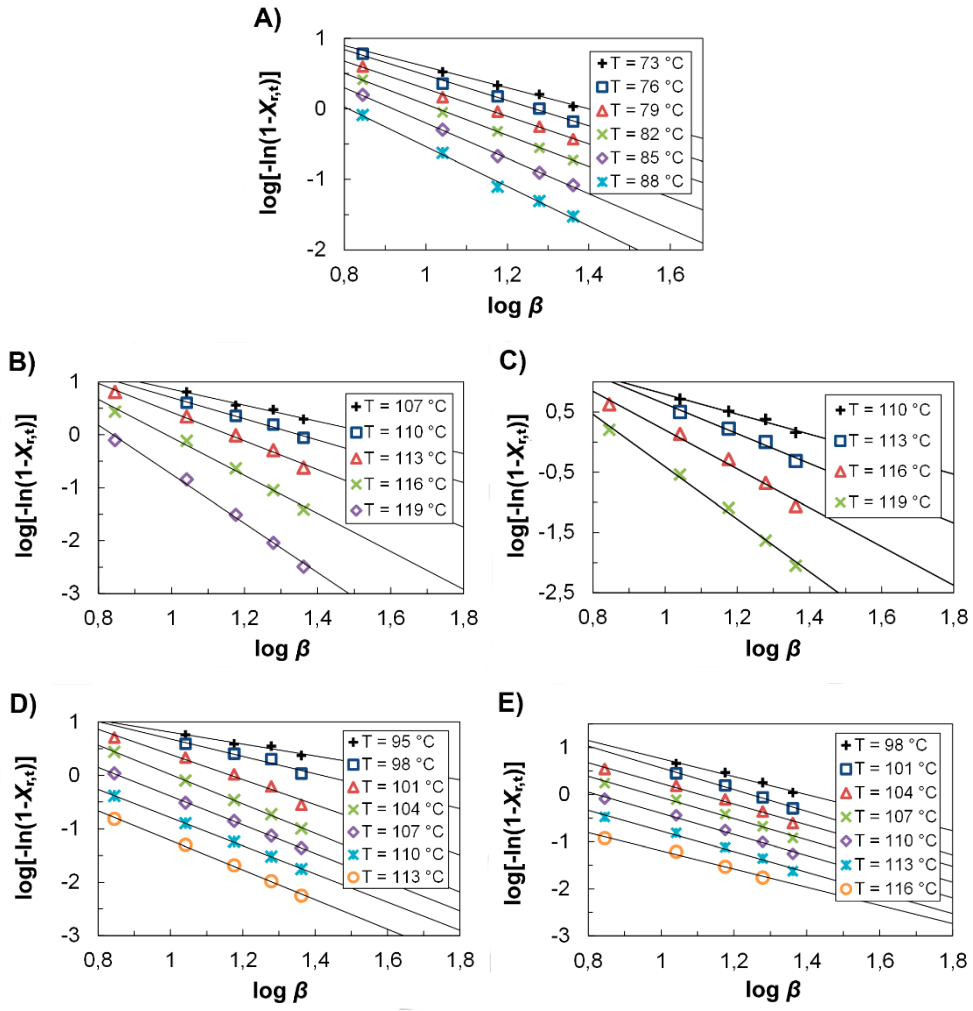

Figure 3-4: Ozawa plots of A) neat PHBV and PHBV nucleated with B) 0.5 % BN, C) 1 % BN, D) 0.5 % OA and E) 1 % OA

Table 3-3: Non-isothermal crystallization kinetic parameters based on Ozawa model (n = 3)

Sample	*T* (°C)	r^2	n_O (± 0.2)	k_O
PHBV	88	0.9944	2.8	188 ± 61
	85	0.9984	2.5	199 ± 30
	82	0.9992	2.2	183 ± 18
	79	0.9962	2.0	173 ± 32
	76	0.9934	1.8	190 ± 43
	73	0.9896	1.5	124 ± 38
PHBV + 0.5 % BN	119	0.9939	4.5	5300 ± 3300
	116	0.9914	3.6	3500 ± 1800
	113	0.9920	2.7	1390 ± 520
	110	0.9838	2.0	520 ± 270
	107	0.9777	1.5	250 ± 110
PHBV + 1 % BN	119	0.9943	4.4	8800 ± 4400
	116	0.9850	3.2	2600 ± 1600
	113	0.9786	2.5	1280 ± 930
	110	0.9770	1.7	288 ± 150
PHBV + 0.5 % OA	113	0.9985	2.7	30 ± 6
	110	0.9998	2.6	71 ± 4
	107	0.9996	2.7	200 ± 20
	104	0.9984	2.8	590 ± 60
	101	0.9787	2.7	560 ± 280
	98	0.9381	1.6	210 ± 170
PHBV + 1 % OA	116	0.9868	1.9	5 ± 2
	113	0.9877	2.2	26 ± 10
	110	0.9911	2.2	71 ± 23
	107	0.9905	2.2	153 ± 52
	104	0.9905	2.2	270 ± 90
	101	0.9912	2.3	760 ± 330
	98	0.9843	1.9	480 ± 230

Finally, the Mo model, which is a combination of both previous models, is also applied to the experimental data. Plots of log β in function of log t can be found in Figure 3-5. The calculated kinetic parameters F(T) and b are given in Table 3-4 for each sample.

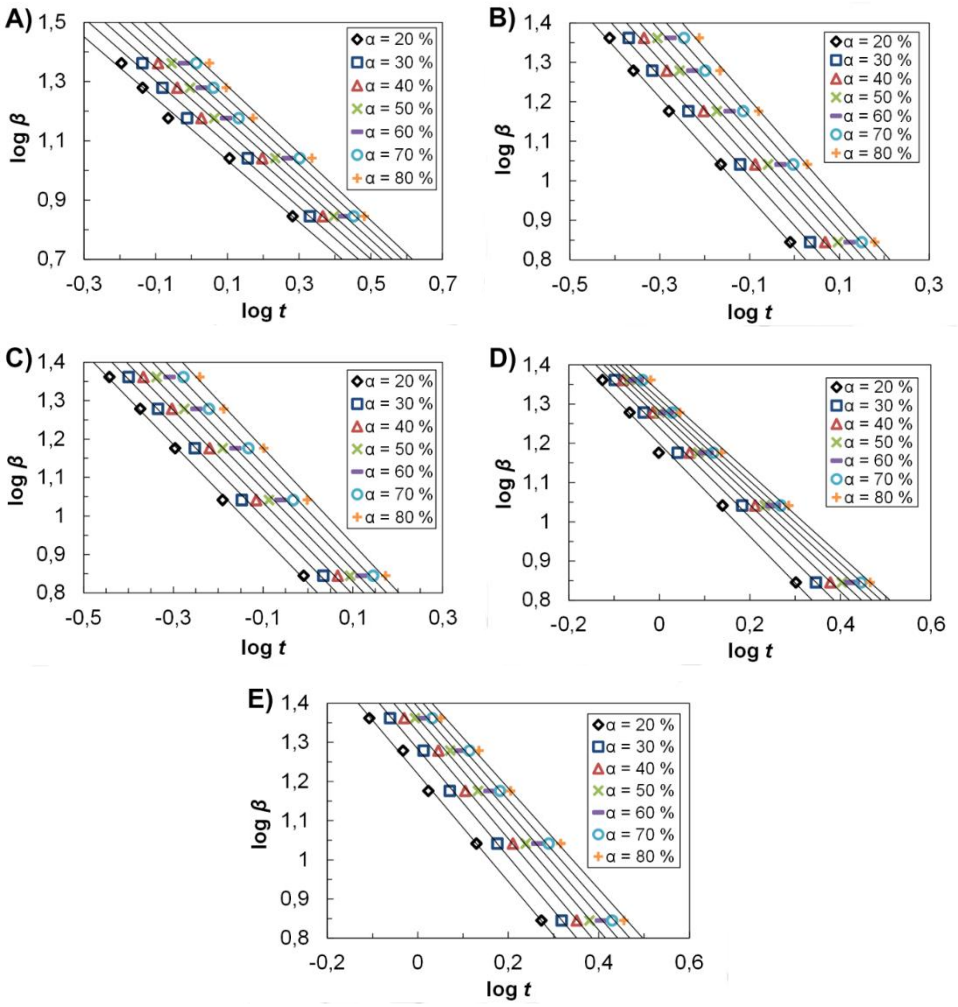

Figure 3-5: Mo plots of A) neat PHBV and PHBV nucleated with B) 0.5 % BN, C) 1 % BN, D) 0.5 % OA and E) 1 % OA

For neat PHBV, it can be immediately seen that for every relative degree of crystallinity $X_{r,t}$ a relatively high degree of correlation is obtained, with r^2 ranging between 0.988 and 0.992. F(T) increases systematically with rising relative degree of crystallinity, which means that at unit crystallization time, a higher cooling rate

is needed to obtain a certain degree of relative crystallinity. The values of b increase only slightly from 1.04 to 1.13 with rising $X_{r,t}$, with an average value of about 1.1. These observations lead to believe that the Mo model is fairly successful in describing the non-isothermal crystallization kinetics of neat PHBV.

The BN nucleated samples also correlate very well with the Mo model, as can be derived from the high degree of correlation ($r^2 \geq 0.997$). For both concentrations of BN, F(T) increases with higher cooling rates, indicating again that at unit crystallization time, a higher relative degree of crystallinity can be obtained with a higher cooling rate. The kinetic parameter b is quasi constant for both samples, with average values of 1.3 and 1.2 for respectively 0.5 % BN and 1 % BN. The constancy of b is another indication that the Mo model is successful in describing the non-isothermal crystallization kinetics of PHBV nucleated with BN. It is also clear from the results that adding 0.5 % of BN to PHBV is practically equally as effective as adding 1 %.

Both OA nucleated samples also showed a very high correlation with the Mo model, with correlation coefficients higher than 0.994. F(T) increases with higher cooling rates, indicating that at unit crystallization time, a higher relative degree of crystallinity can be obtained with a higher cooling rate. Parameter b decreases only slightly with increasing degrees of relative crystallinity. The average value of b is 1.1 for 0.5 % OA and 1.4 for 1 % OA. Thus, the Mo model is fairly successful in describing the crystallization kinetics of PHBV nucleated with OA. Important to note is that F(T) values of BN nucleated samples are substantially lower than those nucleated with OA, indicating that a higher crystallization rate is achieved upon addition of BN, rather than OA.

Table 3-4: Non-isothermal crystallization kinetic parameters based on Mo model (n = 3)

Sample	$X_{r,t}$ (%)	r^2	$F(T)$ (± 0.4)	b (± 0.06)
neat PHBV	20	0.9912	13.8	1.04
	30	0.9900	15.7	1.06
	40	0.9891	17.3	1.08
	50	0.9882	19.0	1.09
	60	0.9875	20.7	1.10
	70	0.9874	23	1.11
	80	0.9888	25	1.13
PHBV + 0.5 % BN	20	0.9987	6.8	1.26
	30	0.9986	7.7	1.26
	40	0.9985	8.5	1.26
	50	0.9984	9.2	1.26
	60	0.9982	10.0	1.27
	70	0.9983	10.8	1.28
	80	0.9983	11.9	1.30
PHBV + 1 % BN	20	0.9983	6.7	1.20
	30	0.9983	7.5	1.20
	40	0.9983	8.2	1.20
	50	0.9982	8.9	1.20
	60	0.9981	9.6	1.21
	70	0.9980	10.3	1.22
	80	0.9978	11.3	1.24
PHBV + 0.5 % OA	20	0.9949	15.8	1.18
	30	0.9970	17.4	1.14
	40	0.9976	18.4	1.11
	50	0.9978	19.2	1.08
	60	0.9979	19.9	1.06
	70	0.9979	20.6	1.05
	80	0.9978	21.5	1.04
PHBV + 1 % OA	20	0.9977	16.5	1.41
	30	0.9978	19.2	1.41
	40	0.9978	21.3	1.40
	50	0.9975	23.1	1.39
	60	0.9970	24.7	1.36
	70	0.9965	26.2	1.34
	80	0.9961	27.8	1.31

3.3.3 Determination of nucleation ability

In order to quantitatively assess the efficiency of a nucleating agent in a certain concentration, the method as proposed by Dobreva and Gutzow [19, 20] was used. Plotting of ln β versus $1/\Delta T_p^2$ for neat and nucleated PHBV will yield, respectively, a slope -B and -B*. The ratio of B* to B can be used as a measure of nucleation ability of a foreign substrate in a polymer melt. These results, along with the correlation coefficient of the data to the applied model, are given in Table 3-5. BN yields a rather low value of ϕ of about 0.5, indicating its excellent nucleation ability, as was to be expected. From the results, it can again be concluded that doubling the concentration of BN from 0.5 to 1 % does not show a significant effect on nucleating agent efficiency.

Table 3-5: Nucleation ability according to Dobreva and Gutzow (n = 3)

Sample	r^2	ϕ
PHBV + 0.5 % BN	0.9994	0.53 ± 0.01
PHBV + 1 % BN	0.9988	0.52 ± 0.01
PHBV + 0.5 % OA	0.9806	0.83 ± 0.07
PHBV + 1 % OA	0.9925	0.53 ± 0.02

PHBV nucleated with 1 % OA also yields a nucleation ability ϕ of about 0.5, indicating an effectiveness similar to boron nitride. However, it is important to note that the nucleation ability does not take the crystallization half time into account (see results in Table 3-1). The addition of OA in a 1 % concentration resulted in a crystallization half time approximately twice as long as was the case for BN. This means that overall BN is still a more effective nucleating agent than OA. This also means, that the method designed by Dobreva and Gutzow is not an ideal tool for comparison of nucleating agents, but can certainly provide useful insights, if combined with other characteristic parameters, such as crystallization half time. Contrary to BN, the concentration plays a significant role. The fact that 0.5 % OA yielded a nucleating ability of about 0.8, but with a very similar crystallization half time, indicates that OA is a less attractive nucleating agent at lower concentrations. The slightly lower correlation results in a greater uncertainty on ϕ.

3.4 CONCLUSIONS

In this chapter, OA was proposed as an alternative nucleating agent for PHBV and compared with the more conventional BN. Several conclusions can be made:

1. The addition of OA shows a clear positive effect on the non-isothermal crystallization of PHBV, increasing the peak temperatures of crystallization by 18 to 23 °C. Despite its significant positive effect on crystallization, OA does not perform as well as BN, which raised crystallization peak temperatures by 30 to 36 °C.
2. Neat and OA and BN nucleated PHBV correlated well with the Mo model for non-isothermal crystallization kinetics. The Avrami and Ozawa model failed to successfully describe the non-isothermal crystallization kinetics. Modelling showed that a substantially higher crystallization rate is obtained upon addition of BN as compared to OA.
3. The nucleation ability of the sample nucleated with 1 % orotic acid was similar to that of both samples nucleated with boron nitride, with a value of φ of approximately 0.5. It was also concluded that the method proposed by Dobreva and Gutzow provides valuable information, but other significant parameters, such as crystallization half time for example, should be taken into account in order to successfully compare the effectiveness of nucleating agents.
4. Lowering the concentration of boron nitride from 1 % to 0.5 % does not seem to influence the non-isothermal crystallization properties. However, this does not seem to be the case for orotic acid, where raising the concentration to 1 % does appear to have a positive influence on the nucleation ability.

Overall, it can be concluded that the alternative nucleating agent, orotic acid, has a significant positive effect on the non-isothermal crystallization properties of PHBV, albeit not as drastic as boron nitride. However, orotic acid should still be taken into account as a possible biodegradable alternative to boron nitride, especially since it can also be used for other biopolyesters, such as PLA, PHB and PHBHHx [7]. Despite the positive results regarding enhancement of PHBV crystallization, it was decided to no longer continue using PHBV as base material, due to its inherently poor mechanical properties.

It could be an alternative route to add plasticizers to PHBV in order to overcome its inherent brittleness. However, it has been demonstrated by Corrêa et al. (2012) that the addition of plasticizers to PHBV also drastically increases its oxygen permeability [29]. In turn, it would be necessary to reduce the gas permeability again through selected modifications, which would results in an even more complex polymeric multiphase system.

3.5 REFERENCES

1. Muthukumar, M., *Nucleation in Polymer Crystallization*, in *Advances in Chemical Physics*. 2004, John Wiley & Sons, Inc. p. 1-63.

2. Wunderlich, B., *CHAPTER V - The Nucleation Step*, in *Macromolecular Physics*, B. Wunderlich, Editor. 1976, Academic Press. p. 1-114.

3. Binsbergen, F.L., *Natural and artificial heterogeneous nucleation in polymer crystallization.* Journal of Polymer Science: Polymer Symposia, 1977. **59**(1): p. 11-29.

4. Mercier, J.P., *Nucleation in polymer crystallization: A physical or a chemical mechanism?* Polymer Engineering & Science, 1990. **30**(5): p. 270-278.

5. Thierry, A. and B.A. Lotz, *Epitaxial Crystallization of Polymers: Means and Issues*, in *Handbook of Polymer Crystallization*. 2013, John Wiley & Sons, Inc. p. 237-264.

6. Kai, W., Y. He, and Y. Inoue, *Fast crystallization of poly(3-hydroxybutyrate) and poly(3-hydroxybutyrate-co-3-hydroxyvalerate) with talc and boron nitride as nucleating agents.* Polym Int, 2005. **54**(5): p. 780-789.

7. Jacquel, N., et al., *Effect of Orotic Acid as a Nucleating Agent on the Crystallization of Bacterial Poly(3-hydroxybutyrate-co-3-hydroxyhexanoate) Copolymers.* Journal of Applied Polymer Science, 2009. **114**(2): p. 1287-1294.

8. Liu, W.J., et al., *Effect of nucleating agents on the crystallization of poly(3-hydroxybutyrate-co-3-hydroxyvalerate).* J Appl Polym Sci, 2002. **86**(9): p. 2145-2152.

9. Qian, J., et al., *Comparison of different nucleating agents on crystallization of poly(3-hydroxybutyrate-co-3-hydroxyvalerates).* Journal of Polymer Science Part B-Polymer Physics, 2007. **45**(13): p. 1564-1577.

10. Zhu, C.J., et al., *The effect of nucleating agents on physical properties of poly-3-hydroxybutyrate (PHB) and poly-3-hydroxybutyrate-co-3-hydroxyvalerate (PHB-co-HV) produced by Burkholderia cepacia ATCC 17759.* Polymer Testing, 2012. **31**(5): p. 579-585.

11. Ma, P.M., et al., *Effects of fumed silica on the crystallization behavior and thermal properties of poly(hydroxybutyrate-co-hydroxyvalerate).* Journal of Applied Polymer Science, 2008. **108**(3): p. 1770-1777.

12. Pan, P., et al., *Crystallization kinetics of bacterial poly(3-hydroxylbutyrate) copolyesters with cyanuric acid as a nucleating agent.* J Appl Polym Sci, 2013. **129**(3): p. 1374-1382.

13. Qiu, Z.B. and Z.S. Li, *Effect of Orotic Acid on the Crystallization Kinetics and Morphology of Biodegradable Poly(L-lactide) as an Efficient Nucleating Agent.* Industrial & Engineering Chemistry Research, 2011. **50**(21): p. 12299-12303.

14. Di Lorenzo, M.L. and C. Silvestre, *Non-isothermal crystallization of polymers.* Progress in Polymer Science, 1999. **24**(6): p. 917-950.

15. Jeziorny, A., *Parameters characterizing kinetics of nonisothermal crystallization of poly(ethylene-terephthalate) determined by DSC.* Polymer, 1978. **19**(10): p. 1142-1144.

16. Liu, T.X., et al., *Isothermal melt and cold crystallization kinetics of poly(aryl ether ether ketone ketone) (PEEKK).* European Polymer Journal, 1997. **33**(9): p. 1405-1414.

17. Lu, S.F., et al., *Nonisothermal Crystallization Kinetics of Biodegradable Poly(butylene succinate-co-propylene succinate)s.* Journal of Polymer Science Part B-Polymer Physics, 2010. **48**(12): p. 1299-1308.

18. Wu, M., et al., *Nonisothermal crystallization kinetics of ZnO nanorod filled polyamide 11 composites.* Materials Chemistry and Physics, 2008. **109**(2-3): p. 547-555.

19. Dobreva, A. and I. Gutzow, *Activity of substrates in the catalyzed nucleation of glass-forming melts .1. Theory.* Journal of Non-Crystalline Solids, 1993. **162**(1-2): p. 1-12.

20. Dobreva, A. and I. Gutzow, *Activity of substrates in the catalyzed nucleation of glass-forming melts .2. Experimental evidence.* Journal of Non-Crystalline Solids, 1993. **162**(1-2): p. 13-25.

21. Duan, B., et al., *Nonisothermal Melt-Crystallization Behavior of Calcium Phosphate/Poly(3-hydroxybutyrate-co-3-hydroxyvalerate) Nanocomposite Microspheres.* Polymer Engineering and Science, 2011. **51**(8): p. 1580-1591.

22. Supaphol, P., *Nonisothermal bulk crystallization and subsequent melting behavior of syndiotactic polypropylenes: Crystallization from the melt state.* Journal of Applied Polymer Science, 2000. **78**(2): p. 338-354.

23. Antoniadis, G., et al., *Non-isothermal crystallization kinetic of poly(ethylene terephthalate)/fumed silica (PET/SiO2) prepared by in situ polymerization.* Thermochimica Acta, 2010. **510**(1-2): p. 103-112.

24. Ozawa, T., *Kinetics of non-isothermal crystallization.* Polymer, 1971. **12**(3): p. 150-158.

25. Qiu, Z.B., et al., *Isothermal melt and cold crystallization kinetics of poly(aryl ether ketone ether ketone ketone).* Journal of Polymer Science Part B-Polymer Physics, 2000. **38**(15): p. 1992-1997.

26. Xiao, J., et al., *Crystallization kinetics of new copoly(ethylene terephthalate-imide)s.* Polymer, 2002. **43**(13): p. 3683-3690.

27. Naffakh, M., et al., *Dynamic Crystallization Kinetics and Nucleation Parameters of a New Generation of Nanocomposites Based on Isotactic Polypropylene and MoS2 Inorganic Nanotubes.* Journal of Physical Chemistry B, 2011. **115**(12): p. 2850-2856.

28. Di Lorenzo, M.L. and B. Wunderlich, *Temperature-modulated calorimetry of the crystallization of polymers analyzed by measurements and model calculations.* Journal of Thermal Analysis and Calorimetry, 1999. **57**(2): p. 459-472.

29. Corrêa, M.C.S., et al., *Elaboration and Characterization of Nano-Biocomposites Based on Plasticized Poly(Hydroxybutyrate-Co-Hydroxyvalerate) with Organo-Modified Montmorillonite.* Journal of Polymers and the Environment, 2012. **20**(2): p. 283-290.

Chapter 4.

EFFECT OF ULTRA-FINE TALC ON CRYSTALLIZATION AND END-USE PROPERTIES OF POLY(3-HYDROXYBUTYRATE-CO-3-HYDROXYHEXANOATE)

In this chapter, the effect of ultra-fine talc (0.5 to 2 wt%) on selected end-use properties of poly(3-hydroxybutyrate-co-3-hydroxyhexanoate) is investigated. The focus of this chapter lies on thermal stability, color, crystallization, gas permeability and tensile properties. This chapter was submitted for review in Journal of Applied Polymer Science as Vandewijngaarden, J., Murariu, M., Dubois, P., Carleer, R., Yperman, J., Peeters, R., Buntinx, M.: 'Effect of ultra-fine talc on crystallization and end-use properties of poly(3-hydroxybutyrate-co-3-hydroxyhexanoate)'

4.1 INTRODUCTION

Talc is a phyllosilicate with ideal chemical formula $Mg_3Si_4O_{10}(OH)_2$ [1-3]. It is a crystalline layered silicate without charge and thus without interlayer cations, this in contrary to montmorillonite clay (see Chapter 5). Talc consists of three hydrated layers. The elemental layer is an octahedral plane, comprised of linked $[MgO_4(OH)_2]^{8-}$ octahedrons. This layer is confined between two tetrahedral sheets of linked $(SiO_4)^{4-}$ tetrahedrons [2, 3]. A representation of the crystal structure of talc is given in Figure 4-1. Talc is made up of stacks of the triple-sheet crystalline units, which are held together by Van der Waals forces between surface oxygen atoms [4].

Talc is a widely used additive/filler in paints, pigments and paper. It is also extensively used in plastics engineering. PP is often modified by addition of talc. At concentrations of 2 to 10 wt%, crystallization rates are increased significantly and mold shrinkage is reduced. At higher loading (up to 40 wt%) it is possible to achieve a reinforcing effect, drastically increasing PP stiffness. On the other hand,

it has also been proven to be efficient at a concentration of 0.5 wt% in PE, but as an anti-blocking agent in order to avoid sticking of film [3].

Research has been published regarding the effect of talc on PHA as well. Most of these publications focus on crystallization properties, from which it can be clearly derived that talc has a beneficial effect on the crystallization rate of PHB and PHBV, in concentration of 1 and 5 wt% [5, 6], as well as poly(3-hydroxybutyrate-co-4-hydroxybutyrate) (0.5 wt% talc) [7]. A limited amount of publications regarding the combination of PHBHHx and talc (in concentrations ranging from 1 to 15 wt%) can be retrieved as well, but do not provide an in-depth characterization [8, 9]. Zhang et al. reported an increase in toughness of PHBHHx at low talc concentrations and a decrease in thermal stability, as measured by TGA [9].

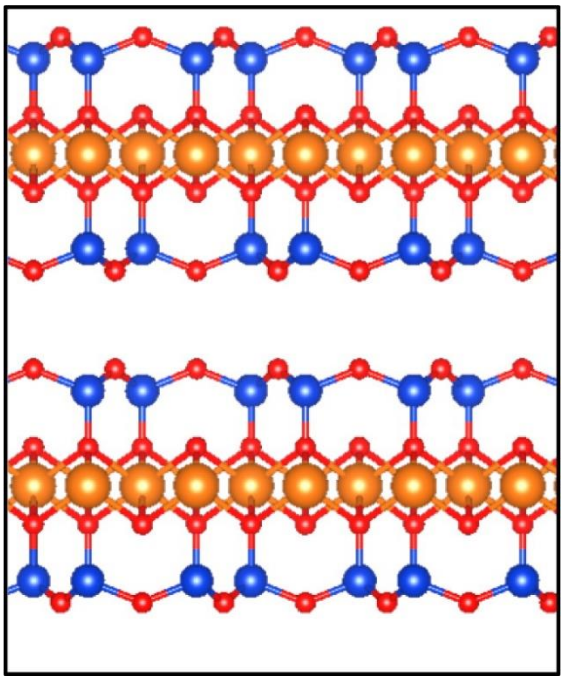

Figure 4-1: Crystal structure of talc. The positions of the hydrogen atoms are not shown. (Si, blue; Mg, bronze; O, red) [10]

In this chapter, a novel grade of talc (Jetfine® 3 C A by Imerys) was employed. The median diameter of this grade of talc is about 1 µm, whereas the median diameter for more conventional grades lies between 2 and 10 µm. The heavily reduced median diameter could lead to significant changes in properties, but at lower concentrations. A beneficial effect by reducing particle size has already been

observed for PP [11], PLA [12, 13] and polycarbonate/poly(butylene terephthalate) blends [14]. Petchwattana et al. (2014) have studied the effects of up to 10 wt% talc in promoting the crystallization of poly(lactic acid) (PLA). Three different talc particle sizes, namely 1, 5 and 30 µm, were used as nucleating agent. Talc was found to be an effective nucleating agent for accelerating the crystallization rate in PLA, whereas the finer talc particles were found to lead slightly to higher degrees of crystallinity [12].

Besides the effect on intrinsic polymer properties (thermal stability and crystallization), an in-depth characterization of specific end-use properties (gas permeability, tensile properties etc.) is given as well. Rather low concentrations of 0.5 to 2 wt% talc were employed due to the fact that enhanced crystallization, without damaging mechanical properties, was the main objective.

4.2 EXPERIMENTAL

4.2.1 Materials and sample preparation

Pure PHBHHx powder, with a 3-hydroxyhexanoate content of 10.5 mol%, was provided by Kaneka Corporation (Westerlo-Oevel, Belgium) and dried at 70 °C *in vacuo* for 3 days.

Ultra-fine talc powder (spherical morphology, tradename Jetfine® 3 C A) was kindly provided by Imerys Talc. According to the technical sheet, the median diameter d_{50} of the talc particles was 1 µm, as measured by sedimental analysis. The powder was dried at 120 °C for 1 day prior to use. Samples containing 0.5, 1 and 2 wt% were prepared, along with a reference sample containing no talc.

Firstly, samples with a total weight of 55 g were dry-mixed in a Rondol mini-mix high speed mixer, before being processed in a Brabender counter-rotating internal mixer equipped with roller blades at a temperature of 140 °C. During feeding of the mixer, a rotation speed of 30 rpm was used for 3 min to avoid the excessive increase of the torque during polymer melting. Then the rotation speed was increased to 70 rpm for 8 min.

Subsequently, samples of about 1.8 g were compressed and molded at 140 °C to prepare films in a polyimide mold (100 mm x 100 mm x 0.150 mm) using an Agila PE20 hydraulic press. The polymer was pre-heated for 90 s without pressure, after

which it was pressed at 30 bar for 150 s, followed by three degassing cycles. Finally, the films were pressed at high pressure of 150 bar for 120 s, followed by a slow cooling at 50 bar for 20 min at 60 °C to allow film crystallization and easy demolding [15].

Thicker plates for tensile testing were produced in a stainless steel mold (100 mm x 100 mm x 0.5 mm) at 140 °C with a pre-heating time of 3 min before being pressed at 30 bar for 200 s. Subsequently two degassing cycles were used before finally molding the sample at 150 bar for 150 s. The samples were slowly cooled at 50 bar for 20 min at 60 °C.

4.2.2 Differential scanning calorimetry (DSC)

Thermal properties of the prepared films were analyzed in sealed aluminium pans under inert atmosphere (50 ml/min nitrogen) using a TA Instruments Q200 DSC and sample weights of about 3.5 mg.

For non-isothermal crystallization experiments, the sample was heated from -30 °C to 150 °C or 170 °C at a heating rate of 10 °C/min. After being kept isothermal for 2 min, the sample was cooled at 10 °C/min to -30 °C and kept constant for 2 min prior to heating to 170 °C at 10 °C/min.

For isothermal crystallization experiments, the sample was heated from -30 °C to 150 °C or 170 °C at a heating rate of 10 °C/min. After an isothermal period of 3 min, the sample was rapidly cooled to 70 °C at 45 °C/min and kept isothermal until crystallization was completed.

For all samples, only the weight fraction of polymer in the composites was considered to allow a more accurate determination of enthalpy values.

Measurements were performed at least in duplicate.

4.2.3 Gel permeation chromatography (GPC)

The molecular weight distribution of the samples was analyzed using a GPC apparatus composed of a SpectroSeries P100 pump, equipped with a Shodex RI71 refractometer detector and two PL-gel 10 µm Mixed-B columns in series, thermostated at 35 °C. The eluent was chloroform (VWR, HPLC grade) at a flow rate of 1.0 ml/min. Samples were dissolved in chloroform at a concentration of 1

g/l and filtered over a 0.45 µm syringe filter. The injection volume was 100 µl. Calibration was performed using polystyrene standards (474 to 3 150 x 10^3 g/mol) dissolved in chloroform with a concentration of 1 g/l.

4.2.4 Thermogravimetric analysis (TGA)

The thermal stability of the samples was analysed using a TA Instruments Hi-Res TGA 2950 thermogravimetric analyser. Samples of about 10 mg were heated from room temperature to 350 °C at a heating rate of 20 °C/min with a N_2 gas flow of 80 ml/min. Measurements were performed at least in duplicate.

4.2.5 Colorimetric analysis

Colorimetric analysis was performed using a Datacolor MicroFlash 200d. Results are presented in CIELAB color coordinates (L^*, a^* and b^*). The total color change ΔE_{ab} is calculated as:

$$\Delta E_{ab} = \sqrt{\Delta L^2 + \Delta a^2 + \Delta b^2} \quad (4\text{-}1)$$

With ΔL, Δa and Δb respectively the difference in L^*, a^* and b^* between the reference (0 wt% talc) and the samples containing talc. A sample was measured 4 times (twice on each side) in order to obtain a representative average.

4.2.6 Opacity

The opacity of the prepared films was determined according to the Hunter Lab method in the reflectance mode, using a Datacolor Microflash 100D. The opacity Y (in %) can be calculated as the relationship between the opacity of a sample on a black standard Y_b and the opacity on a white standard Y_w:

$$Y = Y_b / Y_w \times 100 \quad (4\text{-}2)$$

A sample was measured 4 times (twice on each side) in order to obtain a representative average.

4.2.7 Polarization optical microscopy (POM)

POM experiments were performed using a Nikon Optiphot-Pol polarized optical microscope. Solutions of 5 mg/ml of each sample in chloroform were prepared. A few drops were placed on a microscopy glass and left to dry for 5 min before being placed for 1 day in a vacuum oven at 70 °C. After drying, each sample was

isothermally crystallized, using a DSC oven, in the following way: heating to 170 °C at 10 °C/min, isothermal period at 170 °C for 10 min, cooling to 70 °C at 45 °C/min and finally isothermal crystallization for 40 min at 70 °C.

4.2.8 Thickness measurements

Sample thickness was measured prior to permeability testing using a MTS MI20 thickness gauge. The thickness was taken as the average of five measurements at different locations of each sample.

4.2.9 Barrier properties

The oxygen transmission rate (OTR), at 23 °C and 0 % relative humidity (RH), of the produced samples was measured using a Mocon Ox-Tran 702 (ASTM D3985). Carbon dioxide transmission rate (CO_2TR) at 23 °C and 0 % RH was measured using a Mocon Permatran-C 4/41 (ASTM F2476). Water vapor transmission rate (WVTR) was measured using a Mocon Permatran-W 700 (ASTM F1249). Test gases (O_2 and CO_2) and carrier gas (N_2, N_2/H_2) with a purity of 99.999 % were purchased from Westfalen, Münster (Germany). Samples were placed between 2 aluminium masks with an effective testing area of 5 cm². The sample was exposed to the test gas on one side and to a continuously flushing carrier gas on the other side, both at a total pressure of 1 atm. For OTR measurements a carrier gas N_2/H_2 (95/5) was used, for all other measurements pure N_2. The test gas diffuses through the sample and is guided by the carrier gas towards the detector. The gas transmission rate or gas flux J, in cm³/m².day.atm (for OTR and CO_2TR) or g/m².day (for WVTR) of the specific test gas, is reported when equilibrium is reached (i.e. the concentration of test gas in the carrier gas changes less than 1 % during a test cycle of 30 min). The gas flux J can be defined as the quantity of test gas or permeant Q, which passes through the polymeric film per unit area A during one unit of time t at equilibrium: [16-18]

$$J = Q / (A.t) \tag{4-3}$$

In order to obtain a thickness-independent criterion for comparison, the gas flux J can be normalized for sample thickness d and permeant pressure p to obtain the permeability coefficient P: [16-18]

$$P = J.d / p \tag{4-4}$$

For each sample, two specimens were measured in duplicate.

4.2.10 Tensile testing

The tensile test was performed according to ASTM D638-02 using a MTS/10 tensile tester at a crosshead speed of 1 mm/min and a distance of 25.4 mm between the grips. Samples were cut into dumbbell shapes (ASTM D638-02 type V) and were conditioned at 23 °C and 50 % relative humidity for 48 h before testing. At least 10 specimens were tested for each sample.

4.3 RESULTS AND DISCUSSION

4.3.1 Crystallization properties

For the non-isothermal crystallization experiments, the most important parameters related to crystallization, that can be derived, are the onset temperature of crystallization ($T_{c,o}$), crystallization peak temperature ($T_{c,p}$) and the crystallization enthalpy (ΔH_c). The difference between $T_{c,o}$ and $T_{c,p}$ is calculated as well for each sample in order to observe any changes in crystallization peak width. These results are presented in Table 4-1. The non-isothermal crystallization curves are given in Figure 4-2.

Two melting temperatures from which crystallization must occur during cooling were selected. The first melting temperature is 150 °C, as this is the maximum processing temperature, suggested by the supplier. It is clear that $T_{c,o}$ and $T_{c,p}$ are raised to higher temperatures with increasing amounts of talc. A maximum in crystallization temperature is observed upon addition of 2 wt% talc, resulting in an increase of about 4 °C in $T_{c,o}$ and $T_{c,p}$. This is a clear indication that talc acts as a nucleating agent and thus promotes crystallization of PHBHHx. The crystallization enthalpy ΔH_c and the width of the crystallization peak ($T_{c,o}$ - $T_{c,p}$) remain fairly constant.

A second experimental melting temperature of 170 °C was employed in order to observe if it is possible to enlarge the temperature range at which PHBHHx can be processed and still achieve successful crystallization with a high rate. This can be an promising feature, as some industrial processing require lower viscosity, which is achieved by raising processing temperature.

Upon cooling from the molten state at 170 °C, pure PHBHHx is not able to display any significant crystallization behavior. However, upon addition of ultra-fine talc, an outspoken crystallization peak can be observed. It is also clear that $T_{c,o}$ and $T_{c,p}$ are raised to higher temperatures with increasing amounts of talc. Adding 0.5 wt% talc results in a $T_{c,p}$ of 65.9 °C, whereas $T_{c,p}$ is 70.3 °C for 2 wt% talc.

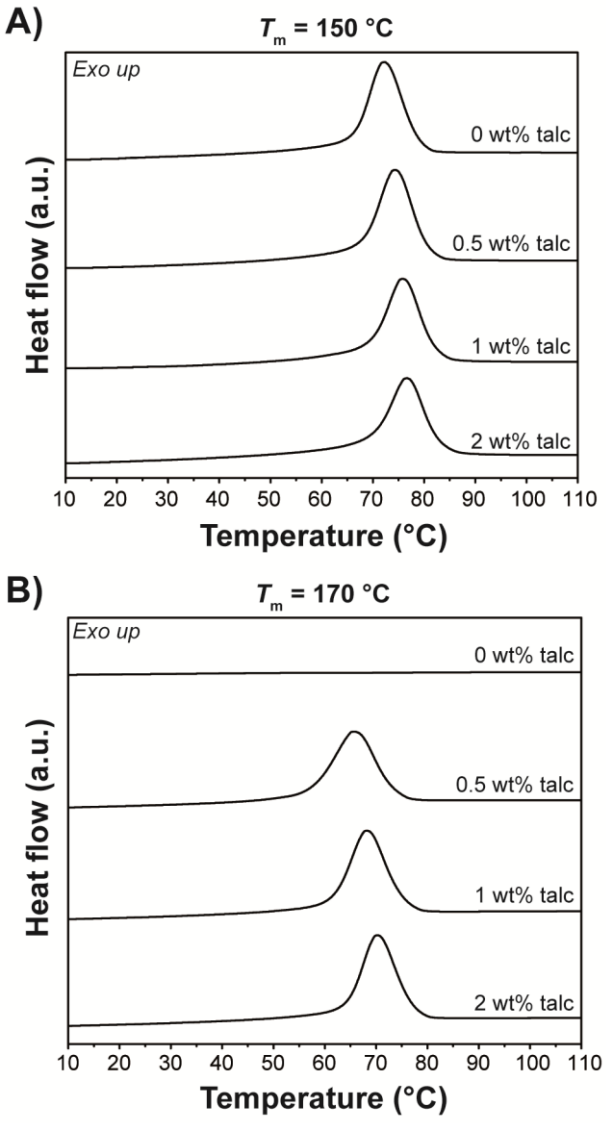

Figure 4-2: Non-isothermal crystallization curves from melting temperatures of A) 150 °C and B) 170 °C

Pure PHBHHx also presents cold crystallization during subsequent heating (onset temperature and enthalpy of 54.1 °C and 6.3 J/g, respectively), whereas the samples containing talc do not present any kind of cold crystallization behavior under these testing conditions. This is also a clear indication of higher crystallinity achieved during cooling from the melt, with ΔH_c of the samples containing talc being about 33 J/g. The crystallization enthalpy ΔH_c is constant for all samples containing talc. Important to note is that the width of the crystallization peak ($T_{c,o}$ - $T_{c,p}$) decreases slightly from 7.6 to 7.1 °C, for respectively 0.5 and 2 wt%, which is indicative of an increasingly narrower crystallization peak. These results clearly confirm that ultra-fine talc acts as a nucleating agent for PHBHHx.

Table 4-1: Non-isothermal crystallization properties of PHBHHx/talc composites (n.d. = not detected, n = 2 or 3)

Talc content	$T_{c,o}$ (± 0.1 °C)	$T_{c,p}$ (± 0.1 °C)	ΔH_c (± 0.5 J/g)	$T_{c,o}$ - $T_{c,p}$ (°C)
T_m = 150 °C:				
0 wt%	79.0	72.2	33.3	6.9
0.5 wt%	80.7	74.3	33.1	6.5
1 wt%	82.1	75.8	32.1	6.3
2 wt%	83.1	76.6	31.6	6.5
T_m = 170 °C:				
0 wt%	n.d.	n.d.	n.d.	n.d.
0.5 wt%	73.5	65.9	33.6	7.6
1 wt%	75.4	68.1	33.8	7.3
2 wt%	77.4	70.3	32.9	7.1

In order to gain more insights into the effect of talc on the crystallization properties of PHBHHx, isothermal crystallization experiments were performed as well. From the molten state, either 150 °C or 170 °C, samples were cooled with 45 °C/min to an isothermal crystallization temperature of 70 °C. For this type of experiment, it is necessary to calculate the crystallization half-time $t_{1/2}$, which is defined as the time needed to reach 50 % relative crystallinity. The crystallization half-time $t_{1/2}$, as well as the change in crystallization half-time $\Delta t_{1/2}$ (in comparison to pure PHBHHx), are presented in Table 4-2. The DSC curves are presented in Figure 4-3.

Isothermal crystallization from the molten state at 150 °C results in a significant decrease in $t_{1/2}$ of 21.7 %, 37.3 % and 47.0 % for the samples containing 0.5 wt%, 1 wt% and 2 wt% talc, respectively. For 2 wt% ultra-fine talc, $t_{1/2}$ is reduced to 0.44 min. The shape of the peak becomes slightly more narrow as well.

Table 4-2: Isothermal crystallization properties of PHBHHx/talc composites (n = 2 or 3)

Talc content	$t_{1/2}$ (± 0.02 min)	$\Delta t_{1/2}$ (%)
T_m = 150 °C:		
0 wt%	0.83	/
0.5 wt%	0.65	-21.7
1 wt%	0.52	-37.3
2 wt%	0.44	-47.0
T_m = 170 °C:		
0 wt%	15.28	/
0.5 wt%	1.54	-89.9
1 wt%	0.52	-96.6
2 wt%	0.44	-97.1

Similar to the non-isothermal experiments, the effect of ultra-fine talc on pure PHBHHx is most outspoken at the higher melting temperature of 170 °C. Pure PHBHHx displays a very broad crystallization peak (marked with a red dotted line for emphasis), corresponding to a high $t_{1/2}$ of 15.28 min. The addition of ultra-fine talc dramatically reduces $t_{1/2}$ to only a fraction of pure PHBHHx. A talc content of 0.5, 1 and 2 wt% leads to a $t_{1/2}$ of 1.54, 0.52 and 0.44 min, respectively, which corresponds to reduction of up to 97 %. The crystallization peak is rendered much more narrow as well, which can be clearly seen from the DSC curves. The isothermal experiments clearly display that the addition of talc to PHBHHx is highly beneficial for the crystallization properties. These experiments also further clarify the importance of talc concentrations. By adding 1 wt% talc, the value of $t_{1/2}$ is only one third of $t_{1/2}$ at a concentration of 0.5 wt%. Increasing the talc content to 2 wt% has a slightly lower $t_{1/2}$, but the effect is not as outspoken.

An important detail to note is that the addition of 1 and 2 wt% results in practically the same $t_{1/2}$ at both experimental melting temperatures, which is a clear indication that the addition of ultra-fine talc can facilitate higher processing temperatures and thus expanding the processability

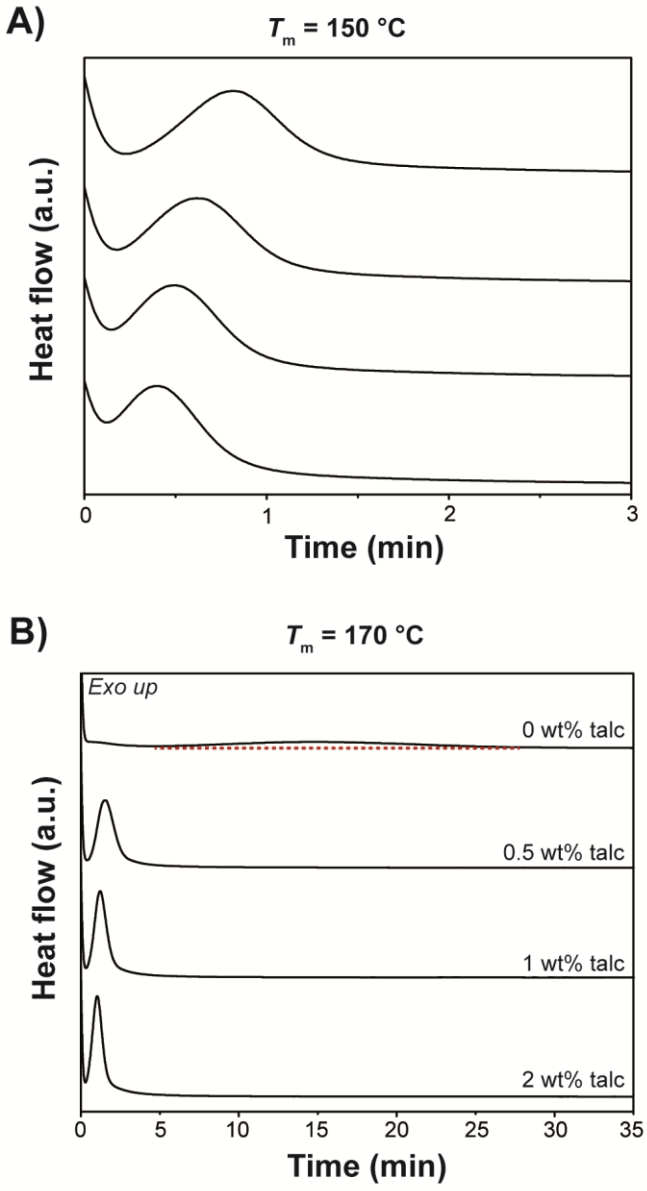

Figure 4-3: Isothermal crystallization curves from melting temperatures of A) 150 °C and B) 170 °C

In order to assess the effect of ultra-fine talc on spherulite size of PHBHHx, some polarization optical microscopy (POM) experiments were performed for isothermal crystallization at 70 °C from a melting temperature of 170 °C. These images are presented in Figure 4-4 at a 20x magnification. The differences in spherulite size can be discerned immediately. Pure PHBHHx presents very large spherulites, with diameters ranging between approximately 100 and 150 μm. The addition of talc in all tested concentrations, results in a much larger number of smaller spherulites, with a diameter of approximately 20 μm.

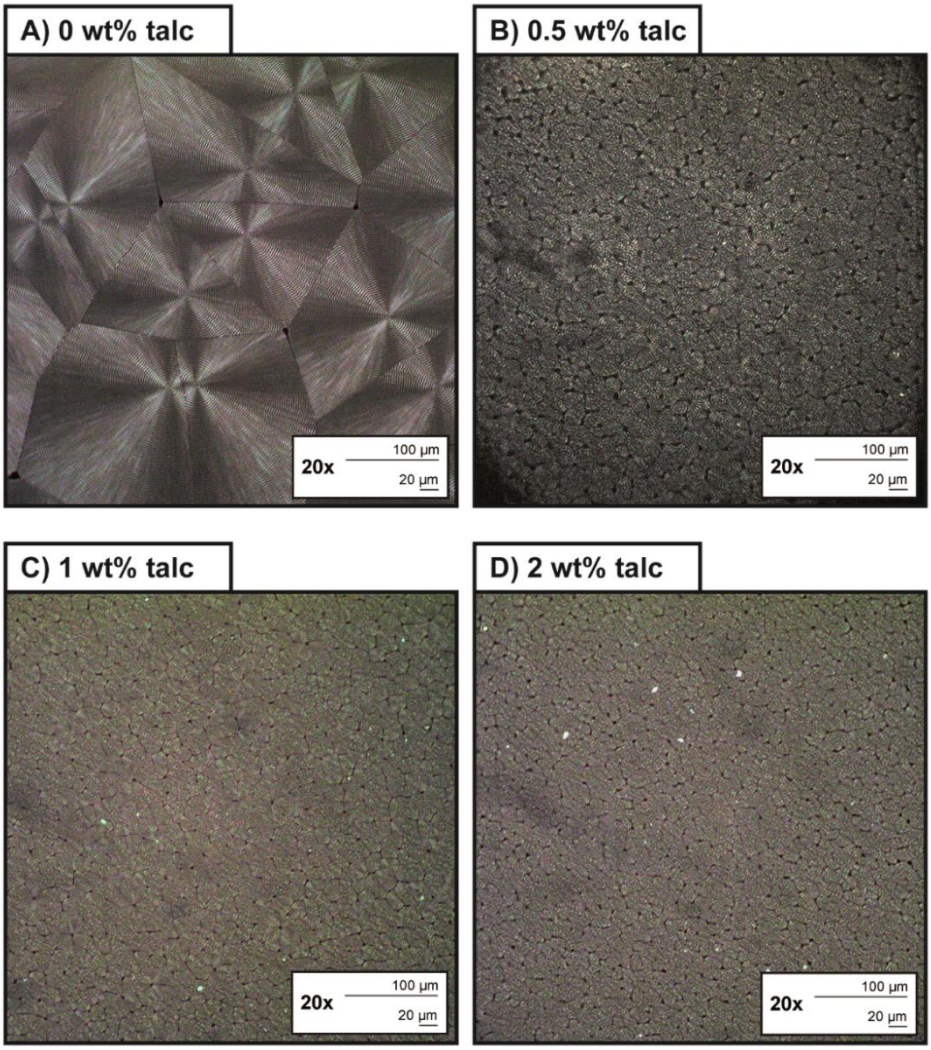

Figure 4-4: POM images of PHBHHx/talc composites containing A) 0 wt%, B) 0.5 wt%, C) 1 wt% and D) 2 wt% of ultra-fine talc

By combining DSC experiments with POM, it can be concluded that ultra-fine talc is a highly performant nucleating agent for PHBHHx containing 10.5 mol% 3-hydroxyhexanoate units. This in contradiction with the study performed by Jacquel et al. (2010), in which talc appeared to have no significant effect on the crystallization of a similar type of PHBHHx. Unfortunately, the particle size of the talc was not disclosed, so it is not possible to make a direct comparison. One must also consider that the studied composites were prepared by solvent casting [8]. In this study however, the samples were prepared by dry-mixing followed by melt compounding, which could play a key role in determining the final properties. The above results, however, clearly show the enhanced crystallization properties of the samples at hand.

4.3.2 Thermal degradation during processing

Using GPC, the thermo-mechanical degradation occurring during melt blending of the polymer and talc was investigated. The number average molecular weight $\bar{M}_n$, weight average molecular weight $\bar{M}_w$ and dispersity ($Đ_M$), defined as the ratio of $\bar{M}_w$ to $\bar{M}_n$, were determined before (virgin) and after melt processing. These results are presented in Table 4-3. It becomes immediately clear that melt processing induces a significant decrease in molecular weight, due to thermal and shear-induced degradation. Upon comparison of the composites, it is possible to observe some fluctuation in results, however no correlation between the talc content and reduction in molecular weight is found. Thus, it must be concluded that the presence of the ultra-fine talc particles during melt processing will not induce a significant amount of extra polymer degradation. It is also important to note that typically processing itself does not seem to affect the dispersity severely, despite the significant reduction in $\bar{M}_w$ and $\bar{M}_n$.

Table 4-3: Molecular weight distribution of PHBHHx/talc composites

Talc content	$\bar{M}_n$ (x 10^3 g/mol)	$\bar{M}_w$ (x 10^3 g/mol)	$Đ_M$
virgin PHBHHx	272	686	2.5
0 wt%	179	489	2.7
0.5 wt%	176	525	3.0
1 wt%	222	523	2.4
2 wt%	194	488	2.5

4.3.3 Thermal stability

The thermal stability of the prepared composites was investigated using TGA under pure nitrogen atmosphere from room temperature to 350 °C with a heating rate of 20 °C/min. The results of the thermogravimetric analysis are presented in Table 4-4.

It can be observed that all three indicative parameters increase slightly at higher talc contents, thus implying a higher thermal stability. The addition of 2 wt% talc to PHBHHx led to the greatest effect, with T_o, T_{50} and T_{max} raised with 4.0 °C, 3.6 °C and 2.5 °C, respectively. Zhang et al. (2007) observed a slight increase of 4 °C in T_{max} in solvent cast PHBHHx samples containing 3 wt% talc [9], similar to the results presented in this study. An increase in thermal stability due to the presence of talc in the polymer matrix has also been observed in other polymeric systems, such as poly(lactid acid)/poly(ε-caprolactone) blends [19] and poly(butylene succinate) [20]. In both studies, this increase in stability was attributed to the so-called barrier effect, due to the fact that the presence of an inorganic filler (with a platelet morphology in this study) hinders the release of volatile degradation products by creating a tortuous path.

Table 4-4: Thermal properties of PHBHHx/talc composites (n = 2 or 3)

Talc content	$T_{d,o}$ (°C)	$T_{d,50}$ (°C)	$T_{d,p}$ (°C)
0 wt%	288.9 (± 0.2)	300.7 (± 0.2)	307.6 (± 0.1)
0.5 wt%	289.9 (± 0.3)	301.8 (± 0.5)	306.5 (± 0.7)
1 wt%	292.9 (± 0.8)	304.2 (± 0.2)	310.1 (± 0.4)
2 wt%	292.9 (± 0.1)	304.3 (± 0.3)	310.1 (± 1.6)

4.3.4 Colorimetric analysis and opacity

The change in color coordinates (ΔL, Δa and Δb) and the total color change (ΔE_{ab}) of the prepared samples are presented in Table 3, with neat PHBHHx used as a reference to calculate color change upon addition of talc. The impact of talc on the colorimetric properties of PHBHHx is rather limited, with ΔL becomes more negative upon increasing the amount of talc, indicative of the samples becoming slightly darker. Δb is positive and increasing with higher talc loading, implying more yellowness. The total color change ΔE_{ab} is only limited, reaching a maximum value of 0.9 for 2 wt% talc.

The results of the opacity measurements are given in the right-hand column of Table 4-5. It can be concluded that the samples are rendered slightly more opaque upon addition of increasing amounts of talc. This can be expected because foreign particles are introduced in increased concentration, which can reflect light and thus induce opacity. However, this effect is not very extensive, as the opacity increases from 10 % to only 13.9 % at a talc loading of 2 wt%.

Table 4-5: Colorimetric properties and opacity of PHBHHx/talc composites

Talc content	Δ*L*	Δ*a*	Δ*b*	ΔE_{ab}	Opacity *Y* (%)
0 wt%	/	/	/	/	10.0
0.5 wt%	-0.2	0	0	0.2	10.3
1 wt%	-0.2	0	0	0.2	11.1
2 wt%	-0.8	0	0.4	0.9	13.9

4.3.5 Barrier properties

The barrier properties, with relevance for packaging applications, were investigated through analysis of permeability of the produced samples for oxygen, carbon dioxide and water vapor (PO_2, PCO_2 and PH_2O). The results of the experiments are presented in Table 4-6. The permeability coefficients of the pure PHBHHx film are fairly similar to the ones obtained in Chapter 2, remaining within the same range of applicability. Since the talc particles in the PHBHHx matrix can be considered as physically impermeable to gas or vapor molecules, a reduction in gas permeability due to creation of an enhanced tortuous path was initially expected, with the filler amount being a key parameter that must be taken into account. However, upon addition of 0.5 wt% talc, the values for PO_2, PCO_2 and PH_2O, unexpectedly, were slightly increased. By increasing the talc content further to 1 and 2 wt%, PO_2, PCO_2 and PH_2O start to decrease again, with the 2 wt% sample performing slightly better than the neat PHBHHx.

It is noteworthy to mention that the literature information about the effects of talc addition in different polymer systems is somewhat contradictory, but in many cases a significant improvement of gas and water vapor barrier properties is reported (e.g. in PLA-talc based composites [19]). We suspect also that using

extrusion techniques, the improvements in barrier properties of PHBHHx – talc films are to be even more obvious with respect to neat PHBHHx films: a) owing to the effectiveness of the nucleating agent which leads to uniform microcrystalline structure and higher crystallinity, b) due to possible orientation of talc platelets following the extrusion and drawing process.

Table 4-6: Gas permeability properties of PHBHHx/talc composites (n=4)

Talc content	PO_2 (cm^3 mm m^{-2} day^{-1} atm^{-1})	PCO_2 (cm^3 mm m^{-2} day^{-1} atm^{-1})	PH_2O (g mm m^{-2} day^{-1})
0 wt%	7.9 (± 0.2)	37.0 (± 0.7)	1.27 (± 0.01)
0.5 wt%	9.0 (± 0.7)	41.9 (± 0.4)	1.54 (± 0.09)
1 wt%	8.4 (± 0.2)	39.9 (± 0.9)	1.32 (± 0.04)
2 wt%	7.5 (± 0.2)	38.6 (± 0.7)	1.21 (± 0.05)

A possible explanation for the observed trend might be related to the enhanced nucleation, induced by the ultra-fine talc particles in the PHBHHx matrix. It is well known that the addition of a nucleating agent results in the formation of a larger amount of nuclei, which will finally grow into crystallites [5]. However, due to the higher number of crystallites, they will be significantly smaller in size, in comparison to the lower amount of larger crystallites formed in a non-nucleated polymer. This effect was clearly shown in Figure 4-4. The crystalline fraction of the polymer acts as a barrier to gas permeability, but if the crystallites are smaller, the tortuous path is reduced as well, which is the case for the sample containing 0.5 wt% talc. Upon increasing the talc content, a second phenomenon comes into play. The physical impermeability of the talc platelets will become more important than the reduced crystallite size, which could explain the subsequent reduction in gas permeability at higher talc concentrations.

4.3.6 Tensile properties

In order to assess the effect of a variable concentration of ultra-fine talc on the tensile properties, stress-strain curves were measured, as shown in Figure 4-5. From these measurements, it is possible to determine Young's modulus, tensile strength (calculated from the maximum in load), the nominal strain at break and the nominal strain at the point of maximum load, which are presented in Table 4-7.

Table 4-7: Tensile properties of PHBHHx/talc composites (n = 10)

Talc content	Young's modulus (MPa)	max. tensile strength (MPa)	nominal strain at max. load (%)	nominal strain at break (%)
0 wt%	804 (± 24)	21.5 (± 0.4)	6.8 (± 0.2)	8.3 (± 0.2)
0.5 wt%	838 (± 18)	22.0 (± 0.2)	6.7 (± 0.1)	8.3 (± 0.4)
1 wt%	860 (± 16)	21.7 (± 0.4)	6.4 (± 0.1)	8.2 (± 0.4)
2 wt%	907 (± 20)	21.9 (± 0.3)	6.3 (± 0.2)	7.9 (± 0.2)

From these results, it can be concluded that adding small amounts of ultra-fine talc has only a limited effect on the tensile properties. The max. tensile strength stays constant, whereas the nominal strain at max. load and nominal strain at break show a decreasing trend, though very limited.

The most outspoken change can be found in the Young's modulus, which increases gradually from 804 MPa to 907 MPa upon addition of 2 wt% talc. Zhang et al. (2007) observed a Young's modulus twice as high as pure PHBHHx upon addition of 3 wt% talc [9], which is much higher than the results presented here.

Globally, the addition of ultra-fine talc, with a maximum concentration of 2 wt%, renders PHBHHx slightly stiffer, but it still retains its ductile nature. As a result, the potential for applications, where flexibility is a necessity, was not compromised.

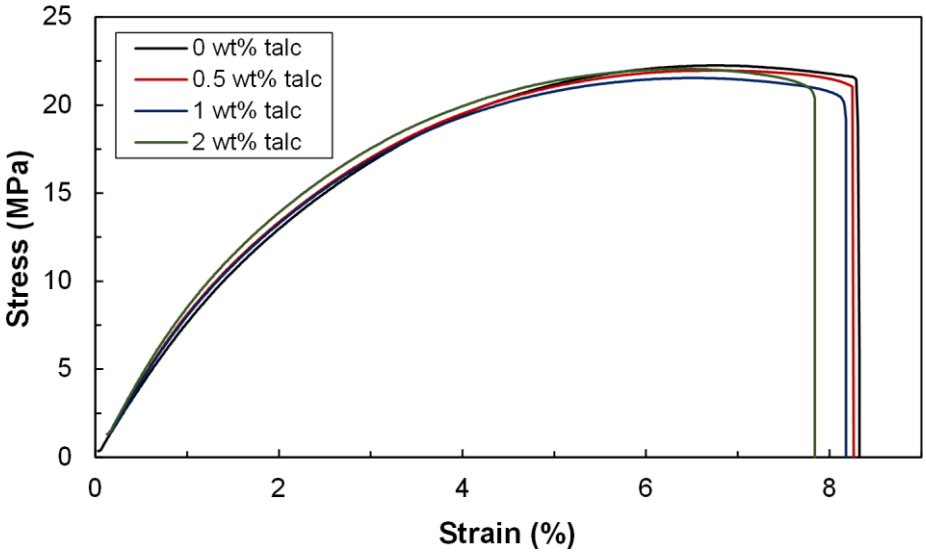

Figure 4-5: Examples of stress-strain curves of PHBHHx/talc composites with 0-2 wt% talc

4.4 CONCLUSIONS

In this study a comprehensive characterization of composites consisting of PHBHHx and 0, 0.5, 1 and 2 wt% ultra-fine talc (median diameter = 1 µm) was performed with a focus on the end-use properties as packaging material.

Via an isothermal and non-isothermal crystallization study, it was proven that ultra-fine talc is an excellent nucleating agent for PHBHHx. Isothermal crystallization half time at 70 °C was reduced by 97 %, in comparison to neat PHBHHx by adding 2 wt% ultra-fine talc, which is highly advantageous for the processability of PHBHHx. It was also observed that the processing temperature could be raised by use of ultra-fine talc. Upon increasing the melt temperature of the DSC experiments from 150 °C to 170 °C, neat PHBHHx was not able to sufficiently crystallize, whereas the samples containing talc still displayed a strong crystallization peak.

Thermal stability was shown to increase slightly, by about 4 °C. Color changes were only minor and a slight increase in opacity from 10.0 to 13.9 %, upon addition of 2 wt% ultra-fine talc, was observed. The gas permeability properties (O_2, CO_2 and water vapor), which can be highly important for food packaging

applications, of the samples containing 0.5 and 1 wt% of talc were slightly higher than that of neat PHBHHx.

The gas permeability upon addition of 2 wt% on the other hand was slightly lower. This unusual trend can be attributed to changes in tortuous path, due to a combinatory effect of smaller spherulites and the presence of impermeable talc particles. It is, however, important to note that all samples were still in the same range of applicability, in terms of food packaging materials.

Regarding the mechanical properties, the addition of ultra-fine talc in low concentrations lead to a slight increase in Young's modulus, whereas tensile strength and elongation at break remained practically the same.

Overall, it can be concluded that minor concentrations (up to 2 wt%) of ultra-fine talc could be very promising to further enhance the industrial processability of PHBHHx. It is a highly efficient nucleating agent, rendering the PHBHHx matrix slightly stiffer and causing a minor increase in thermal stability. The addition of highly effective nucleating agents is considered an valuable possibility to improve its processing properties and to expand the applications of this biopolymer.

4.5 REFERENCES

1. Gatta, G.D., et al., *On the crystal structure and compressional behavior of talc: a mineral of interest in petrology and material science.* Phys. Chem. Miner., 2013. **40**(2): p. 145-156.

2. Malandrini, H., et al., *Interactions between Talc Particles and Water and Organic Solvents.* J. Colloid Interface Sci., 1997. **194**(1): p. 183-193.

3. Kogel, J., et al., *Industrial minerals & rocks: Commodities, markets and uses*. 2006, Colorado: Society for Mining, Metallurgy, and Exploration, Inc. 1548.

4. Zazenski, R., et al., *Talc: Occurrence, Characterization, and Consumer Applications.* Regul. Toxicol. Pharm., 1995. **21**(2): p. 218-229.

5. Kai, W., Y. He, and Y. Inoue, *Fast crystallization of poly(3-hydroxybutyrate) and poly(3-hydroxybutyrate-co-3-hydroxyvalerate) with talc and boron nitride as nucleating agents.* Polym. Int., 2005. **54**(5): p. 780-789.

6. Zhu, C., et al., *The effect of nucleating agents on physical properties of poly-3-hydroxybutyrate (PHB) and poly-3-hydroxybutyrate-co-3-hydroxyvalerate (PHB-co-HV) produced by Burkholderia cepacia ATCC 17759.* Polym. Test., 2012. **31**(5): p. 579-585.

7. Wang, L., et al., *Effect of nucleation agents on the crystallization of poly(3-hydroxybutyrate-co-4-hydroxybutyrate) (P3/4HB).* J. Appl. Polym. Sci., 2010. **116**(2): p. 1116-1123.

8. Jacquel, N., et al., *Nucleation mechanism of polyhydroxybutyrate and poly(hydroxybutyrate-co-hydroxyhexanoate) crystallized by orotic acid as a nucleating agent.* J. Appl. Polym. Sci., 2010. **115**(2): p. 709-715.

9. Zhang, X., et al., *Some novel layered-silicate nanocomposites based on a biodegradable hydroxybutyrate copolymer.* Eur. Pol. J., 2007. **43**(8): p. 3128-3135.

10. Fischer, F.D., et al., *Ultrathin Ti-Silicate Film on a Ru(0001) Surface.* The Journal of Physical Chemistry C, 2015. **119**(27): p. 15443-15448.

11. Švehlová, V. and E. Polouček, *Mechanical properties of talc-filled polypropylene. Influence of filler content, filler particle size and quality of dispersion.* Angew. Makromol. Chem., 1994. **214**(1): p. 91-99.

12. Petchwattana, N., S. Covavisaruch, and S. Petthai, *Influence of talc particle size and content on crystallization behavior, mechanical properties and morphology of poly(lactic acid).* Polym. Bull., 2014. **71**(8): p. 1947-1959.

13. Tábi, T., et al., *Thermal and mechanical analysis of injection moulded poly(lactic acid) filled with poly(ethylene glycol) and talc.* J. Therm. Anal. Calorim., 2014. **118**(3): p. 1419-1430.

14. DePolo, W.S. and D.G. Baird, *Particulate reinforced PC/PBT composites. I. Effect of particle size (nanotalc versus fine talc particles) on dimensional stability and properties.* Polym. Compos., 2009. **30**(2): p. 188-199.

15. Ding, C., B. Cheng, and Q. Wu, *DSC analysis of isothermally melt-crystallized bacterial poly(3-hydroxybutyrate-co-3-hydroxyhexanoate) films.* J. Therm. Anal. Calorim., 2011. **103**(3): p. 1001-1006.

16. Bronlund, J.E., G.P. Redding, and T.R. Robertson, *Modelling Steady-State Moisture Transport Through Corrugated Fibreboard Packaging.* Packag. Technol. Sci., 2013. **27**: p. 193-201.

17. Cagnon, T., et al., *Nanostructuring and Microstructuring of Materials from a Single Agropolymer for Sustainable MAP Preservation of Fresh Food.* Packag. Technol. Sci., 2013. **26**(3): p. 137-148.

18. Kuorwel, K.K., et al., *Physico-Mechanical Properties of Starch-Based Films Containing Naturally Derived Antimicrobial Agents.* Packag. Technol. Sci., 2013. **27**: p. 149-159.

19. Jain, S., et al., *A New Biodegradable Flexible Composite Sheet from Poly(lactic acid)/Poly(ε-caprolactone) Blends and Micro-Talc.* Macromol. Mater. Eng., 2010. **295**(8): p. 750-762.

20. Sun, B., et al., *Effect of different amounts of modified talc on the mechanical, thermal and crystallization properties of poly(butylene succinate).* J. Polym. Eng., 2014. **34**(4): p. 379-385.

Chapter 5.

POLY(3-HYDROXYBUTYRATE-CO-3-HYDROXYHEXANOATE) AND ORGANOMODIFIED CLAY NANOCOMPOSITES FOR USE AS PACKAGING MATERIAL

In this chapter, the applicability of nanocomposites based on organomodified montmorillonite clay blended in poly(3-hydroxybutyrate-co-3-hydroxyhexanoate) is investigated. First a brief introduction to polymer clay nanocomposites is given. This is followed by an in-depth characterization of the melt compounded nanocomposites, with the emphasis on packaging-related properties. This chapter was accepted for publication as Vandewijngaarden, J., Wauters, R., Murariu, M., Dubois, P., Carleer, R., Yperman, J., D'haen, J., Ruttens, B., Schreurs, S., Lepot, N., Peeters, R., Buntinx, M.: 'Poly(3-hydroxybutyrate-co-3-hydroxyhexanoate)/ organomodified montmorillonite nanocomposites for potential food packaging applications' Journal of Polymers and the Environment.

5.1 INTRODUCTION

5.1.1 Organomodified clay nanocomposites

Nanocomposites are a relatively new class of composites, consisting of a polymeric matrix in which particles are introduced, having one or more nanometer dimensions. In this case, these particles are clay nanoparticles. These layered silicates often used in nanocomposites belong to the general family known as 2:1 phyllosilicates. Their structure consists of layers made up of two tetrahedral coordinated silicon atoms fused to an edge-shared octahedral sheet of either aluminium or magnesium hydroxide, as shown in Figure 5-1. The layer thickness is usually around 1 nm, but the lateral dimensions can vary from 30 nm to several microns or larger, dependent on the particular layered silicate [1-3].

The layered stacking leads to a regular van der Waals gap called the interlayer or gallery. Isomorphic substitution within the layers (for example, Al^{3+} replaced by Mg^{2+} or Fe^{2+}, or Mg^{2+} replaced by Li^{+}) generates negative charges that are counterbalanced by alkali and alkaline earth cations, which are situated within the galleries [1-3]. The most used type of clay is montmorillonite.

Two specific characteristics of layered silicates, such as montmorillonite clay, should particularly be kept in mind. The first characteristic is the ability of the some layered silicates to disperse into individual layers. The second one being the ability to fine-tune their surface chemistry through ion exchange of the interlayer cation with cationic surfactants [1, 3]. The latter characteristic is possible due to the fact that the forces holding the layers together are relatively weak and can be disrupted [1].

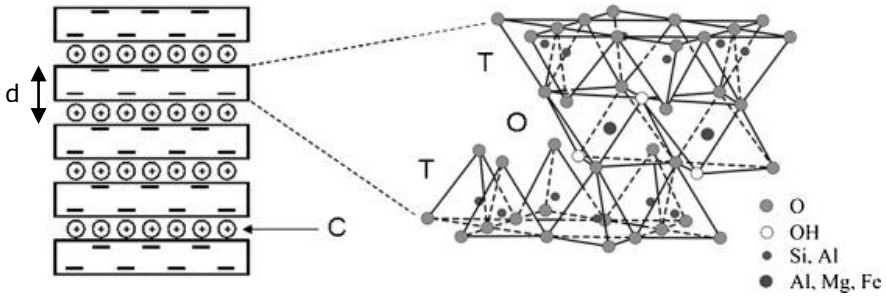

Figure 5-1: A 2:1 layered silicate structure with T a tetrahedral sheet, O an octahedral sheet, C the exchangeable cations and d the interlayer distance [2]

When using pristine clay nanoparticles, there is usually an incompatibility between the organic polymer and inorganic filler, leading to poor mechanical and thermal properties [3]. Only when highly polar polymers are used it is possible to reach sufficient compatibility between matrix and pristine clay, as is the case for poly(ethylene oxide) for example [4]. Most polymers, however, are characterized by an organophilic nature. In order to reduce the hydrophilic nature of the clay, the cations of the interlayer can be replaced with cationic surfactants, such as alkylammonium and alkylphosphonium compounds. This organomodified clay displays a lower surface energy and is much more compatible with polymers, due to its organophylicity [1, 3, 5]. Specific functionalities can be introduced into the surfactant in order to optimize compatibility and increase interlayer distance [1].

Due to the higher degree of compatibility and increased interlayer distance, the chains of the polymeric matrix can penetrate the gallery of the clay. Three possible structures can be formed upon introduction of clay nanoparticles into the polymer [1, 2]:

- If the polymer chains are incapable of intercalating between the silicate layers, a **phase-separated composite** (Figure 5-2a) is formed, with properties in the same range as conventional microcomposites. This inability to intercalate is due to poor polymer-clay affinity.
- An **intercalated structure** (Figure 5-2b) can be formed in which one or more polymer chains are intercalated in the galleries of the silicate layers, resulting in a well ordered morphology of alternating layers of polymer and silicate. Though the layers are still stacked, the interlayer distance has increased significantly.
- In case of complete and uniform dispersion of individual clay platelets, the **exfoliated or delaminated** polymer-clay nanocomposite (Figure 5-2c) is obtained. In a perfect scenario, the layered structure no longer exists.

It is important to note that, depending on the clay content, it is possible to observe multiple types of structures within one sample.

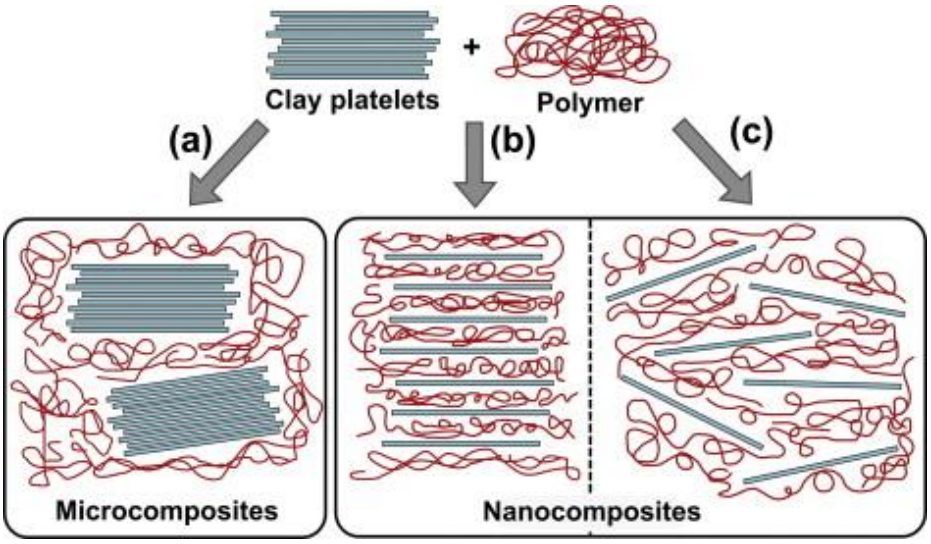

Figure 5-2: Structures of layered silicate composites with a) a phase separated microcomposite, b) an intercalated nanocomposite and c) an exfoliated nanocomposite [6]

Polymer-clay nanocomposites can be prepared using numerous techniques, but the most common three are:

- In situ intercalative polymerization:
  Using this technique, the layered silicate is swollen in liquid monomer (or monomer solution), followed by polymerization in between and around the intercalated layers. Polymerization can be induced by heat or radiation, by a suitable initiator or by an organic initiator or catalyst that was previously introduced into the gallery via cationic exchange [1, 7].
- Exfoliation-adsorption:
  This technique relies on a solvent-based system, in which the polymer (or prepolymer in case of insoluble polymers) is soluble and the layered silicate is swellable. Due to the weak forces, holding the stacks of layers together, it is possible to exfoliate the layered silicates into single layers. The polymer can then adsorb onto the exfoliated sheets. When the solvent is evaporated (or mixture precipitated), the sheets will reassemble and sandwich the polymer chains into an ordered multilayer structure [1, 7].
- Melt intercalation:
  The layered silicate is blended with the polymer matrix in the molten state, using conventional techniques such as twin-screw extrusion. If the layered silicate is sufficiently compatible with the polymer, it is possible to obtain intercalated stacks or in some cases even exfoliated nanocomposites. The main advantage of melt intercalation is that there is no necessity for solvents [1, 7]. The melt intercalation technique is often regarded as the standard procedure for preparation of this type of nanocomposites [3, 7].

5.1.2 Properties of organomodified clay nanocomposites

The addition of layered silicates to a polymeric matrix can have a significant influence on a large array of properties. A selection of properties, that in one way or another, can be related to its application as packaging material, such as gas permeability, tensile properties, biodegradability and thermal stability. These selected properties are discussed in the following paragraphs.

1) Permeability properties

The introduction of organically modified clay into a polymeric matrix can affect the permeability properties of the polymer in two ways. First of all, the dispersion of nanosized fillers creates a tortuous path for gas diffusion [1, 3, 6], which was already discussed in Chapter 1. The layered silicates can essentially be considered as impermeable inorganic platelets and gas molecules must thus diffuse around them.

The second mechanism, through which the clay platelets can influence polymer permeability, is by changing the polymer itself at the interfacial regions. If the interaction between polymer and nanoparticle is favorable, it is possible that polymer chains, located closely to a nanoparticle, can be partially immobilized. As a result, these interfacial zones have altered free volumes or density, which in turn can lower permeability coefficients [6]. It must be noted though that this effect is usually very minor in comparison to the effect of the increased tortuosity.

2) Tensile properties

The Young's modulus of polymers has been shown to significantly increase upon formation of nanocomposites with layered silicates, even at relatively low filler contents. The effect on Young's modulus is mainly influenced by platelet length (larger platelets yield higher Young's modulus) and on the state of dispersion (exfoliated platelets are much more effective than intercalated platelets) [1].

The tensile stress at break can be increased, decreased or remain uninfluenced upon addition of layered silicates. This is highly dependent on the chemical nature of both polymer and particle surfactant. If there is a high degree of interaction between polymer and clay (for example the case of poly(methyl methacrylate)), then the tensile stress at break can be increased. If there is hardly any or no interaction between polymer and clay, then the tensile stress at break can remain unchanged or even decrease [1].

In general, one can state that, for nanocomposites based on thermoplastic polymers and layered silicates, the elongation at break shows a significant decrease upon increasing filler contents [1].

3) Biodegradability

As far as the effect of clay nanoparticles on polymer biodegradability is concerned, a large amount of seemingly contradictory results can be found. The large discrepancies between literature data are mainly due to differences in clay organomodifier, but also in the protocol of testing the biodegradability (composting conditions, soil burial, enzymatic hydrolysis etc.). It is also important to note that the effect on biodegradability is still not completely understood, which adds to large variety within these data and thus rendering them difficult to interpret. For example, Ludueña et al. found that adding Cloisite 30B type organomodified clay reduced the biodegradation rate of PCL from 22 to 15 % weight loss after a 6 month expusre, whereas Cloisite C20A severely increased the weight loss up to 52 % [8]. Stloukal et al., on the other hand, observed an increase in biodegradation rate of PLA for both types of organomodified clay, with a maximum carbon mineralization of 90 % for PLA/Cloisite 20A nanocomposites and only 75 % for pure PLA [9].

Some studies relating to the biodegradability of PHA/clay nanocomposites can be found as well. To indicate the wide variety in results regarding biodegradability, a comparison of three separate studies relating to PHBV/Cloisite 30B nanocomposites is done. Wang et al. found that the biodegradability of PHBV (performed in soil suspension) was reduced with increasing amounts of Cloisite 30B [10]. Iggui et al. found similar results, with a decrease of biodegradability under laboratory-scale composting conditions as well as under aqueous conditions upon addition of Cloisite 30B to the PHBV matrix [11]. Corrêa et al., on the other hand, found that adding a small amount (3 wt% max.) of organomodified clay improved the biodegradability properties of PHBV significantly [12]. It must be concluded that the biodegradability of polymer clay nanocomposites should be investigated on a case-to-case basis and the comparison of the results must take into account a number of critical factors such as co-monomer molar fraction, molecular weight, processing conditions, testing method etc.

4) Thermal stability

The thermal stability of polymer/clay nanocomposites is usually studied using thermogravimetric analysis (TGA). Often it is observed that the introduction of clay nanoparticles in a polymeric matrix enhances the thermal stability, which is

usually attributed to the fact that the layered silicates act as a superior insulator and mass transport barrier to the volatilized degradation products, generated during degradation. The presence of layered silicates can also assist in the formation of a carbonaceous silicate char on the surface of the sample, which further reduces the mass transport of degradation products. The extent of increase in thermal or thermo-oxidative stability varies greatly, dependent on the type of polymer and type of organic modifier incorporated into the clay particles [13, 14].

However, a significant amount of publications can be found, indicating that the addition of organically modified clay nanoparticles can have a deteriorative effect on the thermal stability of the matrix. Several mechanisms have been brought forward in an attempt to explain this phenomenon. The presence of hydroxyl groups on the edges of the clay platelets could possibly catalyze polymer degradation [14]. It is also possible that the layered silicates accumulate heat during the early stages of degradation, acting as a heat source to accelerate the decomposition, in conjuction with the heat flow supplied by the external heat source [13]. Another possible mechanism is the fact that the alkylammonium modifier in the clay nanoparticles can suffer thermal degradation as well, according to the Hofmann elimination reaction. During this type of reaction, the ammonium cation loses an olefin and an amine and leaves an acidic proton on the surface of the layered silicate. The acidic proton, as well as the other reaction products, could have a catalytic effect on polymer degradation [13, 15].

5.2 EXPERIMENTAL

5.2.1 Materials and sample preparation

Pure PHBHHx powder and a commercial PHBHHx granulate (trade name Aonilex X151A) (AON), both with a 3-hydroxyhexanoate content of 10.5 mol%, were provided by Kaneka Corporation (Westerlo-Oevel, Belgium), and dried at 70 °C *in vacuo* for 3 days.

OMMT was purchased from Sigma-Aldrich under the trade name Nanocor I.34 TCN, which is montmorillonite modified with octadecylbis(2-hydroxyethyl)methylammonium chloride, having a mean particle size of 14-18 microns and a basal spacing (d_{001}) of 18-22 Å. The OMMT contained 27.7 wt%

organic modifier, as determined through thermogravimetric analysis. The OMMT was dried at 90 °C *in vacuo* for 3 days.

Firstly, samples with a total weight of 55 g were mixed in a Rondol mini-mix high speed mixer, before being processed in a Brabender counter-rotating internal mixer equipped with roller blades. Mixer temperature was set at 170 °C and 140 °C for respectively, the pure PHBHHx and Aonilex X151A based samples. During feeding of the mixer, a rotation speed of 30 rpm was maintained for 3 min to avoid the excessive increase of the torque during polymer melting. Then the rotation speed was increased to 80 rpm for 8 min.

Subsequently, samples of about 1.8 g were compressed and molded at 140 °C to prepare films in a polyimide mold (100 mm x 100 mm x 0.150 mm) using an Agila PE20 hydraulic press. The polymer was pre-heated for 90 s without pressure before being pressed at 30 bar for 150 s, followed by two degassing cycles. Finally, the films were pressed at high pressure of 150 bar for 120 s, followed by a slow cooling at 50 bar for 20 min at 60 °C to allow film crystallization and easy demolding [16].

Thicker plates for tensile testing and XRD were produced in a stainless steel mold (100 mm x 100 mm x 0.5 mm) at 140 °C with a pre-heating time of 3 min before being pressed at 30 bar for 200 s. Subsequently two degassing cycles were used before finally molding the sample at 150 bar for 150 s. The samples were slowly cooled at 50 bar for 20 min at 60 °C.

OMMT contents of 1, 3, 5 and 10 wt% were used and compared to the neat polymers processed using similar conditions. Samples based on pure PHBHHx powder are denoted as PHBHHx-0, PHBHHx-1, PHBHHx-3, PHBHHx-5 and PHBHHx-10. Samples based on commercial Aonilex X151A (granules) are denoted in a similar manner, but named AON instead of PHBHHx.

The melt-blended samples were used for all following measurements.

5.2.2 Solvent casting

A single set of solvent cast films (based on PHBHHx) was prepared by dispersing the respective amount of OMMT in chloroform for 15 min in an ultrasonic bath to swell the silicate layers of the nanofiller. Then 1 g of PHBHHx was added and the mixture was stirred at 40 °C for 1 hour for complete polymer dissolution and polymer chain intercalation within the galleries of the silicate. The solution was cast in glass petri dishes and left to dry for 3 hours. Complete removal of residual chloroform was obtained using a vacuum oven at 60 °C for 3 days. These samples were only used for further elaboration of the effect of OMMT on crystallization, not for any other measurements.

5.2.3 Polymer recovery

The sample set based on melt-blended PHBHHx (see Paragraph 5.2.1) was dissolved in chloroform, followed by centrifugation for 30 min at 10 000 rpm. The supernatant was cast in glass petri dishes and dried at 70 °C *in vacuo* for 3 days in order to recover the melt-compounded polymer without OMMT nanoparticles. This was done to further investigate the effect of PHBHHx molecular weights on crystallization properties.

5.2.4 Water vapor sorption

The moisture content of OMMT in function of time was measured by weighing about 1 g of OMMT, previously dried for 24 hours at 120 °C, in regular time intervals at a temperature of 23.9 (± 0.4) °C and ambient humidity of 22.8 (± 1.8) %. The moisture content was determined as the ratio of the weight increment to the initial weight. The measurement was performed in duplicate.

5.2.5 Gel permeation chromatography (GPC)

The molecular weight distribution of the samples was analyzed using a GPC apparatus composed of a SpectroSeries P100 pump, equipped with a Shodex RI71 refractometer detector and two PL-gel 10 µm Mixed-B columns in series, thermostated at 35 °C. The eluent was chloroform (VWR, HPLC grade) at a flow rate of 1.0 ml/min. Samples were dissolved in chloroform at a concentration of 1 g/l and filtered over a 220 nm syringe filter. The injection volume was 100 µl. Calibration was performed using polystyrene standards (474 to 3 150 000 g/mol) dissolved in chloroform with a concentration of 1 g/l.

5.2.6 Colorimetric analysis

Colorimetric analysis was performed using a Datacolor MicroFlash 200d. Results are presented in CIELAB color coordinates (L^*, a^* and b^*). The total color change ΔE_{ab} is calculated as:

$$\Delta E_{ab} = \sqrt{\Delta L^2 + \Delta a^2 + \Delta b^2} \quad (5\text{-}2)$$

With ΔL, Δa and Δb respectively the difference in L^*, a^* and b^* between the reference (0 wt% talc) and the samples containing talc. A sample was measured 4 times (twice on each side) in order to obtain a representative average.

5.2.7 Opacity

The opacity of the prepared films was determined according to the Hunter Lab method in the reflectance mode, using a Datacolor Microflash 100D. The opacity Y (in %) can be calculated as the relationship between the opacity of a sample on a black standard Y_b and the opacity on a white standard Y_w:

$$Y = Y_b / Y_w \times 100 \quad (5\text{-}3)$$

A sample was measured 4 times (twice on each side) in order to obtain a representative average.

5.2.8 X-ray diffraction study (XRD)

The XRD study was performed with a Siemens D5000 diffractometer (Cu $K\alpha_1$, λ = 0.1540562 nm), equipped with a scintillation detector, over a 2θ range of 2 to 10° with steps of 0.04°. The interlayer distance of the OMMT in the prepared nanocomposites is calculated using Bragg's law:

$$n \cdot \lambda = 2 \cdot d \cdot \sin \theta \quad (5\text{-}4)$$

With n a positive integer, λ the wavelength of the incident X-ray beams, d the interlayer distance (defined as the spacing between the various planes) and θ the angle between the incident beam and the scattering planes.

5.2.9 Transmission electron microscopy (TEM)

The TEM study was performed with a FEI Tecnai Spirit using an accelerating voltage of 120kV. The images are standard BF (bright field) images. Transparent slices of about 150 nm thick are made with a Leica EM UC6 ultramicrotome.

5.2.10 Thermogravimetric analysis (TGA)

The thermal stability of the samples was analysed using a TA Instruments Hi-Res TGA 2950 thermogravimetric analyser. Samples of about 10 mg were heated from room temperature to 350 °C at a heating rate of 20 °C/min with a N_2 gas flow of 80 ml/min. To provide a mean value, measurements were performed at least in duplicate.

5.2.11 Differential scanning calorimetry (DSC)

Thermal properties of the prepared films were analyzed under inert atmosphere (50 ml/min nitrogen) using a TA Instruments Q200 DSC. About 3.5 mg of the compression molded thin films in an aluminium pan was used to perform the measurements. The sample pan was heated from -30 °C to 150 °C at a heating rate of 10 °C/min. After isothermal period of 2 min, the sample was cooled at 10 °C/min to -30 °C and kept constant for 2 min prior to heating to 170 °C at 10 °C/min. For all samples, only the weight fraction of polymer in nanocomposites was considered to allow a more accurate determination of enthalpy values. Measurements were performed at least in duplicate.

5.2.12 Thickness measurements

Sample thickness was measured prior to permeability testing using a MTS MI20 thickness gauge. The thickness was taken as the average of five measurements at different locations of each sample.

5.2.13 Barrier properties

The oxygen transmission rate (OTR), at 23 °C and 0 % relative humidity (RH), of the produced samples was measured using a Mocon Ox-Tran 702 (ASTM D3985). Carbon dioxide transmission rate (CO_2TR) at 23 °C and 0 % RH was measured using a Mocon Permatran-C 4/41 (ASTM F2476). Water vapor transmission rate (WVTR) was measured using a Mocon Permatran-W 700 (ASTM F1249). Test gases (O_2 and CO_2) and carrier gas (N_2, N_2/H_2) with a purity of 99.999 % were purchased from Westfalen, Münster (Germany). Samples were placed between 2 aluminium masks with an effective testing area of 5 cm². The sample was exposed to the test gas on one side and to a continuously flushing carrier gas on the other side, both at a total pressure of 1 atm. For OTR measurements a carrier gas N_2/H_2 (95/5) was used, for all other measurements pure N_2. The test gas diffuses

through the sample and is guided by the carrier gas towards the detector. The gas transmission rate or gas flux *J*, in $cm^3/m^2.day.atm$ (for OTR and CO_2TR) or $g/m^2.day$ (for WVTR) of the specific test gas, is reported when equilibrium is reached (i.e. the concentration of test gas in the carrier gas changes less than 1 % during a test cycle of 30 min).

The gas flux *J* can be defined as the quantity of test gas or permeant *Q*, which passes through the polymeric film per unit area *A* during one unit of time *t* at equilibrium [17-19]:

$$J = Q / (A.t) \quad (5\text{-}5)$$

In order to obtain a thickness-independent criterion for comparison, the gas flux *J* can be normalized for sample thickness *d* and permeant pressure *p* to obtain the permeability coefficient *P* [17-19]:

$$P = J.d / p \quad (5\text{-}6)$$

Of each sample, two specimens were prepared and were analyzed twice in order to obtain a representative average.

5.2.14 Tensile testing

The tensile test was performed using a MTS/10 tensile tester at a crosshead speed of 1 mm/min and a distance of 25.4 mm between the grips. Samples were cut into dumbbell shapes (ASTM D638-02 type V) and were conditioned at 23 °C and 50 % relative humidity for 48 h before testing. At least 10 specimens were tested for each sample in order to obtain a representative average.

5.3 RESULTS AND DISCUSSION

In this study, a montmorillonite clay, modified with octadecylbis(2-hydroxyethyl)methylammonium chloride was selected due to its proven compatibility with PHB [20] and PHBV [21]. An OMMT concentration range of 1 to 5 wt% was selected, because the main goal is to enhance the barrier properties, which usually requires higher filler loading. A sample with 10 wt% OMMT was also prepared to further emphasize and enhance certain effects.

The potential use of the prepared nanocomposites for food packaging applications is dependent on several properties. Some are related to the processability, i.e.

the effective conversion of the material into a packaging. In this context, thermal stability and crystallization are of importance. Others are directly linked to packaging properties, such as color, gas permeability and mechanical properties (flexible packaging). It is crucial to separately evaluate each property, but also to eventually find a compromise between all properties in order to obtain an all-round performant packaging material.

5.3.1 Degradation during processing

Using GPC, the thermo-mechanical degradation occurring during melt blending of the polymer and OMMT was investigated. The number average molecular weight $\bar{M}_n$, weight average molecular weight $\bar{M}_w$ and dispersity $Đ_M$, defined as the ratio of $\bar{M}_w$ to $\bar{M}_n$, were determined before (virgin) and after melt processing. These results are presented in Table 5-1 for both PHBHHx as well as AON samples. A first observation is that PHBHHx-0 shows a significant decrease in molecular weight upon comparison with the virgin PHBHHx, which suggests the severity of the thermal processing at 170 °C (actual temperature in mixer was 180 °C). Furthermore, it is clear that the degree of degradation increases with higher OMMT content, suggesting that OMMT has a critical role in catalyzing thermal degradation. $\bar{M}_w$ and $\bar{M}_n$ decrease gradually, while the polymer dispersity increases at higher OMMT content, also a clear indication of chain scission.

To reduce the effect of thermal degradation due to the processing itself, the set of AON samples was produced at a lower temperature, i.e. at 140 °C (actual temperature in mixer was 150 °C). The PHBHHx sample set was not prepared at this lower temperature, as the AON sample set shows more promise, which will be demonstrated in the following paragraphs. The results in Table 5-1 clearly show that thermal degradation still occurs but is much less severe as compared to pure PHBHHx processed at 170 °C. $\bar{M}_w$ and $\bar{M}_n$ values decrease after melt processing immediately for neat PHBHHx-0 to less than 1/3 of the value of the virgin PHBHHx sample, whereas the molecular weight of AON-0 was about 40 % lower than that of virgin Aonilex. Virgin PHBHHx displays a significantly higher molecular weight than virgin Aonilex, which is due to the fact that Aonilex is a melt-processed granulate (based on PHBHHx) and has thus already undergone a first thermo-mechanical degradation. These results indicate that a great deal of thermal degradation can be avoided by using a processing temperature of 140 °C.

For the AON samples, it is also clear that thermal degradation increases again at higher OMMT content as reflected in the decreasing $\bar{M}_n$ and $\bar{M}_w$ values and increasing dispersity. Thus it is believed that the OMMT works as a catalyst towards the thermal degradation of the polymer.

Table 5-1: Molecular weight of PHBHHx and Aonilex based OMMT nanocomposites

Sample	$\bar{M}_n$ (x 10^3 g/mol)	$\bar{M}_w$ (x 10^3 g/mol)	$Đ_M$
virgin PHBHHx	380	870	2.3
PHBHHx-0	117	262	2.2
PHBHHx-1	113	257	2.3
PHBHHx-3	99	247	2.5
PHBHHx-5	80	222	2.8
PHBHHx-10	70	204	2.9
virgin Aonilex	251	614	2.4
AON-0	149	371	2.5
AON-1	127	353	2.8
AON-3	116	303	2.6
AON-5	111	304	2.7
AON-10	90	278	3.1

A reduced thermal stability of polymers upon addition of OMMT is most often attributed to Hofmann elimination reaction of the quaternary alkyl ammonium functional group, which is used to modify the clay surface [5, 20, 22-24]. Xie et al. have demonstrated that Hofmann elimination of quaternary ammonium modified clay can start from temperatures as low as 180 °C, depending on the type of quaternary ammonium group [25]. Thus, this degradation reaction could be a possible cause of the advanced thermal degradation in the PHBHHx set of samples. However, since a similar trend is observed in the AON sample set, produced at temperatures well below the degradation temperature of 180 °C, other mechanisms must be considered.

It is also plausible that during melt blending, a rapid moisture uptake by OMMT took place. Despite being organically modified, OMMT takes up significant amounts of ambient moisture in very short time. During melt blending, the

moisture will be released causing hydrolysis of the polymer chains, resulting in a lower molecular weight and altered molecular weight distribution [26].

Figure 5-3 shows the increase in moisture content in function of time for a fully dried sample of OMMT at a temperature of 23.9 (± 0.4) °C and ambient humidity of 22.8 (± 1.8) %. After only 5 min, about 0.45 wt% moisture has been taken up by the OMMT and even 0.65 wt% after 15 min. Although the amount of moisture is very low in terms of weight, it is sufficient to hydrolyze polymer chains. The average handling time between weighing and actual melt blending lies around 10 min. therefore it is possible that water has been absorbed and can be considered a viable cause of the degradation.

Furthermore, it is not excluded that other factors could have contributed to the degradation of the polymer matrix: presence of transition metal ions in the nanofiller as impurities, PHBHHx chain scissions induced by both, high shear forces (typically for the utilization of roller blades) and processing at high temperature etc. [27]

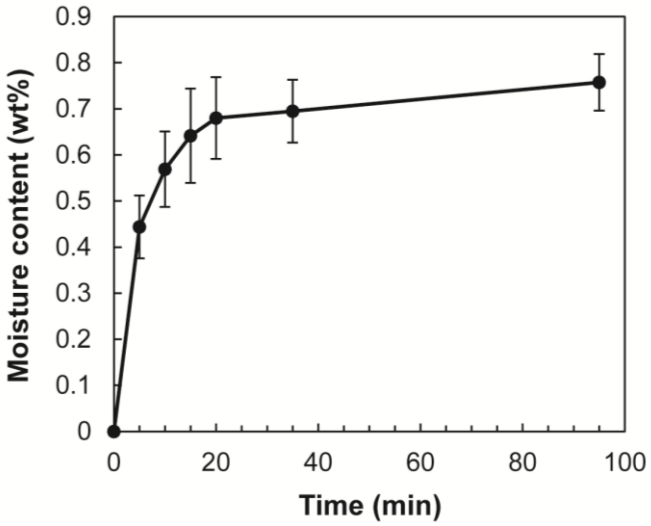

Figure 5-3: Moisture content of OMMT powder in function of time

5.3.2 Dispersion study

The interlayer distance of OMMT nanoparticles in the polymer matrix is investigated using X-ray diffraction analysis. The diffraction patterns of pure OMMT powder and the melt-compounded sample sets are given in Figure 5-4. The diffraction peak at a 2θ of around 2.5° is attributed to the d_{001} reflection. Broader diffraction peaks between 2θ 4.5 and 5.5° are due to the d_{002} reflection. For AON-10 and PHBHHx-10 even the reflection of d_{003} can be observed at around 3.4 – 3.8°. From these reflections, the interlayer distance (d_{001}) of clay platelets in the polymeric matrix can be calculated using Bragg's law and are given in Table 5-2.

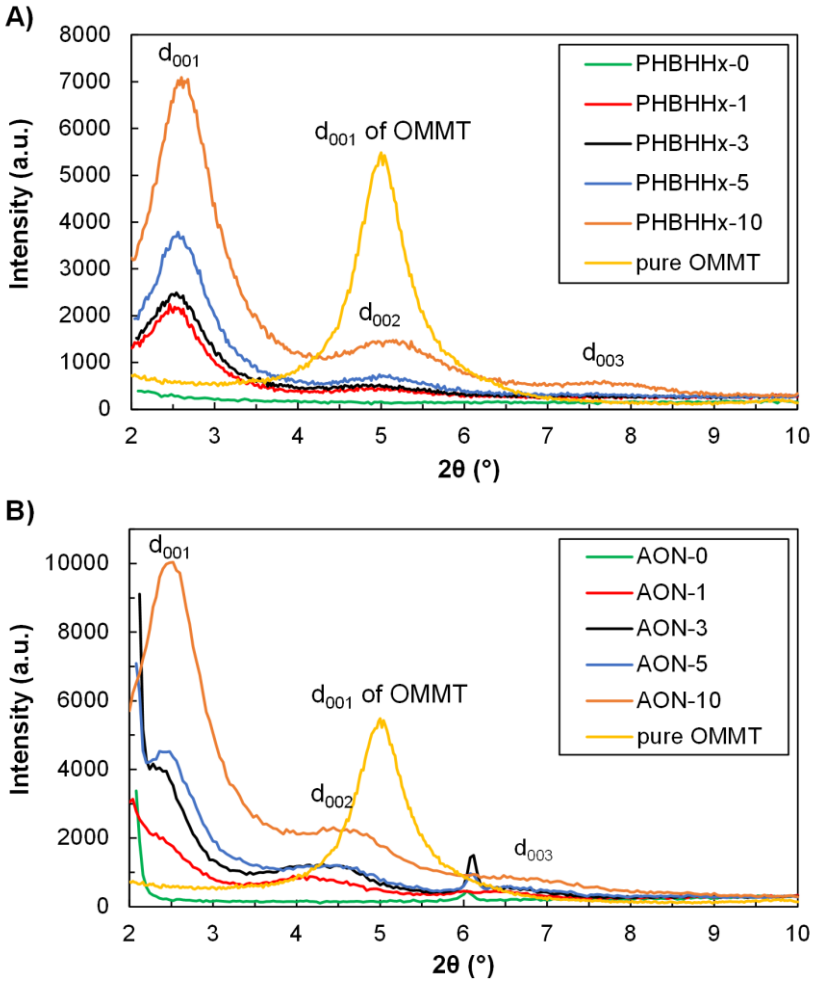

Figure 5-4: X-ray diffraction patterns of A) PHBHHx sample set and B) AON sample set

PHBHHx-1 shows an interlayer distance about twice as high (3.53 nm) as the pure OMMT, which is a clear indication that intercalation of the polymer chains between the clay layers has occurred. As the OMMT content increases, the interlayer distance decreases, reaching a value of 3.32 nm for PHBHHx-10. This can be explained by the fact that the intercalation of the polymer chains between clay platelets becomes more and more difficult as the filler volume fraction increases.

The AON sample set displays a similar trend as the PHBHHx samples, however the interlayer distances are even slightly higher and the shape of peaks are slightly different, which can be indicative of an intercalated/partially exfoliated structure. The interlayer distance of AON-1 (3.76 nm) is about 2 times higher than those of OMMT nanofiller. In the AON-10 sample the interlayer distance has decreased to a value of 3.56, which is even higher than the distance found for PHBHHx-1.

The higher interlayer distances in samples AON-1 to AON-10 could be due to the fact that they were processed at a lower temperature, which leads to less thermal degradation of the OMMT surface modification and thus leading to better swelling of the clay platelets and therefore higher interlayer distances. Moreover, by processing at the temperature of 140°C, the viscosity of the molten polymer was higher (statement based on the torque values recorded during mixing), which can be favorable for good nanofiller dispersion and for the delamination/even exfoliation of clay layers [28]. According to the XRD spectra, especially at lower OMMT loading, some nanocomposites (e.g., AON-1 and AON-3) even show an intercalated-exfoliated morphology.

Table 5-2: Interlayer distance (nm) calculated from XRD results

Sample	Calculated interlayer distance (nm)
pure OMMT	1.78
PHBHHx-1	3.53
PHBHHx-3	3.48
PHBHHx-5	3.37
PHBHHx-10	3.32
AON-1	3.76
AON-3	3.68
AON-5	3.63
AON-10	3.56

To further investigate the morphology, TEM analysis was performed on both sample sets, as can be seen in Figure 5-5 and Figure 5-6. For the PHBHHx sample set, a uniform distribution and dispersion of nanoparticles throughout the matrix is observed at low magnification, however some micron-sized agglomerations are found as well, especially at higher OMMT concentrations. The right hand side in each TEM image shows the OMMT at higher magnification, displaying the stacked silicate layers, thus confirming the intercalated state. For the Aonilex based samples, a uniform distribution and dispersion is observed as well. However, at high magnification it is possible to observe that there is a combination of mostly stacked layers with some single OMMT platelets, confirming the intercalated/partially exfoliated structure presumed from the XRD results.

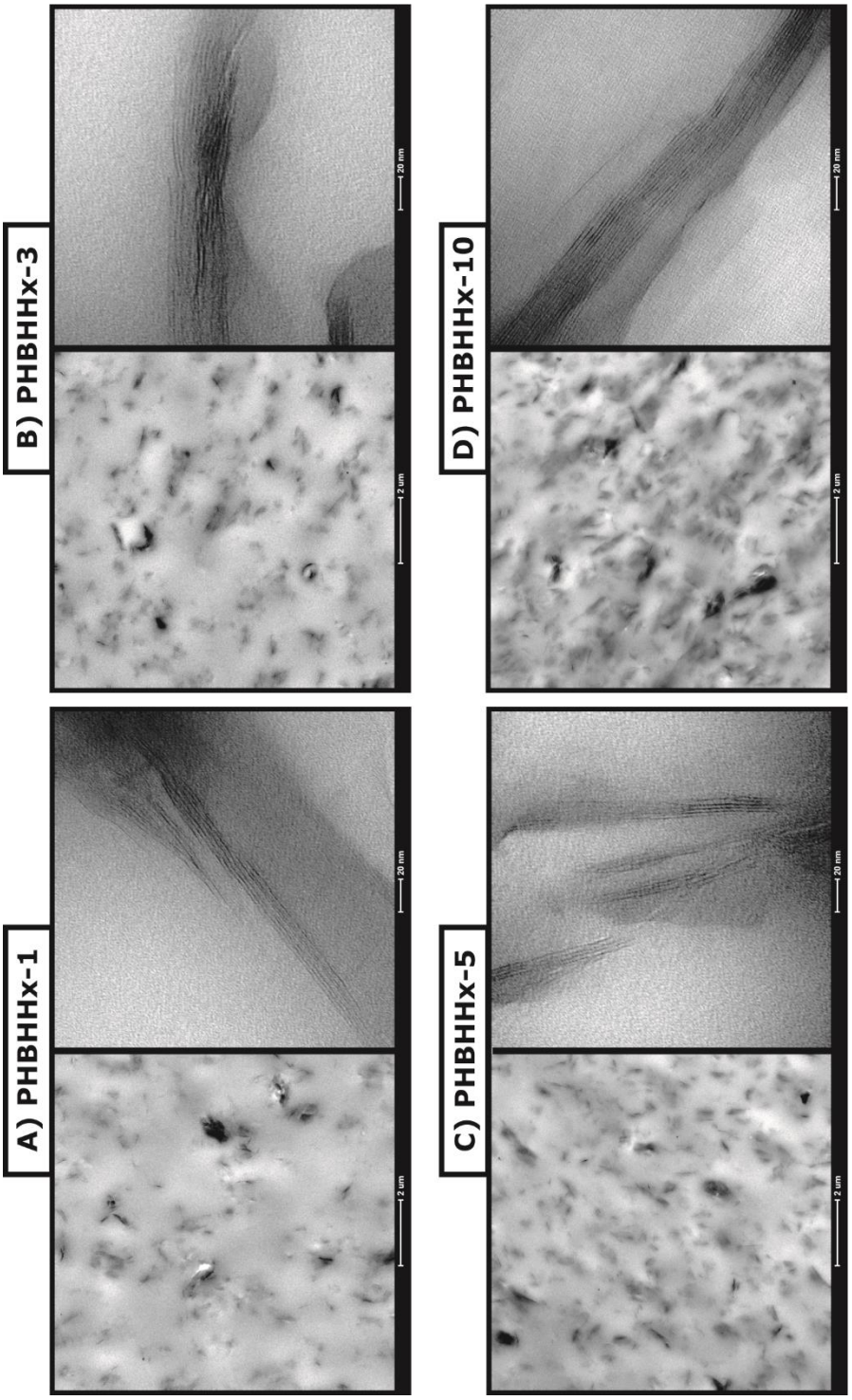

Figure 5-5: TEM images of A) PHBHHx-1, B) PHBHHx-3, C) PHBHHx-5 and D) PHBHHx-10

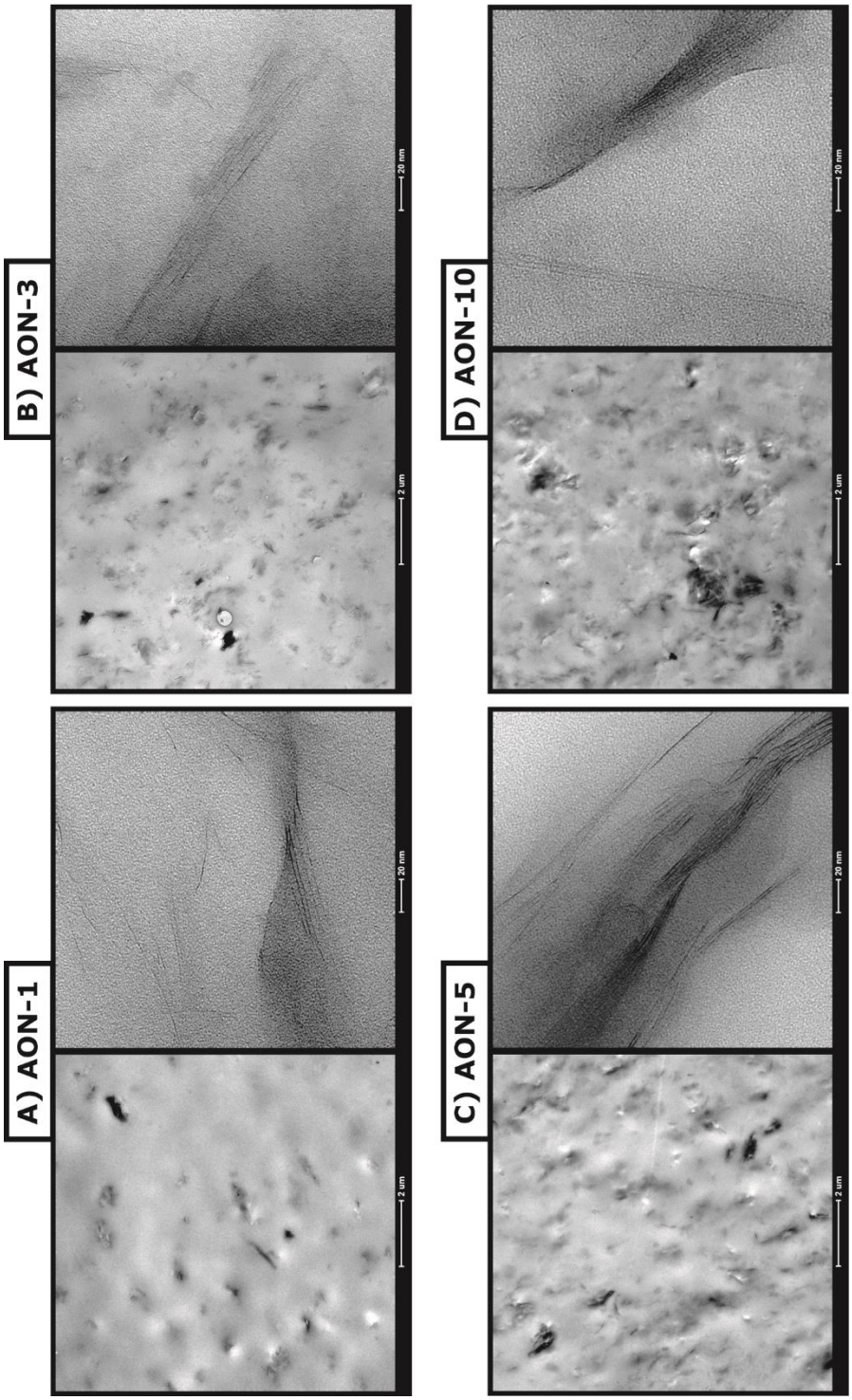

Figure 5-6: TEM images of A) AON-1, B) AON-3, C) AON-5 and D) AON-10

5.3.3 Thermal stability

The thermal stability of the prepared nanocomposites was investigated using TGA under inert atmosphere (N_2). The results of the thermogravimetric analysis of both sample sets are given in Table 5-3.

The evolution of $T_{d,o}$, $T_{d,50}$ and $T_{d,p}$ is similar for both sample sets. The onset of degradation $T_{d,o}$ increases with higher OMMT loading, reaching a maximum at a concentration of 5 wt%, followed by a decrease to a value lower than the sample without OMMT. $T_{d,50}$ and $T_{d,p}$ also reach a maximum at an OMMT concentration of 5 wt%, followed by a decrease at 10 wt%. However, $T_{d,50}$ and $T_{d,p}$ of the 10 wt% samples do not drop below the values of the neat polymer samples. This means that thermal degradation of the samples filled with 10 wt% OMMT starts at a slightly lower temperature than in the unmodified polymer, but the degradation spans out over a larger temperature interval, mainly due to degradation of the organomodifier (present in significant amount) as well as due to the important decrease in molecular weights.

Table 5-3: Thermal stability of OMMT nanocomposites (n = 2 or 3)

Sample	$T_{d,o}$ (°C)	$T_{d,50}$ (°C)	$T_{d,p}$ (°C)
PHBHHx-0	290.5 (± 0.5)	303.7 (± 0.1)	308.9 (± 0.1)
PHBHHx-1	291.6 (± 1.1)	305.8 (± 0.6)	310.2 (± 0.1)
PHBHHx-3	292.9 (± 0.5)	308.2 (± 0.1)	311.9 (± 0.1)
PHBHHx-5	294.4 (± 0.5)	311.5 (± 0.7)	314.4 (± 0.5)
PHBHHx-10	287.8 (± 0.4)	309.4 (± 1.2)	311.1 (± 0.2)
AON-0	291.2 (± 0.1)	304.2 (± 0.4)	309.2 (± 0.3)
AON-1	293.6 (± 0.4)	308.2 (± 0.4)	312.3 (± 0.5)
AON-3	292.9 (± 0.6)	308.9 (± 0.1)	313.1 (± 0.1)
AON-5	293.8 (± 0.6)	312.2 (± 0.6)	316.2 (± 0.4)
AON-10	288.3 (± 0.4)	310.3 (± 0.9)	312.1 (± 0.1)

PHBHHx-5 and AON-5 are the most performant samples in terms of enhanced thermal stability. For PHBHHx-5, an increase of 3.9 °C, 7.8 °C and 5.5 °C can be observed for respectively $T_{d,o}$, $T_{d,50}$ and $T_{d,p}$. For AON-5 these indicative temperatures increase with 2.6 °C, 8.0 °C and 7.0 °C, respectively.

This increase in thermal stability is attributed to the presence of the clay platelets, which act as a barrier against the products volatilized during thermal degradation, thus causing a delay in thermal degradation temperature [21, 29, 30].

The lower thermal stability of PHBHHx-10 and AON-10 is likely due to the fact that a significant amount of thermal degradation has already occurred during processing, as described in paragraph 5.3.1. The high OMMT content will counteract this, but not enough to achieve better results than PHBHHx-5 and AON-5. In general, a better thermal stability (for all investigated OMMT contents) could possibly be achieved by a reduction of thermal degradation during processing and by using optimized melt-mixing parameters to allow the advanced nanofiller dispersion.

In terms of thermal stability, it can be concluded that the samples containing up to 5 wt% OMMT show most potential.

The increase thermal stability by adding 3 wt% OMMT, seems to be fairly comparable to that observed upon addition of 2 wt% ultra-fine talc, which was somewhat to be expected as both fillers have platelet structures.

5.3.4 Colorimetric analysis and opacity

The change in color coordinates (ΔL, Δa and Δb) and the total color change (ΔE_{ab}) of both sample sets are presented in Table 5-4, with PHBHHx-0 and AON-0 used as references to calculate color change upon addition of OMMT. The evolution of color is practically identical for both sample sets. ΔL decreases with higher OMMT concentration, indicative for a slight darkening of samples. Δa also decreases slightly, which means a slight increase in green in the color spectrum of the samples. The most outspoken change can be found in Δb, which increases significantly due to the outspoken yellowing of the prepared nanocomposites. The total color change ΔE_{ab} increases greatly as well, which is normal as this value is calculated from the quadratic values of ΔL, Δa and Δb.

An increase in yellow is common when extensive thermal degradation occurs in samples and this color change can also be slightly observed regarding the reference samples PHBHHx-0 and AON-0, which confirms again the extent of degradation occurring during processing, due to the thermal treatment and is significantly advanced in the presence of OMMT. However, it must be stated that

the yellow color could possibly be partly increased due to the fact that the OMMT powder has a slightly yellowish off-white color on its own.

Table 5-4: Colorimetric properties and opacity of nanocomposites (n = 4)

Sample	**Δ*L*** (± 0.3)	**Δ*a*** (± 0.1)	**Δ*b*** (± 0.3)	**ΔE_{ab}** (± 0.4)	**Opacity *Y* (%)** (± 0.3)
PHBHHx-0	0	0	0	0	9.2
PHBHHx-1	-0.2	-0.5	1.8	1.9	9.8
PHBHHx-3	-0.9	-0.67	2.4	2.6	10.5
PHBHHx-5	-1.0	-1.07	3.8	4.1	11.0
PHBHHx-10	-2.3	-1.97	7.8	8.4	11.2
AON-0	0	0	0	0	11.4
AON-1	-0.1	-0.1	0.5	0.5	11.4
AON-3	-0.8	-0.66	2.72	2.90	12.0
AON-5	-0.9	-0.8	3.4	3.5	12.1
AON-10	-2.1	-1.65	7.33	7.8	12.8

The results of the opacity measurements are given in the right-hand column of Table 5-4. For both sample sets, at increasing OMMT contents, the samples are rendered more opaque. This is to be expected because foreign particles are introduced in increasing concentrations, reflecting light and thus inducing opacity. The opacity of PHBHHx samples ranges from 9.2 % to 11.2 %, whereas the AON samples range from 11.4 to 12.8 %. This slight difference between PHBHHx and AON is most likely due to the presence of some additives in the AON commercial granulate.

5.3.5 Crystallization properties

Unfortunately, the crystallization rate of PHBHHx has been reported to be very slow even at very low 3-hydroxyhexanoate content. Therefore, many efforts are actually devoted to solve this problem (e.g., by addition of nucleating agents, of selected micro- or nanofillers, etc.) [31, 32]. In this context, it was of interest to study the effects of this specific type of OMMT on the crystallization properties.These results are presented in Table 5-5 and Table 5-6.

From the results of the melt-blended PHBHHx/OMMT sample set, it becomes clear that the addition of OMMT has a very severe influence on the crystallization properties. PHBHHx-0 shows a $T_{c,o}$, $T_{c,p}$ and ΔH_c of 77.1 °C, 69.4 °C and 34.8 J/g and no cold crystallization phenomena, indicating a complete crystallization during cooling. However, upon addition of OMMT we can see a clear decreasing trend in $T_{c,o}$ ranging from 73.0 °C to 68.7 °C between 1 wt% and 10 wt% of OMMT. $T_{c,p}$ decreases to 54.9 °C adding only 1 wt% OMMT and appears to remain constant at higher concentrations. Also a clear decrease in ΔH_c is noticed, which becomes more significant at higher concentrations, reaching a value of only 1.0 J/g for PHBHHx-10. Very important to state is that during subsequent heating after cooling, cold crystallization occurs, due to the fact that crystallization was not completed during the first cooling from the molten state. $T_{cc,o}$ and $T_{cc,p}$ increase at higher OMMT loading, whereas ΔH_{cc} decreases.

These phenomena in both crystallization as well as cold crystallization are a clear indication that the addition of OMMT to the PHBHHx matrix severely reduces the overall crystallization rate of the polymer. As a result, lower crystallization temperatures and enthalpies upon cooling are observed, as well as a very outspoken cold crystallization behavior.

Table 5-5: Crystallization properties of PHBHHx and Aonilex based OMMT nanocomposites (n = 2 or 3)

Sample	$T_{c,o}$ (°C)	$T_{c,p}$ (°C)	ΔH_c (J/g)
PHBHHx/OMMT melt-blended:			
PHBHHx-0	77.1 (± 0.2)	69.4 (± 0.3)	34.8 (± 0.8)
PHBHHx-1	73.0 (± 0.2)	54.9 (± 0.4)	2.7 (± 0.1)
PHBHHx-3	72.5 (± 0.6)	54.8 (± 0.2)	2.5 (± 0.1)
PHBHHx-5	70.1 (± 0.8)	55.2 (± 0.1)	0.9 (± 0.1)
PHBHHx-10	68.7 (± 0.6)	55.5 (± 0.1)	1.0 (± 0.2)
PHBHHx/OMMT solvent cast:			
0 wt% OMMT	78.3 (± 0.9)	70.5 (± 0.9)	33.0 (± 0.2)
1 wt% OMMT	77.2 (± 0.1)	69.6 (± 0.1)	32.2 (± 0.1)
3 wt% OMMT	77.1 (± 0.1)	69.4 (± 0.2)	30.9 (± 0.9)
5 wt% OMMT	77.1 (± 0.2)	69.1 (± 0.1)	31.4 (± 0.7)
10 wt% OMMT	74.8 (± 0.3)	66.0 (± 0.4)	29.5 (± 0.3)
PHBHHx recovered from melt-blended PHBHHx/OMMT:			
0 wt% OMMT	78.3 (± 0.1)	70.8 (± 0.1)	33.7 (± 1.2)
1 wt% OMMT	72.8 (± 0.6)	54.3 (± 0.1)	3.2 (± 0.1)
3 wt% OMMT	73.4 (± 0.3)	55.0 (± 0.1)	2.8 (± 0.4)
5 wt% OMMT	72.7 (± 0.2)	54.2 (± 0.1)	2.8 (± 0.9)
10 wt% OMMT	71.7 (± 0.3)	55.3 (± 0.4)	1.1 (± 0.1)
Aonilex/OMMT melt-blended:			
AON-0	77.2 (± 0.1)	70.2 (± 0.2)	34.8 (± 0.8)
AON-1	75.0 (± 0.1)	58.7 (± 0.1)	29.5 (± 1.7)
AON-3	74.2 (± 0.2)	55.7 (± 0.1)	21.5 (± 0.3)
AON-5	73.4 (± 0.3)	54.8 (± 0.2)	20.9 (± 0.2)
AON-10	74.0 (± 1.1)	55.5 (± 0.7)	22.2 (± 1.1)

Table 5-6: Cold crystallization properties of PHBHHx and Aonilex based OMMT nanocomposites (n.d. = not detected, n = 2 or 3)

Sample	$T_{cc,o}$ (°C)	$T_{cc,p}$ (°C)	ΔH_{cc} (J/g)
PHBHHx/OMMT melt-blended:			
PHBHHx-0	n.d.	n.d.	n.d.
PHBHHx-1	48.7 (± 0.7)	72.4 (± 0.6)	8.2 (± 0.3)
PHBHHx-3	49.0 (± 0.4)	72.9 (± 0.1)	9.1 (± 0.9)
PHBHHx-5	52.3 (± 0.2)	74.2 (± 0.1)	6.7 (± 0.3)
PHBHHx-10	52.7 (± 1.3)	74.8 (± 0.6)	5.0 (± 0.1)
PHBHHx/OMMT solvent cast:			
0 wt% OMMT	n.d.	n.d.	n.d.
1 wt% OMMT	n.d.	n.d.	n.d.
3 wt% OMMT	n.d.	n.d.	n.d.
5 wt% OMMT	n.d.	n.d.	n.d.
10 wt% OMMT	n.d.	n.d.	n.d.
PHBHHx recovered from melt-blended PHBHHx/OMMT:			
0 wt% OMMT	n.d.	n.d.	n.d.
1 wt% OMMT	47.73 (± 0.1)	73.1 (± 0.1)	9.3 (± 0.6)
3 wt% OMMT	47.9(± 0.3)	73.5 (± 0.3)	7.9 (± 1.1)
5 wt% OMMT	47.8 (± 1.1)	72.5 (± 0.4)	7.6 (± 1.1)
10 wt% OMMT	52.3 (± 1.7)	74.1 (± 0.5)	3.4 (± 1.0)
Aonilex/OMMT melt-blended:			
AON-0	n.d.	n.d.	n.d.
AON-1	31.9 (± 0.2)	46.1 (± 0.5)	2.0 (± 0.1)
AON-3	37.5 (± 0.2)	57.1 (± 0.1)	6.9 (± 0.1)
AON-5	37.4 (± 0.2)	57.6 (± 0.3)	7.0 (± 0.1)
AON-10	36.1 (± 0.5)	55.7 (± 0.3)	4.2 (± 0.5)

Two possible explanations for the retardation of polymer crystallization can be suggested. One being the reduced polymer mobility due to high interaction between polymer and OMMT surface, which has been identified as the cause of retarded crystallization in PHB/OMMT [33], PHBV/zinc oxide [34] and PLA/zinc oxide [35] nanocomposites. The other possible explanation is the reduction in molecular weight due to thermal degradation, resulting in a lower amount of chain entanglements, which facilitate polymer crystallization. The effect of molecular weight on crystallization properties is known to be highly polymer-dependent [36].

In order to test both hypotheses, two additional sample sets were prepared. One sample set, with OMMT contents of 0, 1, 3, 5 and 10%, was prepared via solvent casting in chloroform. By preparing the samples in dissolved state, rather than in a molten state, it is possible to produce nanocomposites without thermal degradation of the polymer chains. Using these samples, it's possible to observe if the retardation of crystallization still occurs even if no reduction in molecular weight is at play. A separate sample set is produced by recovering the polymer from the original PHBHHx sample set, as described in the experimental section. Via polymer recovery, the polymer after melt blending process, devoid of OMMT, is obtained, to study the influence of a reduction in molecular weight on crystallization, without interference of the presence of OMMT.

The DSC results of these two new sample sets, only used in this specific part of the study, are presented in Table 5-5 and Table 5-6 as well. The solvent cast samples, that have not undergone thermal treatment, display hardly any alteration in crystallization properties, except for the sample containing 10 wt% OMMT. This sample displays a $T_{c,o}$ and $T_{c,p}$ of respectively 3.5 °C and 4.5 °C lower than the solvent cast sample without OMMT. However, ΔH_c remains largely unaffected for the solvent cast samples. Also important to note is that the presence of OMMT in these samples did not induce any cold crystallization during the heating period after the first cooling cycle. Thus, at the highest OMMT concentration crystallization of the polymer is slightly retarded and, due to the fact that molecular weight in all these samples is unmodified, this must be attributed to a lowered polymer mobility in the presence of OMMT. However, the results of the solvent cast samples cannot be directly linked to the results of the

melt intercalated samples. Because of the difference in preparation methods, the dispersion and intercalation state of OMMT within polymer matrix could differ.

It is for this reason that an additional sample set was produced by removing the OMMT from the melt intercalated PHBHHx samples, as described in the experimental section. It is not possible to discern any specific difference, i.e. decreasing or increasing trend in crystallization properties, in comparison to the original melt blended samples. It can be seen that $T_{c,o}$ and $T_{c,p}$ of the recovered PHBHHx-0 sample are slightly higher than those of the original PHBHHx-0. The cold crystallization of PHBHHx before and after polymer recovery is practically identical as well. Therefore, we must conclude that the presence of the OMMT particles does not have a drastic effect on polymer mobility, which was proposed as a possible mechanism for the retarded crystallization. It is possible that this phenomenon has a minor impact, although this effect is completely dominated by the reduced molecular weight, but the influence of other factors can't be totally excluded.

To overcome problems with crystallization, an AON sample set was produced, using the commercial granulate X151A, which demonstrates better crystallization properties than pure PHBHHx. It is therefore believed that the tailored X151A grade already contains processing additives such as nucleating agents. From the results, it becomes immediately obvious that the addition of OMMT has a negative effect on the crystallization properties of AON. However, this effect is not as outspoken, as was the case for the PHBHHx sample set. For example, AON-10 has a slightly higher $T_{c,p}$ and $T_{c,o}$ than PHBHHx-1 and a ΔH_c much higher than PHBHHx-1, despite the major difference in OMMT content. A significant difference in cold crystallization properties can be observed as well. AON/OMMT nanocomposites display a $T_{cc,p}$ of about 56-57 °C, whereas PHBHHx/OMMT nanocomposites have a $T_{cc,p}$ of about 73-74 °C. This much lower temperature indicates as well that crystallization can occur more readily in the Aonilex based samples. Generally, using the commercial granulate, it is possible to obtain a rather high ΔH_c in combination with some minor cold crystallization effects. This is a clear indication that the combination of commercial grade of PHBHHx (Aonilex) and OMMT can be very promising.

When regarding solely the crystallization properties of nanocomposites, it is obvious that the samples based on Aonilex, with a maximum OMMT content of 1 to 3 wt%, are most performant.

5.3.6 Barrier properties

The barrier properties of the produced samples were investigated through analysis of permeability for oxygen, carbon dioxide and water vapor (PO_2, PCO_2 and PH_2O). The results of the experiments are presented in Table 5-7. For the PHBHHx sample set, the permeability coefficients of nanocomposites for all three gases shows a clear decreasing trend upon increasing the OMMT content. Sample PHBHHx-10 even shows a fairly large reduction in PO_2, PCO_2 and PH_2O of 37 %, 42 % and 40 % respectively. The sample set produced from Aonilex pellets were also subjected to the same type of analysis. Here we can observe a similar decreasing trend in permeability coefficients, with PO_2, PCO_2 and PH_2O decreasing with about 47 %, 42 % and 37 % respectively. In general, the permeability of AON based nanocomposites seems to be slightly higher than those from the PHBHHx sample set, however still in the same range.

Table 5-7: Permeability properties of nanocomposites (n = 4)

Sample	PO_2 (cm^3 mm m^{-2} day^{-1} atm^{-1})	PCO_2 (cm^3 mm m^{-2} day^{-1} atm^{-1})	PH_2O (g mm m^{-2} day^{-1})
PHBHHx-0	7.8 (± 0.2)	44 (± 2)	1.34 (± 0.02)
PHBHHx-1	7.4 (± 0.1)	41.5 (± 0.5)	1.26 (± 0.04)
PHBHHx-3	6.3 (± 0.2)	36 (± 1)	1.04 (± 0.06)
PHBHHx-5	6.6 (± 0.1)	37.0 (± 0.7)	1.08 (± 0.02)
PHBHHx-10	4.9 (± 0.1)	25.3 (± 0.4)	0.80 (± 0.01)
AON-0	9.6 (± 0.8)	55 (± 2)	1.51 (± 0.06)
AON-1	8.7 (± 0.2)	51 (± 2)	1.41 (± 0.05)
AON-3	7.8 (± 0.5)	41 (± 2)	1.19 (± 0.02)
AON-5	7.3 (± 0.2)	39 (± 2)	1.0 (± 0.1)
AON-10	5.1 (± 0.3)	32 (± 1)	0.95 (± 0.07)

In terms of gas barrier properties, the samples containing 10 wt% of OMMT display the most promising potential for use as food packaging material, having a PO2 in the range of PET and a PH_2O almost as low as PP (see Table 2-6).

Upon addition of 1 wt% of OMMT, a similar PO_2 value was obtained as for 2 wt% ultra-fine talc (see Chapter 4). A more prominent decrease was observed for OMMT due to the fact that OMMT is a nano-sized filler. Also, the presence of ultra-fine talc increased gas permeability, due to the formation of smaller spherulites, but was compensated for slightly by the increase in tortuous path, formed by the ultra-fine talc particles

Upon comparison with the limited number of references available, it is possible to observe that the permeability results obtained in the frame of this study are very similar. Corrêa et al. obtained a reduction in PO_2 of 12.8 % and 33.8 % by adding 3 wt% of OMMT to respectively PHB and plasticized PHB [12], whereas in this study a reduction of about 19 % was achieved for an OMMT concentration of 3 wt%. The study of Crétois et al. on a PHBV/OMMT system showed an increase in PCO_2 and PH_2O and a fairly constant PO_2, attributed to an increase in gas solubility [22]. Sanchez-Garcia et al. compared PHBV and PHB nanocomposites containing 5 wt% OMMT, resulting in a respective reduction in PO_2 of 26.8 % and 20.5 % [37-39]. Water vapor permeability was reduced by 53.6 % and 5.9 % respectively, this in comparison to AON-5 and PHBHHx-5, showing a reduction of 33.8 % and 19.7 %.

In order to confirm that the mechanism behind the increased barrier properties is solely a physical gas barrier system, the relative permeability of the samples was calculated via the ratio of the permeability coefficients of the nanocomposites to the permeability coefficients of the polymer matrices (PHBHHx-0 and AON-0). These relative permeabilities are presented in Figure 5-7. It is clear that, for both sample sets, the relative permeability for O_2, CO_2 and water vapor shows a similar decreasing trend, indicating that the barrier mechanism for these three gases is similar. The clay platelets create a tortuous path which gas molecules must follow instead of going straight through, thus acting as a physical barrier for gas permeation.

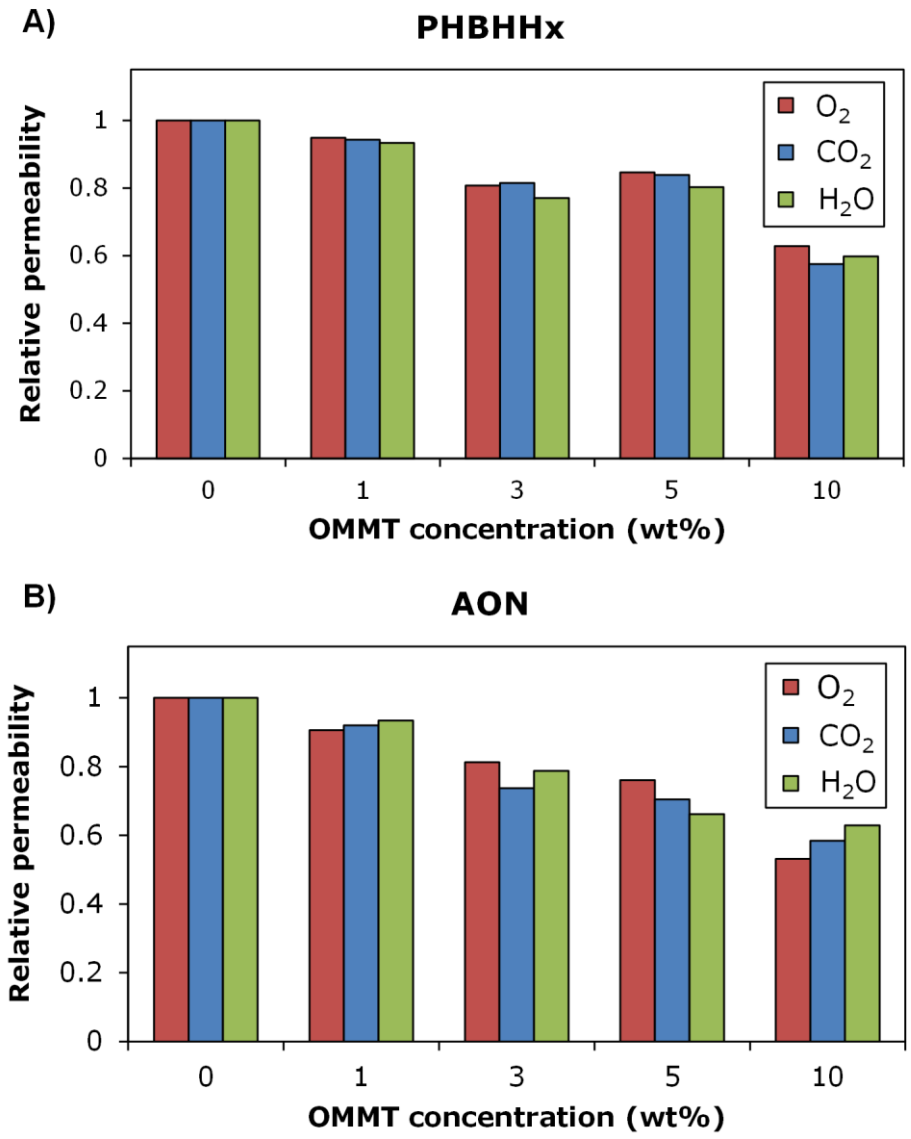

Figure 5-7: Relative permeabiliy of A) PHBHHx sample set and B) AON sample set

5.3.7 Tensile properties

Tensile properties of only Aonilex based sample set were investigated, as these samples are most promising for the properties tested in the previous paragraphs. The results of these tests are comprised in Table 5-8 and Figure 5-8, showing Young's modulus, tensile strength (calculated from the maximum in load), the nominal strain at break and the nominal strain at the point of maximum load.

The reference material AON-0 displays a Young's modulus of 765 MPa and a tensile strength of 19.5 MPa. The addition of OMMT clearly results in a drastic increase in stiffness, demonstrated by the higher values of Young's modulus, almost doubling at a concentration of 10 wt%. The tensile strength on the other hand seems to decrease slightly when adding OMMT, but this effect is not that outspoken. The nominal strain at break shows a severe decrease, going from 6.8 % for AON-0 to 3.8 % for AON-10, indicating that the material is rendered more brittle with rising OMMT concentration.

Table 5-8: Tensile properties of AON/OMMT nanocomposites (n = 10)

Sample	Young's modulus (MPa)	Max. tensile strength (MPa)	Nominal strain at max. load (%)	Nominal strain at break (%)
AON-0	765 (± 24)	19.5 (± 0.3)	5.6 (± 0.2)	6.8 (± 1.6)
AON-1	810 (± 26)	19.7 (± 0.2)	5.5 (± 0.1)	6.4 (± 0.6)
AON-3	937 (± 32)	19.3 (± 0.5)	4.9 (± 0.3)	6.1 (± 0.7)
AON-5	1042 (± 29)	19.0 (± 0.5)	4.6 (± 0.2)	5.1 (± 0.5)
AON-10	1364 (± 23)	18.5 (± 0.3)	3.6 (± 0.3)	3.8 (± 0.2)

Examples of the stress-strain curves of the samples are shown in Figure 5-8, demonstrating the increasing brittleness of the samples. The nominal strain at break is severely reduced. Additionally AON-0 shows clear necking before break, whereas this behavior is gradually reduced with AON-10, where a very brittle break with hardly any necking is observed. This can also be deduced from the gradually reducing difference between the nominal strain at max. load and the nominal strain at break.

For packaging applications however, one would prefer a material to be more ductile, which limits the applicable OMMT concentration range to a maximum of about 3 wt%. However, plasticization of the polymer matrix can be further considered, whereas a material of high stiffness, such as AON-5 and AON-10 with a Young's modulus of up to 1.3 GPa, could find applications in other industries such as the automotive sector.

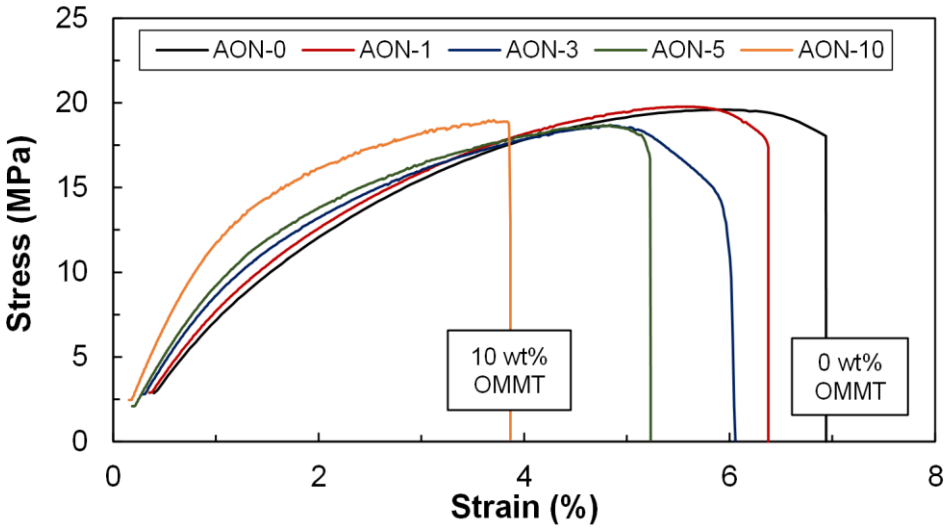

Figure 5-8: Tensile properties of Aonilex based nanocomposites

The effect of OMMT on the mechanical properties was much more outspoken than for ultra-fine talc. The percentual reduction in nominal strain at break and increase in Young's modulus of the sample containing 1 wt% OMMT is very similar to that of the sample containing twice as much ultra-fine talc.

5.4 CONCLUSIONS

In this chapter, PHBHHx and Aonilex were modified through addition of OMMT nanoparticles (1 to 10 wt% loading) in order to improve packaging-related properties. Using the melt-blending technique good nanofiller distribution/dispersion and predominantly intercalated nanostructures were obtained for all OMMT concentrations, as proven by XRD and TEM. Gas permeability properties were significantly improved, reaching a maximum reduction of roughly 40 % as compared to the neat polymer.

The samples were rendered more brittle and stiffer as OMMT content increased, which was to be expected from this type of nanocomposite.

However, some downsides were observed as well:

- An increase in processing-induced thermal degradation, most likely due to an unavoidable rapid moisture uptake of the OMMT. However, upscaling to twin screw extrusion for melt blending, using a continuously heated hopper, might limit moisture absorption.
- Polymer crystallization was severely retarded, due to lowering of molecular weight, but was counteracted for a large part by using a Aonilex instead of PHBHHx.
- The thermal stability of the prepared nanocomposites was enhanced by adding up to 5 wt% nanofiller, but then decreased again at 10 wt%.

Overall, it can be concluded that PHBHHx/OMMT has a certain potential for packaging applications. From a packaging point of view, the sample containing 3 wt% OMMT shows most promise and can possibly be enhanced even further upon application of processing techniques such as biaxial stretching and blow molding. It also should be noted that, despite not useful for packaging, the high stiffness of the nanocomposites with 5 and 10 wt% OMMT could be interesting for other industrial applications, such as the automotive industry.

5.5 REFERENCES

1. Alexandre, M. and P. Dubois, *Polymer-layered silicate nanocomposites: preparation, properties and uses of a new class of materials.* Mater Sci Eng R, 2000. **28**(1–2): p. 1-63.

2. Bordes, P., E. Pollet, and L. Avérous, *Nano-biocomposites: Biodegradable polyester/nanoclay systems.* Prog Polym Sci, 2009. **34**(2): p. 125-155.

3. Sinha Ray, S. and M. Okamoto, *Polymer/layered silicate nanocomposites: a review from preparation to processing.* Prog Polym Sci, 2003. **28**(11): p. 1539-1641.

4. Aranda, P. and E. Ruiz-Hitzky, *Poly(ethylene oxide)-silicate intercalation materials.* Chemistry of Materials, 1992. **4**(6): p. 1395-1403.

5. Bordes, P., et al., *Effect of clay organomodifiers on degradation of polyhydroxyalkanoates.* Polym Degrad Stab, 2009. **94**(5): p. 789-796.

6. Duncan, T.V., *Applications of nanotechnology in food packaging and food safety: Barrier materials, antimicrobials and sensors.* Journal of Colloid and Interface Science, 2011. **363**(1): p. 1-24.

7. Hussain, F., et al., *Review article: Polymer-matrix Nanocomposites, Processing, Manufacturing, and Application: An Overview.* Journal of Composite Materials, 2006. **40**(17): p. 1511-1575.

8. Ludueña, L.N., A. Vázquez, and V.A. Alvarez, *Effect of the type of clay organo-modifier on the morphology, thermal/mechanical/impact/barrier properties and biodegradation in soil of polycaprolactone/clay nanocomposites.* Journal of Applied Polymer Science, 2013. **128**(5): p. 2648-2657.

9. Stloukal, P., et al., *Kinetics and mechanism of the biodegradation of PLA/clay nanocomposites during thermophilic phase of composting process.* Waste Management, 2015. **42**(0): p. 31-40.

10. Wang, S., et al., *Characteristics and biodegradation properties of poly(3-hydroxybutyrate-co-3-hydroxyvalerate)/organophilic montmorillonite (PHBV/OMMT) nanocomposite.* Polymer Degradation and Stability, 2005. **87**(1): p. 69-76.

11. Iggui, K., et al., *A biodegradation study of poly(3-hydroxybutyrate-co-3-hydroxyvalerate)/organoclay nanocomposites in various environmental conditions.* Polymer Degradation and Stability, 2015. **119**(0): p. 77-86.

12. Corrêa, M.C.S., et al., *Elaboration and Characterization of Nano-Biocomposites Based on Plasticized Poly(Hydroxybutyrate-Co-Hydroxyvalerate) with Organo-Modified Montmorillonite.* Journal of Polymers and the Environment, 2012. **20**(2): p. 283-290.

13. Pavlidou, S. and C.D. Papaspyrides, *A review on polymer–layered silicate nanocomposites.* Prog Polym Sci, 2008. **33**(12): p. 1119-1198.

14. Chrissafis, K. and D. Bikiaris, *Can nanoparticles really enhance thermal stability of polymers? Part I: An overview on thermal decomposition of addition polymers.* Thermochimica Acta, 2011. **523**(1–2): p. 1-24.

15. Leszczyńska, A., et al., *Polymer/montmorillonite nanocomposites with improved thermal properties: Part I. Factors influencing thermal stability and mechanisms of thermal stability improvement.* Thermochimica Acta, 2007. **453**(2): p. 75-96.

16. Ding, C., B. Cheng, and Q. Wu, *DSC analysis of isothermally melt-crystallized bacterial poly(3-hydroxybutyrate-co-3-hydroxyhexanoate) films.* Journal of Thermal Analysis and Calorimetry, 2011. **103**(3): p. 1001-1006.

17. Bronlund, J.E., G.P. Redding, and T.R. Robertson, *Modelling Steady-State Moisture Transport Through Corrugated Fibreboard Packaging.* Packag Technol Sci, 2013. **27**: p. 193-201.

18. Cagnon, T., et al., *Nanostructuring and Microstructuring of Materials from a Single Agropolymer for Sustainable MAP Preservation of Fresh Food.* Packag Technol Sci, 2013. **26**(3): p. 137-148.

19. Kuorwel, K.K., et al., *Physico-Mechanical Properties of Starch-Based Films Containing Naturally Derived Antimicrobial Agents.* Packag Technol Sci, 2013. **27**: p. 149-159.

20. Hablot, E., et al., *Thermal and thermo-mechanical degradation of poly(3-hydroxybutyrate)-based multiphase systems.* Polym Degrad Stab, 2008. **93**(2): p. 413-421.

21. Carli, L.N., J.S. Crespo, and R.S. Mauler, *PHBV nanocomposites based on organomodified montmorillonite and halloysite: The effect of clay type on the morphology and thermal and mechanical properties.* Composites Part A, 2011. **42**(11): p. 1601-1608.

22. Crétois, R., et al., *Microstructure and barrier properties of PHBV/organoclays bionanocomposites.* J Membrane Sci, 2014. **467**(0): p. 56-66.

23. Erceg, M., T. Kovačić, and I. Klarić, *Poly(3-hydroxybutyrate) nanocomposites: Isothermal degradation and kinetic analysis.* Thermochim Acta, 2009. **485**(1–2): p. 26-32.

24. Cai, Y., et al., *Morphology, Thermal and Mechanical Properties of Poly (Styrene-Acrylonitrile) (SAN)/Clay Nanocomposites from Organic-Modified Montmorillonite.* Polym Plast Technol Eng, 2007. **46**(5): p. 541-548.

25. Xie, W., et al., *Thermal Degradation Chemistry of Alkyl Quaternary Ammonium Montmorillonite.* Chem Mater, 2001. **13**(9): p. 2979-2990.

26. Davis, R.D., J.W. Gilman, and D.L. VanderHart, *Processing degradation of polyamide 6/montmorillonite clay nanocomposites and clay organic modifier.* Polym Degrad Stab, 2003. **79**(1): p. 111-121.

27. Daly, P.A., et al., *Thermal degradation kinetics of poly(3-hydroxybutyrate-co-3-hydroxyhexanoate).* J Appl Polym Sci, 2005. **98**(1): p. 66-74.

28. Ko, M., et al., *Effect of matrix viscosity on clay dispersion in preparation of polymer/organoclay nanocomposites.* Fibers and Polymers, 2002. **3**(3): p. 103-108.

29. Ojijo, V. and S.S. Ray, *Nano-biocomposites based on synthetic aliphatic polyesters and nanoclay.* Prog Mater Sci, 2014. **62**(0): p. 1-57.

30. Unnikrishnan, L., et al., *Preparation and characterization of poly(methyl methacrylate)–clay nanocomposites via melt intercalation: Effect of organoclay on thermal, mechanical and flammability properties.* Mater Sci Eng A, 2011. **528**(12): p. 3943-3951.

31. Yu, F., et al., *Nucleation Effect of Layered Metal Phosphonate on Crystallization of Bacterial Poly[(3-hydroxybutyrate)-co-(3-hydroxyhexanoate)].* Macromol Mater Eng, 2011. **296**(2): p. 103-112.

32. Zhang, X., et al., *Some novel layered-silicate nanocomposites based on a biodegradable hydroxybutyrate copolymer.* Eur Pol J, 2007. **43**(8): p. 3128-3135.

33. D'Amico, D.A., V.P. Cyras, and L.B. Manfredi, *Non-isothermal crystallization kinetics from the melt of nanocomposites based on poly(3-hydroxybutyrate) and modified clays.* Thermochim Acta, 2014. **594**(0): p. 80-88.

34. Yu, W., et al., *Influence of zinc oxide nanoparticles on the crystallization behavior of electrospun poly(3-hydroxybutyrate-co-3-hydroxyvalerate) nanofibers.* Polymer, 2010. **51**(11): p. 2403-2409.

35. Bussiere, P.O., et al., *Effect of ZnO nanofillers treated with triethoxy caprylylsilane on the isothermal and non-isothermal crystallization of poly(lactic acid).* Phys Chem Chem Phys, 2012. **14**(35): p. 12301-12308.

36. Mandelkern, L., *Crystallization of polymers*. 2nd ed. Vol. Volume 2. Kinetics and mechanisms. 2012, New York: Cambridge University Press. 478.

37. Sanchez-Garcia, M.D., E. Gimenez, and J.M. Lagaron, *Novel PET Nanocomposites of Interest in Food Packaging Applications and Comparative Barrier Performance With Biopolyester Nanocomposites.* J Plast Film Sheet, 2007. **23**(2): p. 133-148.

38. Sanchez-Garcia, M.D., E. Gimenez, and J.M. Lagaron, *Morphology and barrier properties of nanobiocomposites of poly(3-hydroxybutyrate) and layered silicates.* J Appl Polym Sci, 2008. **108**(5): p. 2787-2801.

39. Sanchez-Garcia, M.D. and J.M. Lagaron, *Novel clay-based nanobiocomposites of biopolyesters with synergistic barrier to UV light, gas, and vapour.* J Appl Polym Sci, 2010. **118**(1): p. 188-199.

Chapter 6.

EVALUATION OF PACKAGING PROPERTIES OF POLY(3-HYDROXYBUTYRATE-CO-3-HYDROXYHEXANOATE)/ZINC OXIDE NANOCOMPOSITES

In this chapter, the effect of zinc oxide nanoparticles on packaging-related properties of poly(3-hydroxybutyrate-co-3-hydroxyhexanoate) is investigated. The focus of this chapter lies on gas permeability, tensile properties, thermal stability and crystallization. A single sample containing 3 wt% of TiO_2 was screened as well, for comparison with zinc oxide and as an exploratory test.

6.1 INTRODUCTION

Zinc oxide (ZnO) is a multifunctional material, due to its unique properties, such as high chemical stability, high electrochemical coupling coefficient, broad range of radiation absorption and high photostability. It is classified as a semiconductor in group II-VI [1], which means it is a material of which the cations are from group 12 and anions are from group 16 in the periodic table. Its versatility led to a great variety of applications, such as:

- The major application of ZnO is currently in the **rubber industry**. Here it is used as a vulcanization activator (to increase vulcanization rates) on one hand, but it is also used to increase the thermal conductivity of the rubbers. The latter is crucial for tires, where heat, resulting from deformation under load or cyclic stress, must be dissipated quickly [1, 2].
- ZnO also finds application in the **pharmaceutical and cosmetic industry**. The antibacterial and wound healing properties of ZnO result in its use in dermatological substances against inflammation and itching. It is also used in various nutritional products as source of essential dietary zinc. The addition of ZnO to a wide range of cosmetic products facilitates a better adhesion to

the skin. More importantly, ZnO is a broad-spectrum UV absorber, thus resulting in the utilization in sun creams [1, 2].

- ZnO can be used as a **photocatalyst** for the treatment of waste water streams, contaminated with organic pollutants. The absorption of a photon with an energy equal or greater to the bandgap energy, an electron-hole pair is formed. The positively charged hole in the valence band can react directly with the organic pollutant or indirectly through the formation of hydroxyl free radicals from the reaction with water. The negatively charged electron in the conduction band produces reactive oxygen species from O_2, adsorbed to the ZnO surface, which can attack the organic compounds [1].

ZnO can display three crystal structures: Rocksalt, zinc blende and Wurtzite (Figure 6-1). At ambient conditions however, the thermodynamically stable phase is the Wurtzite structure, in which every zinc atom is tetrahedrally coordinated with four oxygen atoms [3].

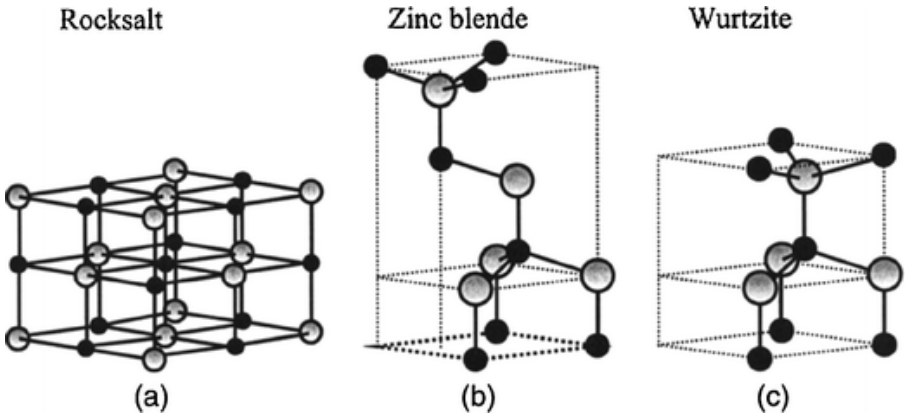

Figure 6-1: Possible crystal structures of ZnO with zinc and oxygen represented by gray and black spheres [3]

According to Espitia et al. (2012), commercial production of ZnO nanoparticles is achieved using two main methods, namely mechanochemical processing (MCP) and physical vapor synthesis (PVS). MCP combines a physical size reduction process in a conventional ball mill with chemical reactions that are mechanically activated at the nanoscale during grinding. PVS involves the vaporization of a solid precursor, using plasma energy. A reactant gas is injected into the vapor, followed by cooling at a controlled rate and condensing to form nanoparticles [3]

Nanosized ZnO can be synthesized in a great variety of structures, resulting in potential applications in many fields of nanotechnology. ZnO nanostructures are classified as one-, two- or three-dimensional. The one-dimensional group comprises most structures, such as nanorods, -needles, -tubes and –wires. Examples of two-dimensional structures are nanoplates/nanosheets and nanopellets. More elaborate three-dimensional structures include flowers and snowflakes [1]. In this study, ZnO nanorods were selected as several studies obtained strongly reduced barrier properties with this type of nanoparticle morphology [4, 5].

Polymer/ZnO nanocomposites are a fairly recent type of material, displaying interesting properties, and synthesized with conventional polymers as well as a large amount of biobased polymers. In order to enhance compatibility between the polymer and ZnO, the surface of the polar ZnO nanoparticles is sometimes chemically modified. Kołodziejczak-Radzimska and Jesionowski (2014) listed the three most used ZnO surface modifications as 1) inorganic compounds (e.g. SiO_2 an Al_2O_3), 2) polymeric compounds (e.g. poly(ethylene glycol) and polystyrene) and 3) organic compounds (carboxylic acids and silanes) [1].

A description of the effect of ZnO nanoparticles on selected properties is given below. One must however keep in mind that the type of nanostructure, as well as a possible surface modification, can play an important role on these properties.

1) Thermal stability:

The effect of ZnO nanoparticles on thermal stability of the polymer matrix appears to be highly dependent on the specific polymer. An increase in thermal stability was observed for PHB [6], PHBV [7], chitosan/poly(vinyl alcohol) blends [8], gelatin [9] and poly(ether ether ketone) [10]. This effect is usually ascribed to the barrier effect that the nanoparticles present against loss of volatiles during degradation. However, PLA displayed a reduced thermal stability upon introduction of ZnO nanoparticles. ZnO acted as a catalyst, enhancing intermolecular transesterification and "unzipping" depolymerization reactions [11]. The gravity of this negative effect was reduced by using surface modified ZnO, in which the surface of the ZnO has been deactivated for a large part.

2) Crystallization:

The crystallization rate shows slight improvement for polymers such as PCL [4], PLA [5] and poly(ether ether ketone) [10]. However, the effect of ZnO nanoparticles on the crystallization rate of PHB and PHBV is rather unclear. The studies of Diez-Pascual et al. [6, 7] showed a rather large increase in crystallization peak temperature for solvent cast samples containing up to 10 wt% of ZnO nanoparticles. A separate study by Yu et al. [12], on the other hand, proved a decrease in crystallization temperature of about 6 °C in electrospun PHBV fibers containing only 1 wt% of ZnO nanoparticles, which was attributed to physical interactions between PHBV and ZnO, resulting in restricted polymer mobility.

3) Barrier properties:

Due to the fact that ZnO is added in the form of inorganic nanoparticles, it is possible that these particles act as an impermeable barrier and cause an increase in tortuous path. Water vapor and oxygen permeability of PHB containing 5 wt% ZnO decreased with 38 % and 53 %, in comparison to neat PHB [6]. For PHBV, a reduction of 46 % and 35 % is observed for water vapor and oxygen permeability, upon addition of 4 wt% ZnO. Elen et al. [4] achieved a reduction of 64 % and 61 % for oxygen and carbon dioxide permeability upon addition of 6 wt% ZnO nanorods to PCL. Pantani et al. [5] reported a 37 % decrease in water vapor permeability of PLA after adding 3 wt% ZnO. Lepot et al. [13] did not find an outspoken effect on oxygen permeability of PP after adding ZnO nanoparticles, which was attributed to the less suitable nanostructure of the ZnO used in that study.

4) Tensile properties:

The addition of nanofillers to a polymeric matrix can induce severe changes in tensile properties. For PHB containing 10 wt% ZnO, Díez-Pascual et al. (2014) found an increase of 43 % in Young's modulus, whereas the elongation at break is reduced with 20 %. The tensile strength increased with 32 % at 5 wt% ZnO and decreased again at higher concentrations [6]. They observed fairly similar patterns for PHBV/ZnO nanocomposites [7]. By adding 6 wt% of ZnO nanorods to PCL, Elen et al. (2012) observed a 36 % increase in Young's modulus, whereas

the elongation at break decreased with 11 %. The tensile strength remained fairly constant [4]. Upon addition of 8 wt% ZnO nanorods, Lepot et al. (2011) observed an increase of 100 % in Young's modulus, whereas the tensile strength remained fairly constant [13]

5) UV blocking:

A great deal of compounds, present in food stuffs, are photosensitive and their degradation during storage will gravely effect their quality. Examples of these food compounds are fatty acids [14], β-carotene [15], chlorophyll [16] and α-tocopherol [17]. Therefore, it could be interesting to provide some light-blocking properties through additives, as is the case for ZnO. Effective UV shielding was observed for PLA [11], HDPE [18] and gelatin [9] upon addition of ≥ 1 wt% ZnO. The UV absorption properties of ZnO arise from the fact that it is a wide band gap semiconductor. When a photon of sufficient energy hits the ZnO surface, its energy is used to form an electron-hole pair. The minimal required energy is called the band gap energy and is about 3.3 eV for ZnO [1-3]. A band gap energy of 3.3 eV corresponds with the ability to absorb all photons with wavelengths of about 376 nm or lower, which comprises a large part of the UV range of the electromagnetic spectrum (200-400 nm).

6) Antibacterial properties:

ZnO nanocomposites based on PHB [6], PHBV [7], gelatin [9], chitosan/poly(vinyl alcohol) blends [8], PLA [5, 11] and poly(ether ether ketone) [10] can possess antibacterial properties, which usually increase at higher concentrations of ZnO. However, it is important to note that the antibacterial properties of ZnO are reduced due to surface modification, as the amount of active ZnO surface, exposed to the bacteria, is reduced. The antibacterial mechanism of ZnO is not yet completely understood, but is usually attributed to 1) the release of antimicrobial Zn^{2+} ions, 2) cell membrane damage due to electrostatic attraction between ZnO surface and bacteria or 3) light-induced formation of reactive oxygen species at the surface of ZnO particles, which can penetrate the cell membrane [3].

6.2 EXPERIMENTAL

6.2.1 Materials and sample preparation

Pure PHBHHx powder and a commercial PHBHHx granulate (trade name Aonilex X151A) (AON), both with a 3-hydroxyhexanoate content of 10.5 mol%, were provided by Kaneka Corporation (Westerlo-Oevel, Belgium), and dried at 70 °C in vacuo for 3 days.

Commercially available ZnO nanorods were kindly provided by Umicore Zinc Chemicals (Belgium) as Zano 20 (rod length ≈ 30 nm, ZnO content ~99.5 %) and Zano 20 Plus (surface coated with a silane especially suitable for the treatment of metal oxides, i.e., triethoxy caprylylsilane; ZnO content: 96.2 %) Surface-treated Zano20 Plus and untreated Zano 20 will be named sZnO and ZnO, respectively.

Rutile TiO_2 nanoparticles (spherical) were kindly provided by Kronos (Germany) as Kronos 2500 (surface treated with aluminum and organic compounds, TiO_2 content ≥ 97.5 %, spherical with particle size ~ 200 nm).

Solvent-cast samples were prepared by sonication of the correct amount of ZnO or sZnO in 10 ml of chloroform for 30 min. Subsequently, the polymer was added and stirred for 30 min at 40 °C. The solutions were cast into glass petri dishes and the chloroform was left to evaporate for 60 min at room temperature. Residual chloroform was removed by drying at 70 °C *in vacuo* for 2 days. Samples containing 1 and 3 wt% of ZnO and sZnO were prepared. These samples were only used for a preliminary screening of the effect on PHBHHx crystallization.

For the melt-blended samples, the following method was employed. Firstly, samples with a total weight of 55 g (polymer + ZnO, sZnO or TiO_2) were mixed in a Rondol mini-mix high speed mixer, before being processed in a Brabender counter-rotating internal mixer equipped with roller blades. Mixer temperature was set at 140 °C. During feeding of the mixer, a rotation speed of 30 rpm was used for 3 min to avoid the excessive increase of the torque during polymer melting. Then the rotation speed was increased to 80 rpm for 8 min. Samples containing 1, 3 and 5 wt% ZnO or sZnO were prepared. A single sample containing 3 wt% TiO_2 was prepared for research and reference purposes, as this is a metal oxide that is commonly used in the plastics and rubbers industry.

Subsequently, samples of about 1.8 g were compressed and molded at 140 °C to prepare films in a polyimide mold (100 mm x 100 mm x 0.150 mm) using an Agila PE20 hydraulic press. The polymer was pre-heated for 90 s without pressure before being pressed at 30 bar for 150 s, followed by two degassing cycles. Finally, the films were pressed at high pressure of 150 bar for 120 s, followed by a slow cooling at 50 bar for 20 min at 60 °C to allow film crystallization and easy demolding.

Thicker plates for tensile testing and XRD were produced in a stainless steel mold (100 mm x 100 mm x 0.5 mm) at 140 °C with a pre-heating time of 3 min before being pressed at 30 bar for 200 s. Subsequently two degassing cycles were used before finally molding the sample at 150 bar for 150 s. The samples were slowly cooled at 50 bar for 20 min at 60 °C.

6.2.2 Transmission electron microscopy (TEM)

The TEM study was performed with a FEI Tecnai Spirit using an accelerating voltage of 120kV. The images are standard BF (bright field) images. Transparent slices of about 150 nm thick are made with a Leica EM UC6 ultramicrotome.

6.2.3 Gel permeation chromatography (GPC)

The molecular weight distribution of PHBHHx was analyzed using a GPC apparatus composed of a SpectroSeries P100 pump, equipped with a Shodex RI71 refractometer detector and two PL-gel 10 µm Mixed-B columns in series, thermostated at 35 °C. The eluent was chloroform (VWR, HPLC grade) at a flow rate of 1.0 ml/min. Samples were dissolved in chloroform at a concentration of 1 g/l and filtered over a 0.45 µm syringe filter. The injection volume was 100 µl. Calibration was performed using polystyrene standards (474 to 3 150 000 g/mol) dissolved in chloroform with a concentration of 1 g/l.

The samples containing ZnO or sZnO were subjected to an acid washing with 0.1 N HCl before analysis, in order to remove the nanosized particles and to avoid damage to the GPC columns. The sample containing TiO_2 was simply filtered over a 0.45 µm syringe filter to remove the particles.

6.2.4 Thermogravimetric analysis (TGA)

The thermal stability of samples was analysed using a TA Instruments Hi-Res TGA 2950 thermogravimetric analyser. Samples of about 10 mg were heated from room temperature to 350 °C at a heating rate of 20 °C/min with a N_2 gas flow of 80 ml/min. Measurements were performed at least in duplicate.

6.2.5 Differential scanning calorimetry (DSC)

Thermal properties of the prepared films were analyzed under inert atmosphere (50 ml/min N_2) using a TA Instruments Q200 DSC. About 3.5 mg of the compression molded thin films in a sealed aluminium pan was used to perform the measurements. The sample pan was heated from -30 °C to 150 °C at a heating rate of 10 °C/min. After being kept isothermal for 2 min, the sample was cooled again at 10 °C/min to -30 °C. For all samples, only the weight fraction of polymer in nanocomposites was considered, this to allow a more accurate determination of enthalpy values. Measurements were performed at least in duplicate.

6.2.6 Thickness measurements

Sample thickness was measured prior to permeability testing, using a MTS MI20 thickness gauge. The thickness was taken as the average of five measurements at different locations of each sample.

6.2.7 Barrier properties

The oxygen transmission rate (OTR), at 23 °C and 0 % relative humidity (RH), of the produced samples was measured using a Mocon Ox-Tran 702 (ASTM D3985). Carbon dioxide transmission rate (CO_2TR) at 23 °C and 0 % RH was measured using a Mocon Permatran-C 4/41 (ASTM F2476). Water vapor transmission rate (WVTR) was measured using a Mocon Permatran-W 700 (ASTM F1249). Test gases (O_2 and CO_2) and carrier gas (N_2, N_2/H_2) with a purity of 99.999 % were purchased from Westfalen, Münster (Germany). Samples were placed between 2 aluminium masks with an effective testing area of 5 cm². The sample was exposed to the test gas on one side and to a continuously flushing carrier gas on the other side, both at a total pressure of 1 atm. For OTR measurements a carrier gas N_2/H_2 (95/5) was used, for all other measurements pure N_2. The test gas diffuses through the sample and is guided by the carrier gas towards the detector. The gas transmission rate or gas flux J, in cm³/m².day.atm (for OTR and CO_2TR) or

g/m².day (for WVTR) of the specific test gas, is reported when equilibrium is reached (i.e. the concentration of test gas in the carrier gas changes less than 1 % during a test cycle of 30 min). The gas flux *J* can be defined as the quantity of test gas or permeant *Q*, which passes through the polymeric film per unit area *A* during one unit of time *t* at equilibrium: [19-21]

$$J = Q / (A.t) \quad (6\text{-}1)$$

In order to obtain a thickness-independent criterion for comparison, the gas flux *J* can be normalized for sample thickness *d* and permeant pressure *p* to obtain the permeability *P*: [19-21]

$$P = J.d / p \quad (6\text{-}2)$$

At least two samples of each blend were measured twice.

6.2.8 Tensile properties

The tensile test was performed using a MTS/10 tensile tester at a crosshead speed of 1 mm/min and a distance of 25.4 mm between the grips. Samples were cut into dumbbell shapes (ASTM D638-02 type V) and were conditioned at 23 °C and 50 % relative humidity for 48 h before testing. At least 10 specimen of each sample were measured.

6.2.9 UV absorption properties

UV-visible absorption measurements were performed on films of approximately 150 µm thickness using an Agilent Cary series UV-Vis-NIR spectrophotometer. Air was used as a blank reference and transmittance spectra were recorded in the wavelength range of 200 to 800 nm.

6.2.10 Opacity

The opacity of the prepared films was determined according to the Hunter Lab method in the reflectance mode, using a Datacolor Microflash 100D. The opacity *Y* (in %) can be calculated as the relationship between the opacity of a sample on a black standard Y_b and the opacity on a white standard Y_w:

$$Y = Y_b / Y_w \times 100 \quad (6\text{-}3)$$

A sample was measured 4 times (twice on each side) in order to obtain a representative average.

6.3 RESULTS AND DISCUSSION

In this study, a ZnO modified with triethoxy caprylylsilane was used, due to its commercial availability, long term stability and most importantly its high compatibility with PLA [11], which is chemically speaking similar to PHBHHx so a similar effect is to be expected. A concentration range of 1 to 5 wt% was selected, because the main goal is to enhance the barrier properties, which usually requires higher filler loading.

6.3.1 Preliminary screening using solvent-cast method

It has been established that the crystallization properties of PHBHHx are far from ideal, but also that the presence of additives can enhance (see Chapter 4) or reduce crystallization properties (see Chapter 5). Therefore a preliminary screening was performed, where solvent cast samples based on pure PHBHHx were prepared, as this is a rapid form of sample preparation. The goal of this screening was to test if crystallization is sufficiently enhanced and if not, whether it is more interesting to change the polymeric matrix to Aonilex.

For the non-isothermal crystallization experiments, the most important parameters related to crystallization, that can be derived from DSC analysis, are the onset temperature of crystallization ($T_{c,o}$), crystallization peak temperature ($T_{c,p}$) and the crystallization enthalpy (ΔH_c). These results are presented in Table 6-1. The pure PHBHHx presents a $T_{c,o}$, $T_{c,p}$ and ΔH_c of 78.1 °C, 70.5 °C and 32.4 °C, respectively. From the results, it can be concluded that the addition of sZnO or ZnO does not have a significant effect on the crystallization properties of PHBHHx, with all three investigated parameters remaining almost unchanged. Therefore, it was decided to perform further experimentation using Aonilex (commercial PHBHHx), abbreviated as AON, which has been tailored for sufficient crystallization after processing, instead of the pure PHBHHx powder.

Table 6-1: Crystallization properties of solvent cast PHBHHx/ZnO and PHBHHx/sZnO nanocomposites (n = 2 or 3)

Sample	$T_{c,o}$ (± 0.2) (°C)	$T_{c,p}$ (± 0.2) (°C)	ΔH_c (± 0.9) (J/g)
PHBHHx pure	78.1	70.5	32.4
PHBHHx + 1 wt% ZnO	78.0	70.4	32.6
PHBHHx + 3 wt% ZnO	77.9	70.1	31.8
PHBHHx + 1 wt% sZnO	78.1	70.6	31.3
PHBHHx + 3 wt% sZnO	78.3	70.6	32.7

6.3.2 Dispersion study

To investigate the nanocomposite morphology, TEM analysis was performed on the ZnO and sZnO nanocomposites. For the ZnO sample set (Figure 6-2A to C), it can be seen that the dispersion is only good at 1 wt% ZnO. At concentrations of 3 and 5 wt%, the ZnO nanoparticles show only a partial fine dispersion in the matrix, the rest is clustered in large agglomerations, as indicated by the red arrows. Some agglomerations are even visible with the naked eye, which is of course unacceptable for actual applications. This is a clear indication that the ZnO and AON are rather incompatible and only low concentrations can be dispersed adequately.

Surface modification of zinc oxide can be of great influence on the dispersion into a polymeric matrix, which can be clearly seen in the TEM images of the AON/sZnO nanocomposites (Figure 6-2E to F). These samples display a fine dispersion at all three tested concentrations, without the formation of large-scaled agglomerations. Due to the silanization of the sZnO surface, the interfacial energy between the nanoparticle surface and the polymer chains is strongly reduced, allowing better mixing and thus the formation of a well-dispersed nanocomposite.

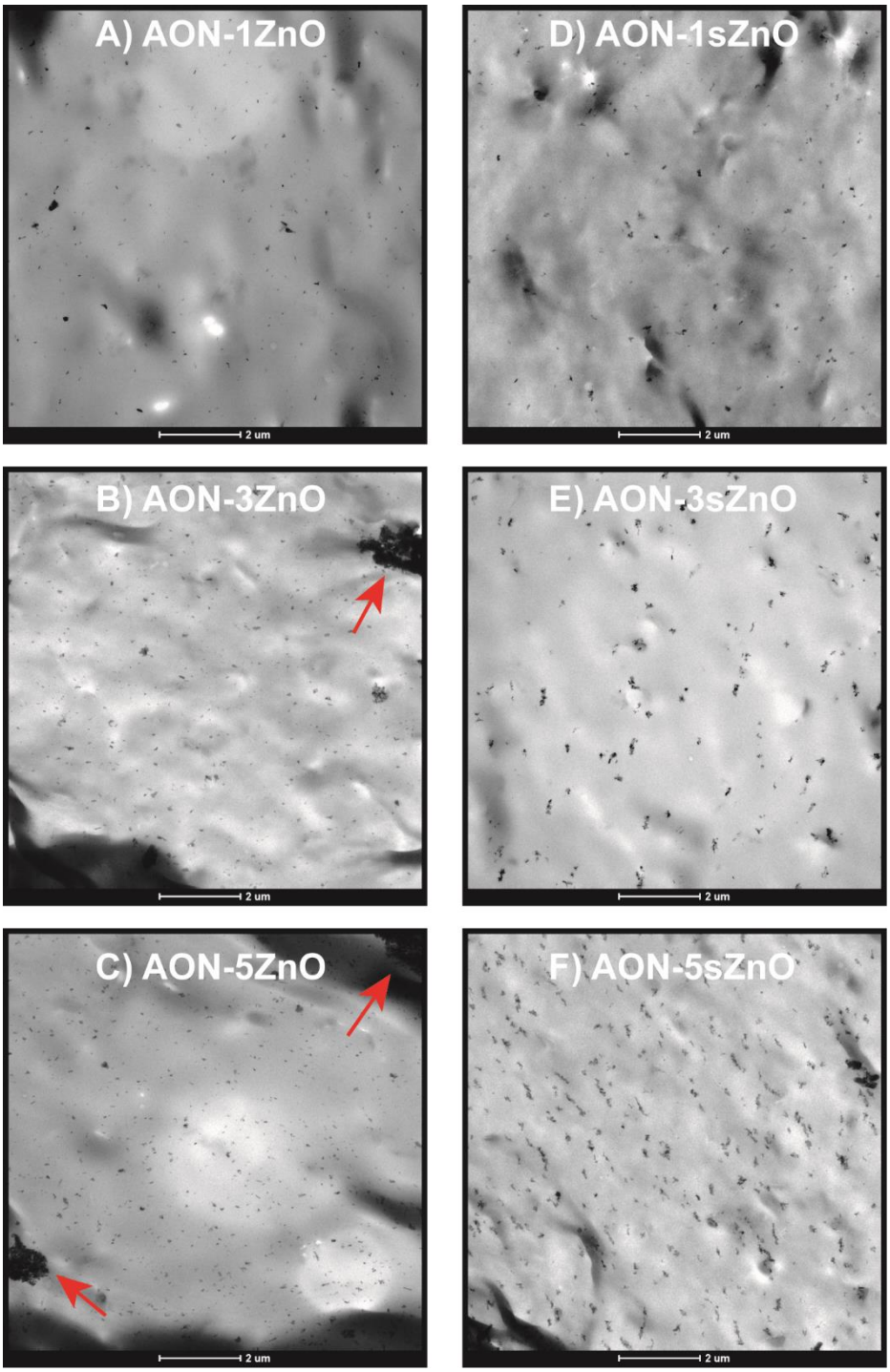

Figure 6-2: TEM images of AON/ZnO and AON/sZnO nanocomposites

6.3.3 Degradation during melt-processing

Using GPC, the thermo-mechanical degradation occurring during melt blending of AON and ZnO, sZnO and TiO_2 was investigated. The number average molecular weight $\bar{M}_n$, weight average molecular weight $\bar{M}_w$ and dispersity ($Đ_M$), defined as the ratio of $\bar{M}_w$ to $\bar{M}_n$, were determined before (virgin) and after melt processing. Table 6-2 is split in two parts, the first part presents the results for the samples that were not acid washed, whereas the second part presents the ZnO or sZnO samples that underwent an acid wash.

When regarding the samples containing ZnO, a decrease in molecular weight at higher ZnO concentrations can be observed, but the dispersity remains fairly constant. $\bar{M}_w$ and $\bar{M}_n$ of the sample containing 5 wt% ZnO are about 9 % and 15 % lower than for AON–0. For the sZnO samples, no explicit changes in molecular weight can be observed with certainty. This is due to the fact that the surface of sZnO is rendered inactive for a large part via surface modification. For example, $\bar{M}_w$ and $\bar{M}_n$ of the sample containing 5 wt% sZnO are only about 5 % lower than AON – 0. The results of the acid washed samples are difficult to interpret, which is most likely due to the fact that the acidic liquid-liquid extraction can possibly cause loss of polymer due to precipitation. However, it is still possible to draw qualitative conclusions.

It is widely accepted that thermal degradation of PHBHHx occurs through random chain scission (*cis*-elimination), following the same degradation mechanism as PHB (See Figure 2-1), involving a six-membered ring transition state, followed by an auto-accelerated degradation due to the formation of low molecular weight reaction products [22-24].

Kim et al. [25] observed that the addition of zinc (in the form of $ZnCl_2$) reduced the thermal stability of PHB, even at concentrations as low as 400 ppm. This effect was attributed to the fact that Zn^{2+} is an intermediate Lewis acid, which could catalyze the *cis*-elimination degradation reaction. This could be a possible explanation for the phenomenon at hand as well.

The addition of 3 wt% of TiO_2 on the other hand does not seem to cause any additional degradation during processing. It is important to note that the TiO_2 used in this study has undergone surface treatment as well in order to increase compatibility with polymeric matrices.

Table 6-2: Molecular weight distribution of AON/ZnO, AON/sZnO and AON/TiO_2 nanocomposites

Sample	$\bar{M}_n$ (x 10^3 g/mol)	$\bar{M}_w$ (x 10^3 g/mol)	$Đ_M$
No HCl treatment:			
Virgin Aonilex	247	557	2.2
AON-0	200	440	2.2
AON-3TiO_2	201	439	2.2
HCl treatment:			
AON-0	183	441	2.4
AON-1ZnO	186	407	2.2
AON-3ZnO	150	378	2.5
AON-5ZnO	167	373	2.2
AON-1sZnO	190	416	2.2
AON-3sZnO	180	426	2.4
AON-5sZnO	176	418	2.4

6.3.4 Thermal stability

The thermal stability of the prepared nanocomposites was investigated using TGA under pure nitrogen atmosphere from room temperature to 350 °C with a heating rate of 20 °C/min. These results are presented in Table 6-3.

The reference sample AON–0 displays a $T_{d,o}$, $T_{d,50}$ and $T_{d,p}$ of 290.6, 301.3 and 305.8 °C, respectively. The addition of increasing amounts of ZnO and sZnO results in a gradual decrease of these indicative parameters. For example, adding 5 wt% ZnO to AON results in a decrease $T_{d,o}$, $T_{d,50}$ and $T_{d,p}$ of about 15 °C, 11 °C and 17 °C. The addition of sZnO results in a similar effect, albeit about 2 °C less. From these results, it can be concluded that zinc oxide has a catalytic effect on the thermal degradation of AON, but this effect can be partially compensated for by using surface modified zinc oxide.

Similar to the results in the previous paragraph, it must be concluded that the addition of 3 wt% TiO_2 does not show any significant effect on the thermal stability, with all three indicative temperatures practically unchanged.

When comparing to the ultra-fine talc and OMMT composites of Chapter 4 and 5, it must be concluded that both ZnO and sZnO nanoparticles present a completely different effect. For OMMT (up to 5 wt%) and ultra-fine talc an increase in thermal stability was observed.

Table 6-3: Thermal stability of AON/ZnO, AON/sZnO and AON/TiO_2 nanocomposites (n = 2 or 3)

Sample	$T_{d,o}$ (°C)	$T_{d,50}$ (°C)	$T_{d,p}$ (°C)
AON-0	290.6 (± 0.5)	301.3 (± 0.8)	305.8 (± 0.7)
AON-1ZnO	278.8 (± 0.3)	291.0 (± 0.8)	294.3 (± 0.9)
AON-3ZnO	275.5 (± 0.3)	289.3 (± 0.4)	289.7 (± 0.4)
AON-5ZnO	275.5 (± 0.4)	290.5 (± 0.3)	288.8 (± 0.7)
AON-1sZnO	281.6 (± 0.3)	293.4 (± 0.2)	296.1 (± 0.2)
AON-3sZnO	278.3 (± 0.2)	291.3 (± 0.2)	291.0 (± 0.7)
AON-5sZnO	277.4 (± 0.5)	291.5 (± 0.3)	290.0 (± 0.7)
AON–3TiO_2	289.1 (± 0.5)	299.6 (± 0.3)	305.5 (± 0.8)

6.3.5 Crystallization properties

From the non-isothermal crystallization study, it is possible to observe the onset of crystallization ($T_{c,o}$), crystallization peak temperature ($T_{c,p}$) and the crystallization enthalpy (ΔH_c), which are presented in Table 6-4.

In general, it can be deduced that the nanofillers do not gravely effect the crystallization properties of AON. However, it is possible to discern a slight decrease in crystallization temperatures upon addition of the unmodified ZnO, with $T_{c,o}$ and $T_{c,p}$ decreasing 1.3 °C and 1.7 °C. Yu et al. [12] observed a decrease in crystallization temperature of about 6 °C in electrospun PHBV fibers with 1 wt% ZnO nanofiller.

They attributed this effect to a high degree of interactions between PHBV and ZnO, which restricted polymer mobility and thus caused a slight decrease which they attributed to a interactions between PHBV and ZnO, resulting in restricted polymer mobility. Given the chemical similarity between PHBV and PHBHHx, a similar phenomenon could be at play. However, it is of high importance to realize that a reduction in crystallization temperatures of about 1 to 2 °C, does not present any technical difficulties. Addition of sZnO instead of ZnO, resulted in no change in crystallization temperatures.

Table 6-4: Crystallization of melt-compounded AON/ZnO, AON/sZnO and AON/TiO_2 nanocomposites (n = 2 or 3)

Sample	$T_{c,o}$ (± 0.2) (°C)	$T_{c,p}$ (± 0.2) (°C)	ΔH_c (± 0.8) (J/g)
AON-0	80.4	73.3	33.8
AON-1ZnO	79.6	72.3	34.7
AON-3ZnO	79.1	71.8	33.9
AON-5ZnO	79.1	71.6	34.4
AON-1sZnO	80.1	72.9	34.1
AON-3sZnO	80.5	73.4	33.9
AON-5sZnO	80.7	73.5	33.6
AON–3TiO_2	80.5	73.4	34.0

Again, the sample containing 3 wt% TiO_2 presented no difference in crystallization properties, in comparison to the reference AON. There is only a limited amount of literature data available on PHA/TiO_2 composites, but the study of Buzarovska et al. (2009) revealed slight increases in crystallization properties and thermal stability of PHBV at high TiO_2 concentrations (≥ 5 wt%) [26].

6.3.6 Barrier properties

For all prepared nanocomposites, a thorough analysis of PO_2, PCO_2 and PH_2O was performed. It can be seen in Table 6-5 that the addition of sZnO, in all tested concentrations, does not have any effect on the gas permeability properties of AON. The addition of 1 and 3 wt% ZnO lowered PO_2, PCO_2 and PH_2O slightly with about 5, 7 and 11 % respectively. It was not possible to measure AON-5ZnO, due to the fact that the permeability values of this sample exceeded the measuring range of the apparatus. The presence of agglomerations larger than the thickness

of the film are responsible for this. As a result, the films are not perfectly formed and cracks and voids are present. The addition of TiO_2 has no effect on the gas permeability properties of AON. This in comparison to the earlier prepared OMMT nanocomposites, which showed a significant reduction in permeability properties with increasing OMMT concentrations.

Table 6-5: Barrier properties of AON/ZnO, AON/sZnO and AON/TiO_2 nanocomposites (n = 4)

Sample	PO_2 (cm^3 mm m^{-2} day^{-1} atm^{-1})	PCO_2 (cm^3 mm m^{-2} day^{-1} atm^{-1})	PH_2O (g mm m^{-2} day^{-1})
AON-0	9.0 (± 0.1)	42.9 (± 0.5)	1.37 (± 0.02)
AON–1ZnO	8.4 (± 0.2)	40 (± 1)	1.22 (± 0.03)
AON–3ZnO	8.6 (± 0.1)	40.0 (± 0.2)	1.22 (± 0.03)
AON–1sZnO	9.0 (± 0.2)	43 (± 1)	1.38 (± 0.05)
AON-3sZnO	9.2 (± 0.1)	42.1 (± 0.3)	1.33 (± 0.03)
AON-5sZnO	9.2 (± 0.1)	42.9 (± 0.5)	1.30 (± 0.05)
AON-3TiO_2	9.0 (± 0.3)	42 (± 1)	1.35 (± 0.03)

The lack of any drastic effect on the gas permeability properties is most likely due to the nanostructure of the zinc oxide nanoparticles used in this study. These nanorods do not form a tortuous path as elaborate as nanoplatelets for example. However, literature data regarding the use of PLA/sZnO nanorods (up to 3 wt% sZnO) [5] and PCL/ZnO nanorods (up to 6 wt% ZnO) [4] indicate severe reductions in gas permeability, in comparison to the neat polymers. It must be concluded that the effect of sZnO and ZnO nanorods on this particular polymeric system is not great. The addition of ZnO reduced the gas permeability a bit, which could be because it is less compatible with the polymer and thus forms larger impermeable clusters, whereas sZnO is highly dispersible and forms very small clusters, which does not create an elaborate tortuous path. These agglomerates can be visually observed for 3 and 5 wt% ZnO and also microscopically in Figure 6-2.

6.3.7 Tensile properties

The results of these tests are comprised in Table 6-6, showing Young's modulus (slope of initial linear part of stress-strain curve), tensile strength (calculated from the maximum in load), the nominal strain at break and the nominal strain at the point of maximum load. Examples of the stress strain curves are given in Figure 6-3.

AON–0 is a fairly ductile material with a Young's modulus, max. tensile strength and nominal strain at break of 704 MPa, 19.1 MPa and 7.4 %, respectively. The addition of ZnO has the greatest effect on the tensile properties. The material becomes gradually stiffer and more brittle. Upon addition of 5 wt% ZnO, the Young's modulus increases with 12 % to 789 MPa, whereas the nominal strain at break and nominal strain at max. load are reduced by 36 % and 28 %, respectively.

Table 6-6: Tensile properties of AON/ZnO, AON/sZnO and AON/TiO_2 nanocomposites (n = 10)

Talc content	Young's modulus (Mpa)	max. tensile strength (Mpa)	nominal strain at max. load (%)	nominal strain at break (%)
AON-0	704 (± 28)	19.1 (± 0.4)	5.8 (± 0.1)	7.4 (± 0.2)
AON-1ZnO	737 (± 23)	19.3 (± 0.3)	5.5 (± 0.2)	6.3 (± 0.1)
AON-3ZnO	792 (± 26)	18.8 (± 0.4)	4.8 (± 0.2)	5.7 (± 0.2)
AON-5ZnO	789 (± 29)	17.1 (± 1.0)	4.2 (± 0.4)	4.7 (± 0.2)
AON-1sZnO	719 (± 19)	19.0 (± 0.5)	5.9 (± 0.2)	6.9 (± 0.2)
AON-3sZnO	728 (± 25)	18.9 (± 0.7)	5.5 (± 0.2)	6.2 (± 0.2)
AON-5sZnO	751 (± 36)	18.8 (± 0.3)	5.4 (± 0.2)	6.0 (± 0.3)
AON-3TiO_2	770 (± 45)	18.8 (± 0.3)	5.4 (± 0.2)	6.2 (± 0.1)

Important to note is that the difference between these latter two properties, becomes smaller and smaller with increasing amounts of ZnO. This is an indication that the necking behavior is reduced, typical of a less ductile material. The max. tensile strength displays a decreasing trend as well, reaching a minimal value of 17.1 MPa at 5 wt% ZnO. This is a clear confirmation of the incompatibility between the polymer and the unmodified ZnO nanoparticles and their poor dispersion.

The addition of surface modified sZnO clearly induces less grave changes in tensile properties. The max. tensile strength remains fairly constant at all sZnO concentrations. The Young's modulus is increased by only 7 % upon addition of 5 wt% sZnO. The nominal strain at break and at max. load are reduced by 19 % and 7 %, reaching values of 6.0 % and 5.4 % respectively. The high degree of compatibility and excellent dispersion of sZnO can be considered as an explanation for these results. All in all, using sZnO it is possible to render AON stiffer, without losing too much of its ductility or tensile strength. Murariu et al. [11] found an increase in Young's modulus of about 24 % and a decrease in nominal strain at break of 41 % upon addition of 3 wt% sZnO (same grade as used in this study) to PLA, which are significantly more severe changes in tensile properties.

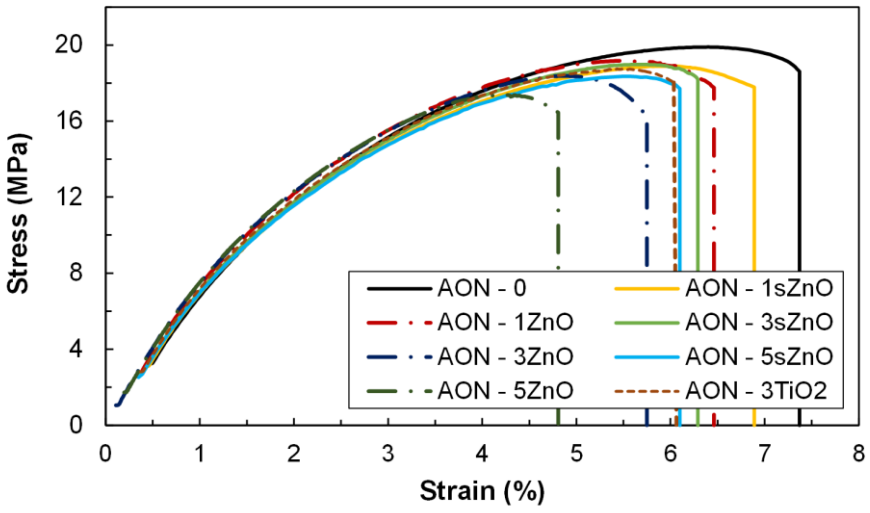

Figure 6-3: Stress-strain curves of AON/ZnO, AON/sZnO and AON/TiO_2 nanocomposites

The addition of unmodified ZnO has similar effects as OMMT on the strain at break, but the effect on the Young's modulus is not as outspoken. The addition of sZnO induced only minor effects on the mechanical properties.

Adding 3 wt% of TiO_2 to AON, results in an increase of Young's modulus of 9 %, reaching a value of 770 MPa. The nominal strain at break and at max. load are reduced to 6.2 % and 5.4 % respectively, whereas the max. tensile strength

remained the same. From these results, it can be seen that the addition of 3 wt% of TiO_2 has a similar effect as adding 5 wt% sZnO.

6.3.8 UV absorption properties

The UV absorption properties of the prepared nanocomposites were characterized through recording of UV-Vis transmittance spectra, which are presented in Figure 6-4. It can be seen that the prepared nanocomposite films are characterized by a highly effective UV-blocking. Upon addition of only 1 wt% of ZnO or sZnO, a complete cut-off of transmission of wavelengths below about 370 nm is observed. This means that wavelengths of the UV-C (200-280 nm), UV-B (280-315 nm) and a major fraction of the UV-A (315-400 nm) cannot pass through the films.

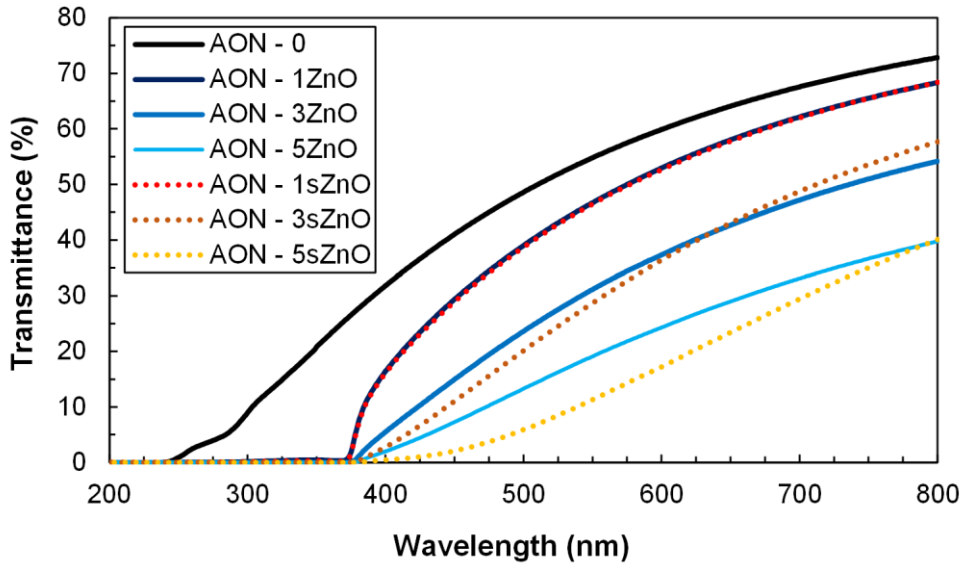

Figure 6-4: UV-Vis spectra of AON/ZnO and AON/sZnO nanocomposites

The films containing 3 and 5 wt% of ZnO or sZnO show a complete blocking below 370 nm as well, but also show a strongly reduced transmittance in the visible range of the electromagnetic spectrum (400-780 nm). The sample containing 3 wt% of TiO_2 is not shown in Figure 6-4, as it showed complete absorption (0 % transmission) for wavelengths between 200 and 800 nm. Thus, for effective UV-shielding and retaining a rather good transmittance in the visible range, it is necessary to limit the ZnO or sZnO content to 1 wt%.

6.3.9 Opacity

The opacity of the samples prepared in this chapter are presented in Table 6-7. From the results it can be immediately seen that the addition of ZnO or sZnO significantly increases the opacity of the films. An increase from 11.5 % to 30.1 % and 37.7 % can be observed upon addition of 5 wt% ZnO and 5 wt% sZnO, respectively. This is due to the whitening effect of zinc oxide. An even more extensive effect was observed for the sample containing 3 wt% TiO_2, which was rendered practically completely non-transparant, with an opacity of 87.6 %. This was to be expected, since TiO_2 is a widely used white pigment. If a good transparency is required for the application, it is important to note that the ZnO or sZnO concentration should be limited to 1 wt%. Photographs of the samples against a white and black background are given in Figure 6-5, in order to clearly display the increase in opacity.

Table 6-7: Opacity of AON/ZnO, AON/sZnO and AON/TiO_2 nanocomposites (n = 4)

Sample	Opacity *Y* (%)
AON-0	11.5 (± 0.2)
AON-1ZnO	17.1 (± 0.3)
AON-3ZnO	24.2 (± 0.3)
AON-5ZnO	30.1 (± 0.9)
AON-1sZnO	15.9 (± 0.3)
AON-3sZnO	26.3 (± 0.6)
AON-5sZnO	37.7 (± 0.4)
AON-3TiO_2	87.6 (± 0.1)

Figure 6-5: Photographs of AON/ZnO, AON/sZnO and AON/TiO_2 nanocomposites

6.4 CONCLUSIONS

In this chapter, the effect of ZnO and sZnO (surface modified) nanorods, in a concentration range of 1 to 5 wt%, on end-use properties of a commercial grade of PHBHHx was investigated. Due to a lack of compatibility, it was not possible to obtain a fine dispersion of ZnO nanoparticles in concentrations above 1 wt%, leading to agglomerations visible to the naked eye. Using sZnO, this problem was solved and the nanorods were finely dispersed at all tested concentrations.

Important observations that were made, are:

- ZnO appears to have a slight catalytic effect on the thermal degradation of the polymer, leading to a reduction in thermal stability and molecular weight after processing. However, this was counteracted partially by using sZnO, in which the zinc oxide surface is deactivated by surface modifications for a large part.
- Barrier properties for O_2, CO_2 and water vapor were hardly influenced, due to the fact that the rodlike nanostructure does not create a tortuous path as elaborate, as for example platelets.
- The presence of sZnO nanorods led to a stiffer material, with slightly lower strain at break, but of equal tensile strength. By adding ZnO nanorods in concentrations higher than 1 wt%, the tensile strength was reduced as well, rendering it brittle.
- An effective UV shielding effect was observed for wavelengths shorter than 370 nm, for all concentrations of sZnO and ZnO.
- The addition of 3 wt% TiO_2 led to a highly opaque material, with tensile properties similar to the film containing 5 wt% sZnO and very efficient UV blocking properties. The presence of these particles did not induce any effect on thermal stability, crystallization or barrier properties.

Even though no outspoken effect on the barrier properties were observed, the potential of Aonilex/zinc oxide nanocomposites can be found in the addition of 1 wt% of sZnO, to produce a slightly stiffer water barrier material with UV protective properties, which can be used as an outer layer in for example EVOH multilayer films.

6.5 REFERENCES

1. Kołodziejczak-Radzimska, A. and T. Jesionowski, *Zinc Oxide—From Synthesis to Application: A Review.* Materials, 2014. **7**(4): p. 2833.

2. Moezzi, A., A.M. McDonagh, and M.B. Cortie, *Zinc oxide particles: Synthesis, properties and applications.* Chemical Engineering Journal, 2012. **185–186**: p. 1-22.

3. Espitia, P., et al., *Zinc Oxide Nanoparticles: Synthesis, Antimicrobial Activity and Food Packaging Applications.* Food and Bioprocess Technology, 2012. **5**(5): p. 1447-1464.

4. Elen, K., et al., *Towards high-performance biopackaging: barrier and mechanical properties of dual-action polycaprolactone/zinc oxide nanocomposites.* Polymers for Advanced Technologies, 2012. **23**(10): p. 1422-1428.

5. Pantani, R., et al., *PLA-ZnO nanocomposite films: Water vapor barrier properties and specific end-use characteristics.* European Polymer Journal, 2013. **49**(11): p. 3471-3482.

6. Díez-Pascual, A. and A. Díez-Vicente, *Poly(3-hydroxybutyrate)/ZnO Bionanocomposites with Improved Mechanical, Barrier and Antibacterial Properties.* International Journal of Molecular Sciences, 2014. **15**(6): p. 10950.

7. Díez-Pascual, A.M. and A.L. Díez-Vicente, *ZnO-Reinforced Poly(3-hydroxybutyrate-co-3-hydroxyvalerate) Bionanocomposites with Antimicrobial Function for Food Packaging.* ACS Applied Materials & Interfaces, 2014. **6**(12): p. 9822-9834.

8. Vicentini, D.S., A. Smania Jr, and M.C.M. Laranjeira, *Chitosan/poly (vinyl alcohol) films containing ZnO nanoparticles and plasticizers.* Materials Science and Engineering: C, 2010. **30**(4): p. 503-508.

9. Shankar, S., et al., *Preparation, characterization, and antimicrobial activity of gelatin/ZnO nanocomposite films.* Food Hydrocolloids, 2015. **45**: p. 264-271.

10. Diez-Pascual, A.M., C. Xu, and R. Luque, *Development and characterization of novel poly(ether ether ketone)/ZnO bionanocomposites.* Journal of Materials Chemistry B, 2014. **2**(20): p. 3065-3078.

11. Murariu, M., et al., *High-Performance Polylactide/ZnO Nanocomposites Designed for Films and Fibers with Special End-Use Properties.* Biomacromolecules, 2011. **12**(5): p. 1762-1771.

12. Yu, W., et al., *Influence of zinc oxide nanoparticles on the crystallization behavior of electrospun poly(3-hydroxybutyrate-co-3-hydroxyvalerate) nanofibers.* Polymer, 2010. **51**(11): p. 2403-2409.

13. Lepot, N., et al., *Influence of incorporation of ZnO nanoparticles and biaxial orientation on mechanical and oxygen barrier properties of polypropylene films for food packaging applications.* Journal of Applied Polymer Science, 2011. **120**(3): p. 1616-1623.

14. Sanches-Silva, A., et al., *Study of the effect of light on fatty acids of potato crisps using a gas chromatographic method.* Analytica Chimica Acta, 2004. **524**(1–2): p. 191-200.

15. Lennersten, M. and H. Lingnert, *Influence of Wavelength and Packaging Material on Lipid Oxidation and Colour Changes in Low-fat Mayonnaise.* LWT - Food Science and Technology, 2000. **33**(4): p. 253-260.

16. Thron, M., K. Eichner, and G. Ziegleder, *The Influence of Light of Different Wavelengths on Chlorophyll-Containing Foods.* LWT - Food Science and Technology, 2001. **34**(8): p. 542-548.

17. Kristensen, D., et al., *Influence of light and temperature on the colour and oxidative stability of processed cheese.* International Dairy Journal, 2001. **11**(10): p. 837-843.

18. Li, S.-C. and Y.-N. Li, *Mechanical and antibacterial properties of modified nano-ZnO/high-density polyethylene composite films with a low doped content of nano-ZnO.* Journal of Applied Polymer Science, 2010. **116**(5): p. 2965-2969.

19. Bronlund, J.E., G.P. Redding, and T.R. Robertson, *Modelling Steady-State Moisture Transport Through Corrugated Fibreboard Packaging.* Packag Technol Sci, 2013. **27**: p. 193-201.

20. Cagnon, T., et al., *Nanostructuring and Microstructuring of Materials from a Single Agropolymer for Sustainable MAP Preservation of Fresh Food.* Packag Technol Sci, 2013. **26**(3): p. 137-148.

21. Kuorwel, K.K., et al., *Physico-Mechanical Properties of Starch-Based Films Containing Naturally Derived Antimicrobial Agents.* Packag Technol Sci, 2013. **27**: p. 149-159.

22. Ariffin, H., et al., *Determination of multiple thermal degradation mechanisms of poly(3-hydroxybutyrate).* Polym Degrad Stab, 2008. **93**(8): p. 1433-1439.

23. Morikawa, H. and R.H. Marchessault, *Pyrolysis of bacterial polyalkanoates.* Can J Chem, 1981. **59**(15): p. 2306-2313.

24. Vogel, C., et al., *Thermal Degradation of Poly(3-hydroxybutyrate) and Poly(3-hydroxybutyrate-co-3-hydroxyhexanoate) in Nitrogen and Oxygen Studied by Thermogravimetric–Fourier Transform Infrared Spectroscopy.* Appl Spectrosc, 2007. **61**(7): p. 755-764.

25. Kim, K.J., Y. Doi, and H. Abe, *Effects of residual metal compounds and chain-end structure on thermal degradation of poly(3-hydroxybutyric acid).* Polymer Degradation and Stability, 2006. **91**(4): p. 769-777.

26. Buzarovska, A., et al., *Poly(hydroxybutyrate-co-hydroxyvalerate)/titanium dioxide nanocomposites: A degradation study.* Journal of Applied Polymer Science, 2009. **114**(5): p. 3118-3124.

Chapter 7.

CONCLUSIONS AND FUTURE POSSIBILITIES

This chapter provides an overview of the main findings from this doctoral study. Considering these findings, some possible and innovative routes for novel research topics are suggested.

7.1 CONCLUSIONS

This doctoral study investigated several modification techniques for three selected polyhydroxyalkanoates, to enhance their potential for food packaging applications, as well as to reduce possible indirect drawbacks (i.e. processing related). Following research questions were set as guideline for the experimental work:

1) How do the selected PHA compare to each other and what are their major positive and negative properties?
2) How can the properties of PHBV be enhanced?
3) How can the properties of PHBHHx be enhanced?

First of all, the three selected PHA, namely PHBV, PHBHHx and Aonilex (commercial granulate of PHBHHx) were thoroughly characterized and compared. It became immediately clear that the former two suffered from slow crystallization rates. PHBHHx and Aonilex were proven to be rather ductile materials, whereas PHBV appeared to be more brittle. In terms of gas barrier properties, all three polymers performed fairly well, displaying a moderate O_2 and CO_2 permeability and a rather low water vapor permeability. Based on these results, it appeared that PHBHHx and Aonilex displayed more potential for application as flexible packaging than the grade of PHBV, used in this study.

As slow crystallization is a common problem for PHBV and PHBHHx, efforts were made to find efficient nucleating agents to increase crystallization rates. This might not be a problem directly related to the packaging properties, it is however

a great nuisance for the industrial production of packaging films from these materials. PHBHHx was modified through the addition of low concentrations of ultra-fine talc (median diameter ≤ 1μm). Crystallization rates were greatly enhanced, without a severe change of other polymer properties (permeability, thermal stability etc.), indicating a great potential for industrial use of the combination PHBHHx and ultra-fine talc. For PHBV, the conventional nucleating agent boron nitride was compared to a biobased/biodegradable alternative orotic acid. These experiments proved that, even though it appears to be quite an effective nucleating agent, orotic acid is less performant than boron nitride. These results, in combination with the inherent brittleness of this type of PHBV, led to the decision to proceed only with PHBHHx and Aonilex in the following parts of the doctoral research.

Attempts to enhance the packaging properties of PHBHHx and Aonilex were made through the preparation of nanocomposites. Firstly, OMMT was added to PHBHHx and Aonilex in concentrations from 1 to 10 wt%. Due to the high aspect ratio of the OMMT nanoparticles, a steady decrease in gas permeability properties (O_2, CO_2 and water vapor) was observed upon increasing OMMT concentrations, with maximum reductions between 37 and 47 %. However, some downsides were observed as well. The addition of OMMT increased thermal degradation during processing, leading to slower crystallization rates. However, this was partially compensated by using Aonilex instead of PHBHHx. Also, high concentrations of OMMT (≥ 5 wt%) rendered the nanocomposites rather brittle and very stiff.

A final modification that was investigated are Aonilex/zinc oxide nanorods composites, with filler concentrations ranging from 1 to 5 wt%. It was shown that the use of unmodified zinc oxide nanorods resulted in a very poor dispersion, leading to a stiffer, yet more brittle nanocomposite. Therefore, surface modified zinc oxide nanorods (sZnO) were used in order to lower interfacial energy and successfully obtain fine dispersions at all tested concentrations. Though literature data indicated that zinc oxide nanorods could induce a significant reduction in gas permeability properties, this was not the case for Aonilex/sZnO nanocomposites. Gas barrier properties remained constant at all temperatures and a slightly reduced thermal stability was observed. However, the addition of sZnO, in concentrations as low as 1 wt%, gave the nanocomposites the remarkable feature

of UV shielding, which could be interesting for food packaging materials. The use of TiO_2 did not result in a material with better characteristics, nor does its zero transparency make it an interesting food packaging material.

In general, even though we were not able to create a high-barrier material based on a PHA, it is necessary to place these findings in their correct context. A successful implementation of PHA as a food packaging material should be done by enhancing negative properties (i.e. faster crystallization with nucleating agent) and correctly using the already present positive properties to its advantage. For example, PHBHHx already presents itself as a fairly good water vapor barrier. Through the addition of low concentrations of ultra-fine talc, a better industrial processability is possible, as processes such as sheet extrusion or injection molding require sufficiently rapid crystallization to avoid sticking to molds and rolls. Adding 1 wt% sZnO to this system, can create a fast crystallizing, UV shielding outer layer, protecting a moisture-sensitive oxygen barrier (i.e. EVOH) for high-end food packaging.

7.2 FUTURE RESEARCH

During this doctoral study, several routes and topics, regarding the implementation of PHA for food packaging, have been found, that deserve further investigation.

It was proven that the addition of OMMT can severely reduce the gas permeability properties of PHBHHx, however at the cost of its ductility at higher OMMT contents. Therefore, it could be interesting to subject PHBHHx/OMMT (with OMMT contents ≤ 3 wt%) to a processing technique that can induce orientation of the nanoparticles, such as stretch blow molding or a combination of sheet extrusion and biaxial orientation. Additional orientation could prove to be a promising route for reaching even lower permeability values, with lower OMMT concentrations.

A modification route that shows a great amount of potential is the formation of multilayer films of PHA and a high oxygen barrier polymer. Taking advantage of the naturally low water vapor permeability of PHA to protect a moisture sensitive oxygen barrier, such as EVOH, can be of great interest for the food packaging industry. However, this would require compatibility between the used polymers in terms of processing temperature and melt viscosity. Therefore, combining two

PHA outer layers with one inner layer of whey protein isolate barrier coating, can be a more interesting route to develop a high-end biobased multilayer. This type of sample preparation requires dedicated equipment, which was not available during this doctoral research unfortunately.

Besides the effect of modifications on packaging-related properties, it can be interesting to investigate the effect of adding different types of (nano)fillers on the biodegradability of the polymers used in this study. If it is possible to retain, or even enhance, the highly biodegradable nature of the final packaging product, some new perspectives regarding its waste management can be regarded.

Finally, the use of ultra-fine talc as a nucleating agent for PHBHHx should be elaborated further, as this can tackle one of the most important drawbacks of this polymer. Testing this composite in lab scale processing equipment, such as sheet extrusion and injection molding, can give a clear idea on its industrial value.

ABOUT THE AUTHOR

Jens Vandewijngaarden was born on July 12th 1988 in Herk-de-Stad. He obtained a Master in Nuclear Engineering Technology,with a specialization in Environmental Technology & Radiochemistry at XIOS University College in 2010. His thesis, titled 'Characterization of activated carbons derived from short rotation hardwood coppice' was nominated for the Paul Donners award. In search of a new challenge, he started his doctoral research in early 2011 as a collaboration between the research groups Applied and Analytical Chemistry and Packaging Technology Center at the University of Hasselt. During the first year of his doctoral research, the author has successfully completed several additional university courses at the University of Hasselt and University of Leuven.

During his PhD research, the author has also taught several practical and theoretical courses on packaging materials, waste management and analytical chemistry. In the Applied and Analytical Chemistry lab, he also assisted in other research projects involving characterization of materials.

The following is a list of scientific publications that the he has (co-)authored.

Journal papers indexed in SCI (A1):

- Smets, K., Adriaensens, P., Vandewijngaarden, J., Stals, M., Cornelissen, T., Schreurs, S., Carleer, R., Yperman, J.: *'Water content of pyrolysis oil: Comparison between Karl Fischer titration, GC/MS-corrected azeotropic distillation and H-1 NMR spectroscopy.'* In Journal of Analytical and Applied Pyrolysis, 2011, Vol. 90, Issue 2, p. 100-105
- Stals, M., Vandewijngaarden, J., Wróbel-Iwaniec, I., Gryglewicz, G., Carleer, R., Schreurs, S., Yperman, J.: *'Characterization of activated carbons derived from short rotation hardwood pyrolysis char.'* In Journal of Analytical and Applied Pyrolysis, 2013, Vol. 101, p. 199-208
- Vandewijngaarden, J., Murariu, M., Dubois, P., Carleer, R., Yperman, J., Adriaensens, P., Schreurs, S., Lepot, N., Peeters, R., Buntinx, M.: *'Gas Permeability Properties of Poly(3-hydroxybutyrate-co-3-hydroxyhexanoate).'* In Journal of Polymers and the Environment, 2014, Vol. 22, Issue 4, p. 501-507

- Mesroghli, Sh., Yperman, J., Jorjani, E., Vandewijngaarden, J., Reggers, G., Carleer, R., Noaparast, M.: *'Changes and removal of different sulfur forms after chemical desulfurization by peroxyacetic acid on microwave treated coals'* In Fuel, 2015, Vol. 154, p. 59-70
- Vandewijngaarden, J., Wauters, R., Murariu, M., Dubois, P., Carleer, R., Yperman, J., D'haen, J., Ruttens, B., Schreurs, S., Lepot, N., Peeters, R., Buntinx, M.: *'Poly(3-hydroxybutyrate-co-3-hydroxyhexanoate)/ organomodified montmorillonite nanocomposites for potential food packaging applications*' In Journal of Polymers and the Environment, 2016, p. 1-15

The following paper is submitted for publication:

- Vandewijngaarden, J., Murariu, M., Dubois, P., Carleer, R., Yperman, J., Peeters, R., Buntinx, M.: '*Effect of ultra-fine talc on crystallization and end-use properties of poly(3-hydroxybutyrate-co-3-hydroxyhexanoate)*' Submitted for review in Journal of Applied Polymer Science.

Book sections (B2):

- Stals, M., Vandewijngaarden, J., Gryglewicz, G., Carleer, R., Schreurs, S., Yperman, J.: *'Activation and Characterization of Pyrolysis Chars from Short Rotation Hardwoods.'* In Essays on Environmental Studies (Ed. Sarin, A.), 2012, p. 291-306, ISBN: 978-960-9549-75-2

Presentations (C2):

- *'Characterization of poly(3-hydroxybutyrate-co-3-hydroxyhexanoate)/ organomodified clay nanocomposites for packaging applications.'* At ChemCYS, Blankenberge, 27th and 28th of February 201